# Immobilisation of an *Aspergillus niger* derived endo-1,4-β-mannanase, Man26A, for the production of prebiotic mannooligosaccharides from soybean meal

A thesis submitted in fulfilment of the requirements for the degree of

MASTERS IN SCIENCE

in

BIOCHEMISTRY

at

RHODES UNIVERSITY

by

AMY SAGE ANDERSON

https://orcid.org/0000-0002-3199-2765

Supervisor: Prof. Brett I. Pletschke

Co-supervisor: Dr. Lithalethu Mkabayi

January 2024

**Abstract**

This study investigated the potential for antibiotic alternatives in the form of prebiotics produced from the enzymatic breakdown of soybean meal (SBM). This study first investigated the immobilisation of an endo-1,4-β-mannanase derived from *Aspergillus niger* on glutaraldehyde-activated chitosan nanoparticles (CTS) and glutaraldehyde-activated chitosan-coated magnetic Fe3O4 nanoparticles (MAGS-CTS) - which could be effectively used to hydrolyse the galactomannan contained in SBM in a recyclable manner. The mannooligosaccharides (MOS) produced from the enzymatic digestion of SBM were then analysed for their prebiotic and antimicrobial capabilities to determine whether the strategy employed was capable of promoting and inhibiting probiotic and pathogenic growth, respectively. An *Aspergillus niger* endo-1,4-β-mannanase, Man26A, was confirmed by FTIR (Fourier-transform infrared spectroscopy) and XRD (X-ray powder diffraction) to be immobilised onto CTS and MAGS-CTS by covalent bonding. The immobilisation (%) and activity yields (%) were 81.14% and 35.45%, and 55.75% and 21.17%, respectively. The biochemical properties (pH and temperature optima, and temperature stability) of both the free CTS and MAGS-CTS immobilised Man26A enzymes were evaluated, with the pH optima shifting to a lower pH range after immobilisation (pH 2.0 – 3.0 vs. 5.0), while the temperature optima and stabilities remaining unchanged (at 60°C). CTS and free enzymes exhibited identical thermal stabilities, maintaining 100% activity for the first 6 hours at 55°C, while MAGS-CTS showed an immediate drop in relative activity after the first 30 minutes of incubation. Recyclability analysis revealed that CTS could be effectively reused for six reaction cycles, while the MAGS-CTS immobilised enzyme could only be used once. Both enzymes could be efficiently stored at 4ºC, showing a relative residual activity of 73% after 120 hours of storage. Substrate kinetic analysis showed that the free enzyme had the highest catalytic capabilities in hydrolysing locust bean gum (LBG), with the CTS immobilised enzyme was the most efficient in hydrolysing SBM, the insoluble, complex substrate. Sugar residues produced from the hydrolysis of LBG illustrated the effective breakdown of galactomannan to mannobiose (M2), mannotriose (M3), mannotetrose (M4), and mannohexose (M6). SBM-produced sugars analysed via TLC and HPLC indicated that the MOS residues were most probably glucose, galactose, and galactomannans (GM2 and GM3). The SBM-produced sugars were then evaluated for their prebiotic effect, illustrating their successful utilisation as a carbon source by probiotic bacteria; *Streptococcus thermophilus, Bacillus subtilis* and *Lactobacillus bulgaricus.* Evaluation of the antimicrobial activities of the SBM-produced

sugars digested by probiotics suggested that their metabolites had the potential to be used as an antibiotic alternative. This study therefore illustrated that an endo-1,4-β-mannanase derived from *Aspergillus niger* could be immobilised successfully, for use in a recyclable reaction to produce MOS products. This study also described the successful use of SBM-sugars as a prebiotic, indicating a successful alternative to antibiotic growth promoters (AGP) by illustrating their positive effect on inhibiting growth of pathogenic bacterial species.

**List of Abbreviations**

| | |
|---|---|
| **%** | Percentage |
| **°** | Degree |
| **2θ** | Diffraction Angle |
| ***A*** | The quantity of enzyme loaded for immobilisation procedure (mg) |
| ***A-B*** | The theoretical immobilised enzyme. |
| ***A. niger*** | *Aspergillus niger* |
| **$A^+$** | Absorbance of the positive control |
| **A-CTS** | Glutaraldehyde-activated chitosan nanoparticles |
| ***Af*** | Absorbance of the background |
| **AGP** | Antibiotic growth promoter |
| $A_i$ | Absorbance of the sample |
| **ANF** | Antinutritional factors |
| ***B*** | Unbound protein after immobilisation (mg) |
| ***B. subtilis*** | *Bacillus subtilis* |
| **BSA** | Bovine serum albumin |
| **Ca** | Calcium |
| **Cl** | Chloride |
| **CLEAs** | Cross-linked enzyme aggregates |
| **CTS** | Endo-1,4-β-mannanase immobilised glutaraldehyde-activated chitosan nanoparticles |
| ***D*** | Crystalline size (nm) |
| **DNS** | 3,5-dinitrosalicylic acid |
| **DP** | Degree of Polymerisation |
| ***E. coli*** | *Escherichia coli* |
| **$Fe_3O_4$** | Iron Oxide |
| **FIIR** | Feed innate immune response |
| **FTIR** | Fourier-transform infrared spectroscopy |
| **g** | Grams |
| ***g*** | Relative centrifugal force |
| **g/L** | Grams per Litre |
| **Gal:Man** | Galactose: Mannose |
| **GHs** | Glycoside hydrolases |

| | |
|---|---|
| **GM2** | Galactosyl-mannobiose |
| **GM3** | Galactosyl-mannotriose |
| **GM5** | Galactosyl-mannopentaose |
| **HPLC** | High-performance liquid chromatography |
| **HPLC-RID** | High-performance liquid chromatography refractive index detectors |
| ***K*** | Scherrer constant |
| ***K. pneumonia*** | *Klebsiella pneumoniae* |
| ***L. bulgaricus*** | *Lactobacillus bulgaricus* |
| **LBG** | Locust bean gum |
| **M** | Molar |
| **M1** | Mannose |
| **M2** | Mannobiose |
| **M3** | Mannotriose |
| **M4** | Mannotetraose |
| **M5** | Mannopentaose |
| **M6** | Mannohexaose |
| **MAGS** | Magnetic $Fe_3O_4$ nanoparticles |
| **MAGS-A-CTS** | Glutaraldehyde-activated chitosan-coated magnetic $Fe_3O_4$ nanoparticles |
| **MAGS-chitosan** | Chitosan-coated magnetic $Fe_3O_4$ nanoparticles; |
| **MAGS-CTS** | Endo-1,4-β-mannanase immobilised glutaraldehyde-activated chitosan-coated magnetic $Fe_3O_4$ nanoparticles |
| **mg** | Milligrams |
| **mg/ml** | Milligrams per millilitre |
| **ml** | Millilitres |
| **ml/min** | Millilitre per minute |
| **mM** | Millimolar |
| **MOS** | Mannooligosaccharides |
| **Na** | Sodium |
| **nm** | Nanometre |
| **NSP** | Non-starch polysaccharides |
| **$^oC$** | Degrees Celsius |
| **$^oC$/min** | Degrees Celsius per minute |

| | |
|---|---|
| **$OD_{600}$** | Optical density at a wavelength of 600 nm |
| **PRR** | Pathogen recognition receptors |
| **PTS** | Phosphoenolpyruvate-sugar |
| **PUL** | Mannose utilisation locus |
| **Rpm** | Revolutions per minute |
| ***S. aureus*** | *Staphylococcus aureus* |
| ***S. thermophilus*** | *Streptococcus thermophilus* |
| **$s^{-1}$** | Per second |
| **SBM** | Soybean meal |
| **SEM** | Scanning electron microscopy |
| **TFA** | Trifluoroacetic acid |
| **TLC** | Thin-layer chromatography |
| **TPP** | Sodium Tripolyphosphate |
| **U/mg** | Specific Activity |
| **v/v** | Volume per volume |
| **w/v** | Weight per volume |
| **XRD** | X-ray powder diffraction |
| ***β*** | Full width of the wavelength at half maximum |
| ***λ*** | Radiation wavelength |
| **µL** | Microlitres |
| **µmol** | Micromolar |

**Plagiarism declaration**

I, Amy Sage Anderson, declare that this thesis is my own, original and unaided work. It is being submitted for the Master of Science at Rhodes University. It has not been submitted before, for any degree or examination, at any other university.

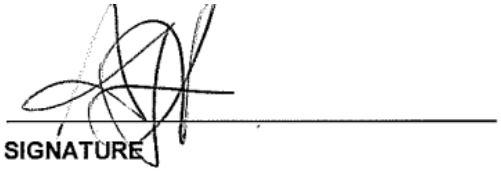


Date: January 2024

**TABLE OF CONTENTS**

**List of Figures**

**List of Tables**

**Acknowledgements**

Throughout the project I have received a great deal of support and assistance. I would like to express my sincere gratitude to my supervisors, Professor Brett I. Pletschke (Supervisor) and Dr. Lithalethu Mkabayi (Co-supervisor). Thank you, Prof. Pletschke, for your constant support and guidance. From the day I arrived in the lab during honours to the day that I left, every moment was enjoyed. Thank you for all the advice and assistance over the past 2.5-years, it was appreciated immensely, and I know that without your guidance I would not be handing in my MSc. Thank you to Dr. Mkabayi, for spending hours with me going through concepts, making comments, as well as helping me with everything else one could imagine facing during an MSc thesis. I am so grateful that you were my co-supervisor, and I appreciate everything you have helped me achieve to date. I would like to thank Dr. Samkelo Malgas for the guidance regarding mannooligosaccharides and mannanases throughout the year. With the above thanks I would also like to mention and thank Prof. Pletschke, Dr. Mkabayi, and Dr. Malgas for assistance in publishing my first research paper, I am forever grateful to have been given the opportunity.

I would like to give special thanks to all the occupants of labs 410 and 412 in the Department of Biochemistry and Microbiology at Rhodes University, where ESP lab is situated. Special mention should be made to Lebogang Ramatsui, Mihle Magenelele, Tariro Sithole, Yuchan Park, Chantal Daub, Arryn Michaels, and finally Blessing Mabate, for the assistance in various experiments, the encouragement as well as enormous amounts of amusement and laughter throughout the year. I would like to thank my diggs mates, Aidan Du Preez, Andrew Meiklejohn, Kowie Meiklejohn, and Bonnie Du Preez, thank you for the constant support which has led to the handing-in of my MSc dissertation. Lastly, I would like to thank Gillian Anderson, Robyn Anderson, Gregg Scott-Brown, Harvy Brownerson, Riley Brownerson, and Darsi Brownerson for their financial and emotional support this year. The ongoing support, throughout my write-up especially, made the procedure highly enjoyable.

**List of outputs emanating from this study**

Anderson, A.; Mkabayi, L.; Malgas, S.; Kango, N.; Pletschke, B. I. Covalent Immobilisation of an *Aspergillus niger* Derived Endo-1,4-β-mannanase, Man26A, on Glutaraldehyde-activated Chitosan Nanoparticles for the Effective Production of Prebiotic MOS from Soybean meal. *Agronomy*. 2022, 12(12), 2993.

# CHAPTER 1: LITERATURE REVIEW

## 1.1 Background

The poultry meat sector is one of the largest contributors to meat production and consumption worldwide, due to its low cost of production, high feed conversion ratios and low product prices (OECD/FAO, 2018). In 2020, worldwide meat consumption was at 323.9 million metric tons, with poultry representing 40.5% of this total. Poultry meat and eggs remain one of the most affordable sources of animal protein, supplying various countries with nutritious food as well as contributing to the direct and indirect employment of approximately 120 000 people in South Africa (OECD, 2021). It is estimated that poultry production will need to increase by 70% by 2050 to meet the population's growing demands. In addition, it has also been estimated that the presence of antibiotics in animal agriculture will be increased by 67% by 2030, to achieve the desired quantities of animal protein – emphasising the world's need for sustainable livestock practices (Nkukwana, 2018; Arunrattanamook et al., 2020; Hedman et al., 2020).

Worldwide, 70% of all synthesised antibiotics are used in animal production (Arunrattanamook et al., 2020; Hedman et al., 2020). Although antibiotics have increased poultry productivity and health, they have also led to the growth of drug-resistant pathogens and antibiotic-related environmental pollutants (Arunrattanamook et al., 2020). These factors have led to a ban on antibiotics in several countries, such as the United Kingdom, Denmark and the Netherlands. South Africa has yet to ban antibiotics in livestock farming practices, though if this does occur, it is suspected to result in a massive drop in production. Antibiotic alternatives are vital for South Africa to maintain high quantities of animal protein while maintaining low costs to compete with cheap international imports (Manyi-Loh, 2015). For a sustainable supply of healthy animal protein, alternative feed additives are being investigated, with prebiotics showing potential as a strong candidate (Markowiak and Śliżewska, 2018). With no direct benefit themselves, the abilities of prebiotics to control pathogenic microbiota, increase nutrient uptake and benefit the intestinal morphology of poultry have made them a competitive contender to antibiotic growth promoters (AGP) (Solis-Cruz et al., 2019). With an indirect virulence to pathogenic bacteria, prebiotics are a sort-after alternative, for creating healthy animal protein.

## 1.2 Poultry feed

Feed is a fundamental aspect of animal production, requiring sustainable and ethical methods of production to ensure long term food stability (van der Poel et al., 2020). A large portion of production costs are allocated to poultry feed. Therefore, it is essential to find affordable grains supplying poultry with the required nutrients for maintenance and growth to support the population's growing demand for animal protein (Ravindran, 2013). Poultry have a short digestive tract that can absorb nutrients more rapidly than other domestic animals. As a result, high-performance birds require nutrient-rich feeds which can be easily digested (Ravindran, 2013). To ensure that poultry grows optimally for production, they need five specific components in their diet to ensure health: energy, protein, minerals, vitamins and water (Blair, 2008). The proportions of these nutrients in the diet depend on age, species, and purpose of production (Ravindran, 2013).

Water, an essential part of a poultry diet, facilitates the absorption of nutrients and excretion of waste products and helps to regulate body temperature (Ravindran, 2013). According to Ravindran (2013) energy is derived from simple carbohydrates, fats, and proteins; the amount of available energy in the feed directly translates to the quantity of feed that needs to be consumed by the individual organism. Energy is typically provided by simple carbohydrates, fats, and proteins (Ravindran, 2013). Minerals in the feed are required for the formation of the skeletal system, health, and maintenance of acid-base balance in the body; the most important minerals are sodium (Na), potassium (K), and chloride (Cl). All vitamins are required in the poultry diet and are often supplied through vitamin premixes; acting as facilitators for biochemical reactions in the body (Ravindran, 2013). Proteins make up the most significant proportion of poultry feed; delivering essential amino acids which support overall maintenance and growth. Twenty amino acids are required by poultry, ten being essential and which must be supplied (Ravindran, 2013). The essential amino acids for poultry are lysine, methionine, threonine, tryptophan, isoleucine, leucine, histidine, valine, phenylalanine, and arginine (Ravindran, 2013). The plant protein source traditionally used in poultry feed formulations is soybean meal (SBM) containing nine essential amino acids required for maintenance and growth (Dei, 2011).

### 1.2.1 Soybean meal

Soybean is a legume plant cultivated worldwide - prominently grown for its high protein content (Fan, 2019; Zahir et al., 2019). This plant is used in soybean oil extraction, making up

55% of global oilseed production. The soybean oil extraction produces a waste product of SBM, a feed ingredient mainly used in the diets of non-ruminant organisms (Ibáñez, 2020). For many years SBM has been considered an asset to the agricultural feed industry due to its high protein delivery, good amino acid balance, and year-round availability (Dozier and Hess, 2011; Zahir et al., 2019). Global soybean production was estimated to 352 million metric tons between 2021 and 2022 (USDA WASDE, 2022). With a drastic increase in the price of dietary protein sources, poultry nutritionists are searching for alternative methods for nutrient utilisation of cheap protein alternatives such as SBM (Suthama and Wibawa, 2018).

The carbohydrate proportion of SBM makes up 30 – 35% of its total mass, divided into non-structural and structural components (Islam et al., 2018). The structural carbohydrate is composed of non-starch polysaccharides (NSPs); this includes the dietary fibre proportion, cellulose, hemicellulose, and pectin (Islam et al., 2018) – the distribution of these components within the primary cell wall can be seen visually in Figure 1.1. The cells of SBM are supported by primary and secondary cell walls composed of various proportions of polysaccharides, phenolic compounds, and proteins (Nakano et al., 2015; Zahir et al., 2019; Holland et al., 2020). Cellulose and hemicellulose are straight-chain and cross-linked polymers, respectively, which serve as the structural components of the SBM cell wall (Nakano et al., 2015; Zahir et al., 2019; Holland et al., 2020). Cellulose fibres run in linear patterns through the cell wall, with hemicellulose intertwining between the cellulose microfibrils to create a cellulose-matrix network that maintains the cell wall rigidity (Wang et al., 2013). The hemicellulose portion of the cell is composed of various sugars within the soluble and structural carbohydrates. It has been estimated that the average total sugar content within SBM is between 5.0% and 16.6% when comparing various species (Choct et al., 2010). This includes rhamnose 0.7 ± 0.02%; glucose 3.1 ± 1.2%; xylose 1.1 ± 0.4% galactose 5.7 ± 1.3%; arabinose 2.7± 0.2%; fructose 0.2 ± 0.3%; and mannose 1.09 ± 0.6% (Islam et al.,2018). When focusing on the non-starch polysaccharides (NSPs) within the water-soluble and in-soluble portions of SBM, these were quantified as 0.07% rhamnose, 0.12% fucose, 1.31% arabinose, 0.64% xylose, 2.32%, glucose 1.92% galactose, and 0.30% mannose. The total compositions of NSPs within SBM constituted 8.26% (Karr-Lilienthal et al., 2005).

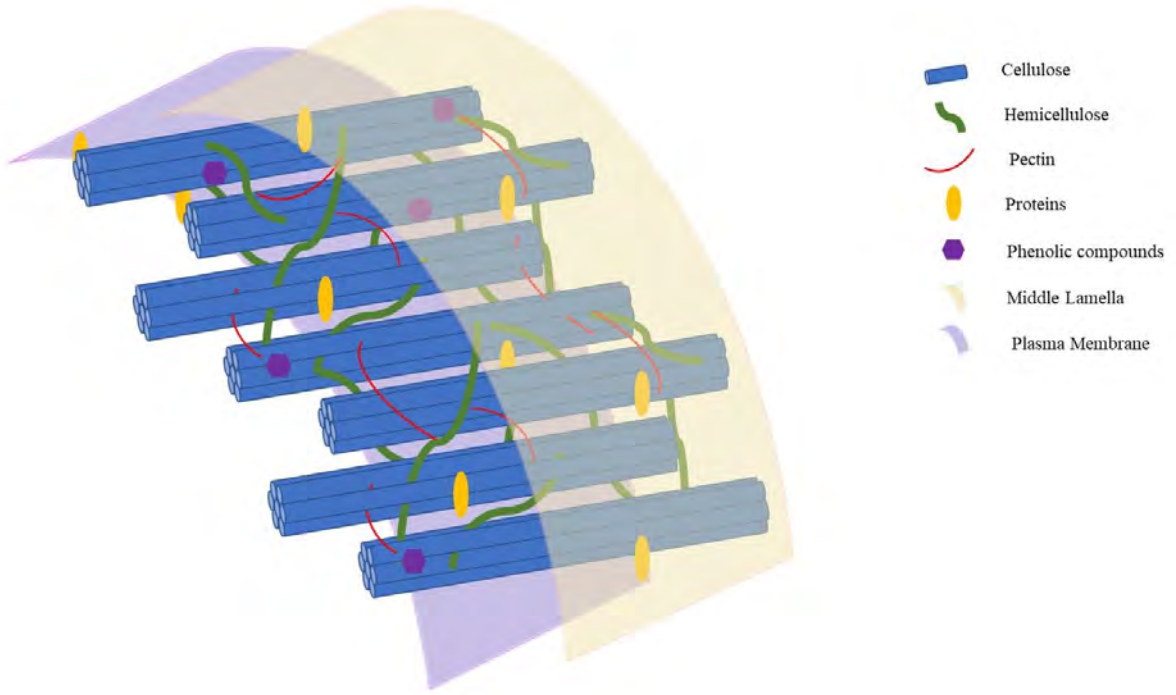


**Figure 1.1** Schematic representation of the primary cell wall of SBM. Modified from Nakano et al. (2015) and Holland et al. (2020).

However, the use of SBM has been limited due to the presence of several antinutritional factors (ANFs) and NSPs that have proven to be deleterious to the health and weight of poultry (Vangroenweghe et al., 2021). Plants have evolved ANFs over time as a defence mechanism to prevent utilisation by potential predators. SBM is highly nutritious, but overconsumptions leads to decreased nutrient uptake and growth due to the biologically active ANFs (Sinha and Khare, 2017). Examples of ANFs in SBM include phytic acid, saponins, cyanide, tannins, trypsin inhibitors, oxalates, and β-mannans (Sinha and Khare, 2017; Vangroenweghe et al., 2021). Though deleterious to metabolic action, many ANFs can be disabled by heat treatments below 100°C, however, this is not always the case for β-mannans (Sinha and Khare, 2017; White et al., 2021). β-Mannans, also typically termed galactomannans, are ANFs found in both the hulled and dehulled forms of SBM (White et al., 2021).

#### 1.2.1.1 β-galactomannans

Cellulose, hemicellulose, and pectin are various polysaccharides found in the cell walls of SBM, with hemicellulose making up 20 – 35% of the cell wall's total dry mass. Hemicellulose composition can vary, categorising them as mannans, xyloglucans, and xylans, respective of

their composition and origin (Wang et al., 2013; Sharma et al., 2020). The hemicellulose portion of SBM has a backbone made primarily of mannan (Arsenault et al., 2017; Sharma et al., 2020). These mannans are termed heteropolysaccharides, being subclassified as galactomannans; this describes the linear chains of β-1,4-linked D-mannose residues with α-1,6-linked D-galactose side chains repeated randomly throughout the polymer's backbone structure (Malgas et al., 2015a; Latham et al., 2018; Sharma et al., 2020 Suryawanshi, 2021), as can be seen in Figure 1.2.

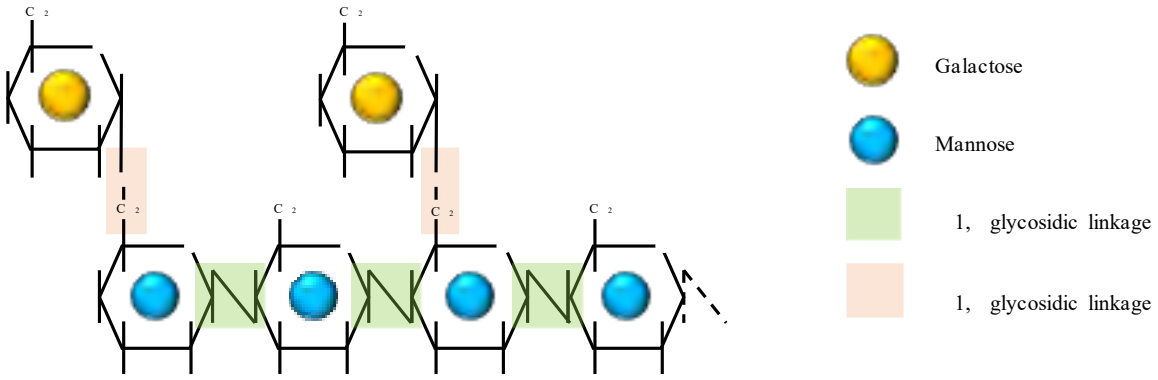


**Figure 1.2.** The general structure of galactomannan subfamilies of hemicellulose in SBM. Modified from Sharma et al. (2020).

There are various sources of galactomannans, three of which are locust bean gum (LBG), guar gum, and SBM with galactose: mannose (Gal:Man) ratios of 1:4, 1:2, and 1:1.8, respectively (Kashef et al., 2008; Malgas et al., 2015b; Surywanshi and Kango, 2021). The ratio of Gal:Man differs according to the origin and species from which the galactomannans were extracted. Galactomannans are stored in the cell walls of plants, being utilised for the growth of the embryo during germination (Sharma et al., 2020). These monosaccharides are synthesised in the lumen of the Golgi apparatus, where they are then delivered to the cell wall via secretory vesicles (Sharma et al., 2020).

Scientific interest in β-mannans has grown due to their configurations being components on the surface of numerous pathogens such as fungi, viruses, and bacteria (Hsiao et al., 2006). Galactomannans are deleterious to poultry health by binding to pathogen recognition receptors (PRR), stimulating a feed innate immune response (FIIR). This is a non-productive, energy-draining process where reactive oxygen and nitrogen species, bacteriolytic enzymes,

antimicrobial peptides and complement proteins are produced in response to a false threat (Hsiao et al., 2006; Scapini et al., 2018; Vangroenwghe et al., 2021). Another adverse side effect of galactomannans is the tendency to increase intestinal viscosity after consumption due to soluble fibres holding a high water retention capacity (Shastak et al., 2015; Scapini et al., 2018). This has the potential to decrease nutrient uptake leading to a decrease in weight gain and overall bird health (Scapini et al., 2018).

Decreasing the galactomannan content in agricultural feedstocks removes many adverse side effects of the heteropolysaccharide. This may be done by hydrolysing the mannan backbone into various degrees of polymerisation (DP) (DP 2-10). This is possible with the use of exogenous enzymes such as an endo-1,4-β-mannanase (Shastak et al., 2015; Scapini et al., 2018).

### 1.3 β-Mannanases

β-Mannanases are enzymes used to catalyse biochemical reactions (Malgas et al., 2015a; Mafa and Malgas, 2023). These enzymes are termed glycoside hydrolases (GHs), specifically endohydrolases. These biocatalysts catalyse the hydrolysis of a β-1,4-glycosidic linkages in β-mannan. There are four families of G s to which β-mannanases belong: GH5, GH26, GH113, and GH134 (Malgas et al., 2015a; Sharma et al., 2018). These families can be further classified into 14 clans, GH-A – GH-N, which then describe the structural fold similarity (Sharma et al., 2018). Three of the four families which contain β-mannanases are part of the GH-A clan, which can be characterised by the dominating class being a TIM barrel catalytic domain with two conserved glutamic acid residues, located in the middle of the catalytic core (Sharma et al., 2018). The characteristic fold of the TIM barrel in clan GH-A is set apart from others by a central β-barrel formed by 8 parallel β-strands (Sharma et al., 2018), which can be clearly visualised in Figure 1.3 – the blue and red indicating the N-terminus and C-terminus, respectively (Sun et al., 2021). The members of clan GH-A have an active site pocket with two pivotal catalytic glutamate residues; for GH26, these residues are Glu 212 and Glu320 (Sharma et al., 2018). For the efficient hydrolysis of galactomannan, the biocatalyst requires several substrate binding sites to be exposed. The β-mannanase enzyme should contain a nucleophilic catalyst and an acid/base catalyst, within a cleft confirmation; being distributed within 5.5 Å from each respective catalyst (Dawood and Ma, 2020). The molecular weight of β-mannanase was determined by SDS-PAGE by Soni et al. (2016) to be 49 kDa.

**Figure 1.3.** The modelled 3D structure of ManAC from *Aspergillus calidoustus,* based on the crystalline structure of β-mannanase from *Aspergillus niger* BK01 (Sun et al., 2021).

This study utilised a thermophilic fungus derived from *Aspergillus niger*, endo-1,4-β-mannanase (CAS number: 37288-54-3). The specificity of this enzyme focuses on the random hydrolysis of the (1,4)-β-D-mannosidic linkages in β-mannans, galactomannans and glucomannans (Sharma et al., 2018). A visual summary of hydrolysis is indicated in Figure 1. , where the β-mannanase enzyme randomly cleaves the (1,4)-β-D-mannosidic linkages to produce various DP lengths of mannose. Further enzymes used in synergy with β-mannanase can assist in the debranching and breakdown of complex galactomannan structures. Examples of these are β-mannosidase, β-glucosidase, α-1,6-D-galactoside galactohydrolase, and acetyl mannan esterase (Arunrattanamook et al., 2020).

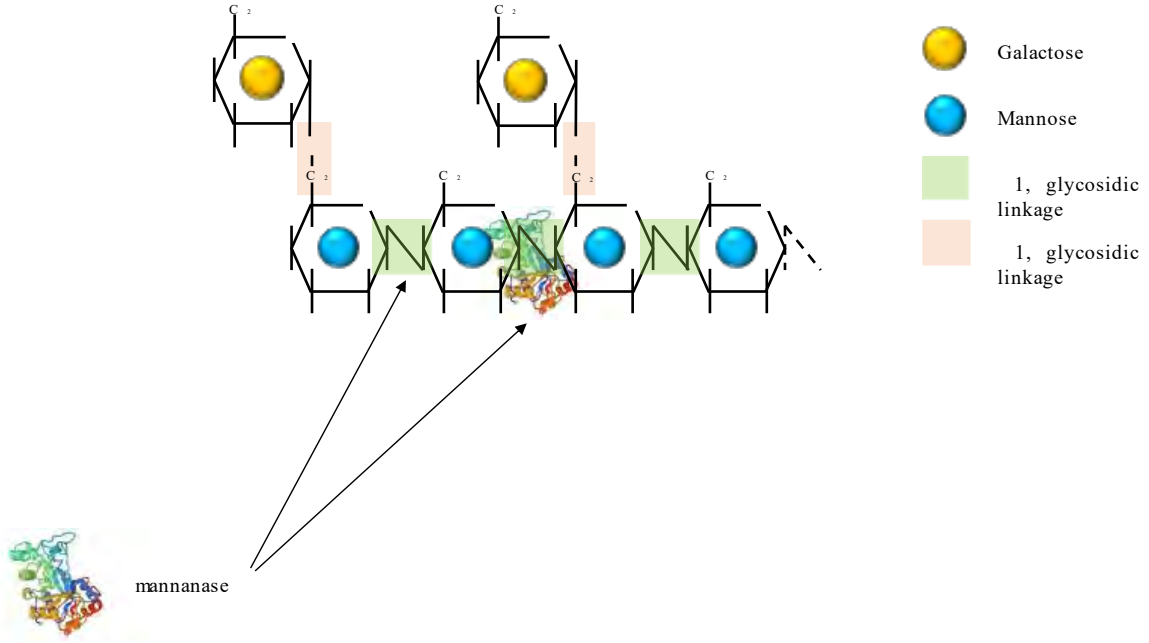


**Figure 1.4.** General structure of galactomannan in SBM undergoing hydrolysis of the β-1,4-glycosidic linkage by a β-mannanase. This image was modified from Sharma et al. (2018) and Sharma et al. (2020).

The optimum conditions of the enzyme were established by Naganagouda et al., (2009) to be at a temperature optimum of 55°C and a pH optimum of 5.0 to 5.5. The optimum conditions of β-mannanase enzymes are dependent on the source from which they are derived. This can be seen by the fact that bacterial β-mannanases prefer neutral to alkaline pH conditions, whilst fungal β-mannanases prefer more acidic conditions (Dawood and Ma, 2020).

The kinetic parameters are vital to understanding the behaviour of an enzyme, and how it functions with a given substrate (Soni et al., 2016). Regarding a β-mannanase from *Aspergillus terreus* it was established by Soni et al. (2016) that the $K_M$ and $V_{max}$ values were 5.9 mg/ml and 39.42 µmol/ml/min, respectively (Soni et al., 2016). Inhibitors of this enzyme included $Hg^{2+}$, $Zn^{2+}$, PMSF and EDTA, which prevented the hydrolysis of the (1,4)-β-D-mannosidic linkages. β-mercaptoethanol was found to enhance the activity of the β-mannanase, increasing the activity by 30% (Soni et al., 2016). It has been established that in a reaction with β-mannanase and a mannan-rich substrate, the enzyme requires a minimum of four mannose residues for hydrolysis to occur. This is due to the enzyme not being able to cleave the linkage between a mannobiose and/or a mannotriose (Soni et al., 2016). Evaluating the hydrolysis products of mannan-rich substrates with a variety of extracellular mannanases for various times

showed that mannanases derived from *Penicillium oxalicum* KUB-SN2-1 produced mainly mannobiose and mannotriose after 3 hours (Chantorn et al., 2013).

Industrially, β-mannanases have become of great importance used in several different industries such as oil extraction, fruit clarification, bioethanol production and the animal feed industry (Shastak et al., 2015; Sharma et al., 2018; Dawood and Ma, 2020). Within the poultry industry, β-mannanases have shown their importance by creating more valuable and nutritious agricultural feedstocks - with modes of action to decrease viscosity, increase metabolism, and improve the overall performance of birds (Shastak et al., 2015; Dawood and Ma, 2020). Literature has described the potential for β-mannanase enzymes to reduce the thickness of the ileal mucosal layer within the small intestine – a location characteristic for the proliferation of pathogenic bacteria. This results in the indirect reduction of pathogenic bacteria and an increase in overall gut health (Ayoola et al., 2015; Dawood and Ma, 2020).

Various strategies have been employed to improve the industrial applications of β-mannanases – with examples in bioengineering, genetic modification and immobilisation (Puri and Abraham, 2016; Dawood and Ma, 2020). The immobilisation of enzymes strives to overcome current limitations by increasing storage stability, activity, reusability and recovery of the biocatalyst (Puri and Abraham, 2016). This study investigated the immobilisation of an endo-1,4-β-mannanase to increase the reusability of the biocatalyst whilst improving its stability.

### 1.3.1 Immobilised β-mannanase

Enzyme immobilisation is the attachment of an enzyme to a stationary organic, inorganic, and/or insoluble material – forming a heterogenous enzyme system (Homaei et al., 2013). Immobilisation of a biocatalyst imitates the natural functioning of the enzyme *in vitro*, as most enzymes are attached to a cytoskeleton, membrane and/or an organelle structure (Homaei et al., 2013). Enzyme immobilisation, when used in large-scale processes, provides a cost-effective strategy to enhance an enzyme's thermal and operational stability, decrease product/substrate inhibition, and decrease the risk of product contamination with enzyme residues (Vaz and Filho, 2019; Alnadari et al., 2020; Arunrattanamook et al., 2020). Immobilisation strategies have gained increasing interest, as enzymes in industrial settings have been shown to be associated with high costs, instability, and high loading demands (Vaz and Filho, 2019; Verma et al., 2020).

Four major strategies exist for enzyme immobilisation on to a solid carrier: physical adsorption, entrapment in a matrix, covalent binding, and cross-linking (Homaei et al., 2013) – these have

been depicted visually in Figure 1.5. Physical adsorption is the attachment of an enzyme to a stationary molecule by weak attractive forces such as hydrogen bonds or Van der Waals forces (Homaei et al., 2013). With this technique, there is little effect on enzyme activity; however, potential leaching of the biocatalyst can occur (Rehm et al., 2016). Entrapment/encapsulation encases the enzyme in a gel, polymer, and/or fibre matrix (Rehm et al., 2016; Vaz and Filho, 2019). This technique typically preserves the original conformation of the enzyme; however, due to the pores of the matrix, can also be prone to biocatalyst leaching (Rehm et al., 2016). Cross-linking combines entrapment and covalent attachment, and functions to create enzyme-enzyme links as well as covalent attachment to a solid carrier. This technique is often facilitated with the help of a cross-linking agent such as glutaraldehyde (Blibech et al., 2011; Rehm et al., 2016; Vaz and Filho, 2019). Covalent binding is a method of immobilisation which uses the functional groups on both the stationary surface and the enzyme to allow for attachment. This attachment forms covalent bonds between the enzyme and the solid carrier (Homaei et al., 2013). This process can be assisted with help of a bi-functional agent such as glutaraldehyde – a solvent which facilitates the formation of robust inter- and intra-covalent bonds between the enzyme and the support (Reshmy et al., 2022). The formation of imine bonds between the free aldehydes of glutaraldehyde (-CHO) and amino groups ($-NH_2$) of the enzyme assists in the strong attachment of enzymes to a surface material – with minimal loss in enzyme activity (Collins et al., 2011; Klein et al., 2012; Morsy et al., 2019; Mohapatra et al., 2021; Sadaqat et al., 2022).

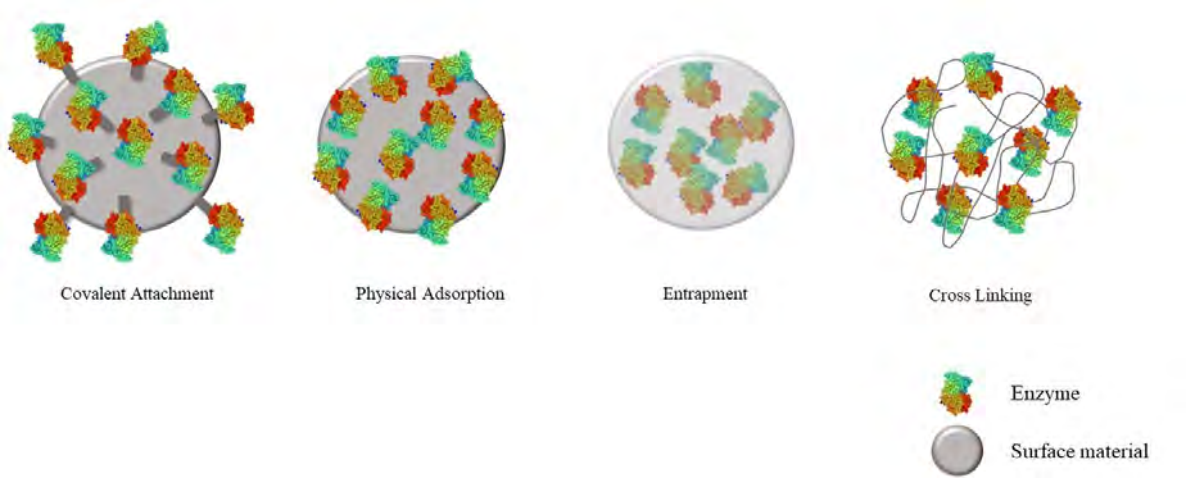


**Figure 1.5.** Visual representation of various immobilisation strategies. Adapted from Homaei et al. (2013), Rehm et al. (2016), and Reshmy et al. (2022).

There are disadvantages associated with the immobilisation of biocatalysts, with one disadvantage being a decrease in catalytic activity caused by a modification in the enzyme's structure (Arunrattanamook et al., 2020).

Various factors should be considered when selecting an appropriate surface for immobilisation – these include size, shape, surface chemistry, processibility, and accessibility (Rehm et al., 2016). Carrier dimensions can range from nano- to micro-, with nano-structured materials recently rapidly gaining more interest (Bilal et al., 2018; Nguyen et al., 2019). These particles range in dimension from 1 – 100 nm, synthesized from various methods such as milling, high-pressure homogenisation, and sonication (Divya and Jisha, 2018). Nanoparticles have a high surface area compared to micro- or macro- particles, facilitating a higher enzyme loading with immobilisation (Nguyen et al., 2019). Surface chemistry does not always facilitate binding directly; however, this can be improved by addition of a bifunctional agent, such as glutaraldehyde (Homaei et al., 2013; Nguyen et al., 2019). The choice of solid carrier for immobilisation is important; various supports include biopolymers, synthetic polymers, hydrogels, inorganic supports, magnetic particles, and cross-linked enzyme aggregates (CLEAs) (Homaei et al., 2013).

Chitosan is a biopolymer commonly employed to facilitate immobilisations. Chitosan has a diverse range of applications within immobilisation, being functional as an antimicrobial agent, copolymer, polymer coating, and immobilisation support (Zuluaga et al., 2012; Homaei et al., 2013; Bilal et al., 2018; Divya and Jisha, 2018). Chitosan is the N-acetyl derivative of chitin,

produced from the partial deacetylation of chitin. This modified biopolymer consists of alternating units of 1-4 linked 2-acetamido-2-deoxy-β-D-glucopyranose and 2-amino-2-deoxy-β-D-glucopyranose (Divya and Jisha, 2018), visualised in Figure 1.6.

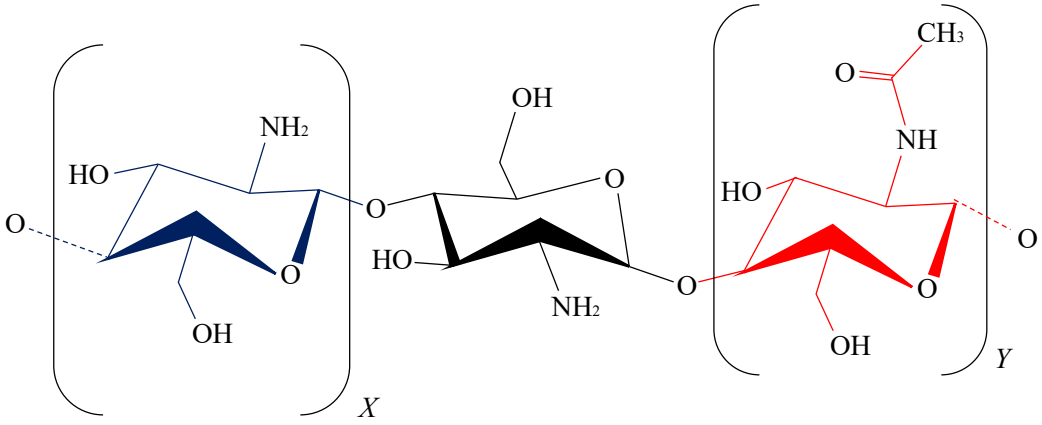


**Figure 1.6.** Chemical structure of chitosan showing the 1-4 linked 2-acetamido-2-deoxy-β-D-glucopyranose (*X*) and 2-amino-2-deoxy-β-D-glucopyranose (*Y*) rings (Divya and Jisha, 2018).

Chitosan has shown great potential as an antimicrobial agent, elongating the shelf life of immobilised enzymes by its natural antibacterial activity (Raafat and Sahl, 2009; Divya and Jisha, 2018; Shoaib and Zhouping, 2020). Major mechanisms of action promoting antimicrobial activity focus on ionic interactions with bacterial surface molecules, penetration of the microbial cell membrane and inhibition of protein synthesis, and chelation of essential metal ions needed for microbial growth (Raafat and Sahl, 2009; Younes and Marguerite, 2015; Shoaib and Zhouping, 2020). Chitosan's application as a copolymer, when used in combination with alginate, reduces stress on peptides and proteins – increasing the enzyme's stability during immobilisation (Homaei et al., 2013). Chitosan is commonly used as a polymer coating for magnetic particles. These carriers tend to aggregate with chitosan, weakening the magnetic and Van der Waals interactions, resulting in steric repulsion and preventing the clumping and direct immobilisation of enzymes onto metal surfaces (Bilal et al., 2018; Nguyen et al., 2019). Chitosan has shown its value in the immobilisation process by its resistance to chemical degradation, its amino functional groups which provide optimal enzyme attachment sites and its ability to be enhanced with the use of chemical treatments and bifunctional reagents (Silva et al., 2015, Divya and Jisha, 2018; Nguyen et al., 2018).

A major goal of this study is to immobilise an endo-1,4-β-mannanase derived from *A. niger* onto a solid support. This should promote enzyme recovery and reusability, reducing the cost of the reaction with the immobilised biocatalyst. Strategies which focus on the use of chitosan nanoparticles and chitosan-coated magnetic nanoparticles were also evaluated (Bilal et al., 2018).

### 1.4 Mannooligosaccharides

Mannooligosaccharides (MOS) are a by-product of the chemical or enzymatic hydrolysis of a mannan-rich substrate such as the galactomannan portion present in hemicellulose (Jana et al., 2021). MOS are short chain oligosaccharides consisting of repeating mannose moieties, linked by β-1,4-glycosidic bonds (Jana et al., 2021). The MOS residues of galactomannan are composed of D-mannopyranosyl residues linked by a β-1,4-glycosidic bond with a single 1,6-linked α-D-galactopyranosyl group positioned along the chain (Jana et al., 2021; Zhang et al., 2021). These chains can be further classified into α-/β-MOS, determined by the position of the hydroxyl group on the first carbon of the pyranose ring – as displayed in Figure 1.7 (Jana et al., 2021). α-/β-M S are differentiated by the glycosidic linkage, with α-MOS derived from the α-1,6-linkage present in the cell wall of yeast and β-MOS derived from the hydrolysis of a β-1,4-linkage present in plant mannans such as LBG and SBM (Jana et al., 2021).

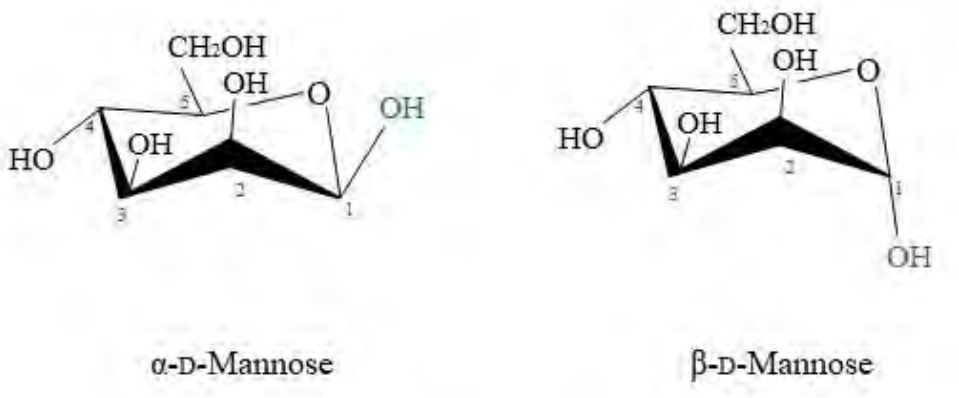


**Figure 1.7.** Chemical structure of α-D-Mannose and β-D-Mannose from LBG.

The varying length of the M S chains results from β-mannanase randomly cleaving the β-1,4-glycosidic bonds in the mannan backbone (Malgas et al., 2015a; Malgas et al., 2015b; Sharma et al., 2018; Jana et al., 2021). These chains can contain 1-10 mannose residues – with this study focusing on the first six: mannose (M1), mannobiose (M2), mannotriose (M3), mannotetraose (M4), mannopentaose (M5), and mannohexaose (M6) – as can be seen in Figure

1.8. MOS has been frequently employed in poultry feed formulations as an AGP – due to its benefits in altering populations of pathogenic bacteria whilst improving nutrient utilisation (Kocher et al., 2004; Chacher et al., 2017; Dawood and Ma, 2020; Tiwari et al., 2020). Chains of MOS can be defined as linear homomannans or heteromannans – with differences being based on whether sugars other than mannose are present within the structure (Kango et al., 2022). The various distribution of sugars other than mannose, such as glucose, galactose, and xylose to form a heteromannan structure will effect the oligosaccharide produced, this being affected by the branches of sugars present on the mannan backbone after hydrolysis (Kango et al., 2022).

MOS is frequently used in agriculture for monogastric organisms as a prebiotic fibre to enhance growth and nutrient uptake in monogastric organisms such as poultry (Shastak et al., 2015; Chacher et al., 2017; Saeed et al., 2017; Dawood and Ma, 2020; Jana et al., 2021). As stated by a las and Nochta (2012), "a prebiotic is a specialised plant fibre that makes up the non-digestible components of food that stimulate the growth and/or activity of beneficial bacteria in the digestive system and promotes the gut and general health of the host organism". M S can be classified as both a simple sugar and a polysaccharide, with a tendency to behave like both a dietary fibre and prebiotic (Tiwari et al., 2020).

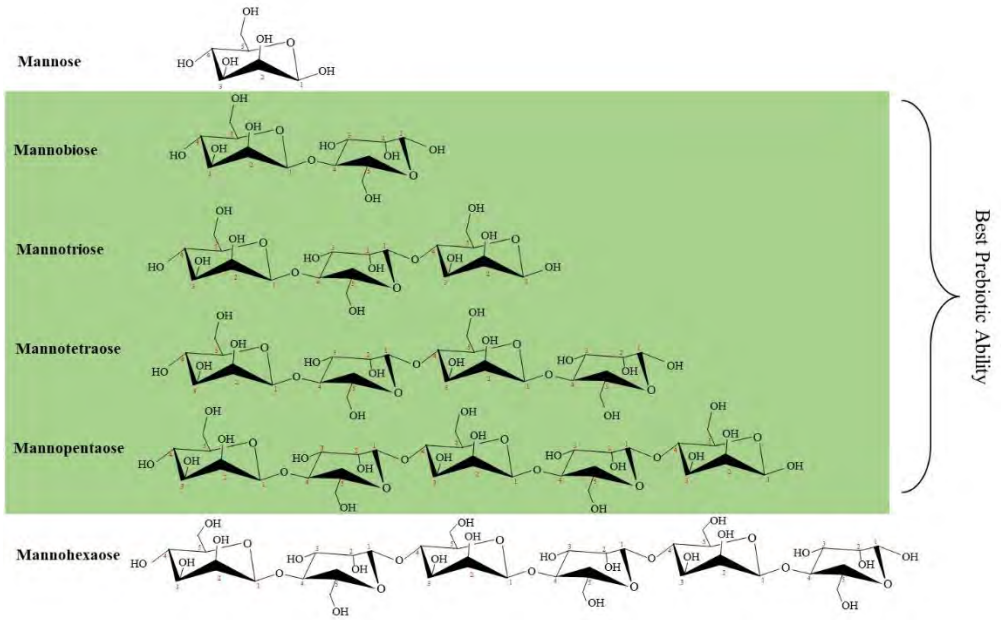


**Figure 1.8.** Diagram showing the chemical structure of M1 – M6.

Prebiotics such as MOS stimulate the accumulation of probiotics, live microorganisms, or microbial feed supplements, which improve intestinal microbial balance (Hazrati et al., 2019). The large influence of bacterial colonisation is due to the requirements needed for optimal growth, which are commonly pH, nutrient availability and the effect of host enzymes and digestive juices (Kamada et al., 2013; Pan and Yu, 2014). It is common for bacteria to reside in colonies with various strains – acquiring nutrients from complex ecological networks (Kamada et al., 2013; Pan and Yu, 2014). From the various DP lengths of MOS residues, it has been established that M2 has the best prebiotic potential. However, MOS residues of M2 – M5 have all been shown to play an active role as prebiotics – stimulating probiotics such as Lactobacillus and inhibiting pathogenic bacteria such as Salmonella (Srivastava and Kapoor, 2017; Tiwari et al., 2020; Zhang et al., 2021).

M S are not susceptible to breakdown by the host's enzymes or immune system and, therefore, can have no nutritional benefit (Saeed et al., 2017; Kim et al., 2019). M S's success as a prebiotic compound is defined by the capability for probiotics to utilise it as a nutritional source – breaking it down into beneficial compounds which can help prevent disease and colonisation of pathogenic bacteria (Kango et al., 2022). *Bacillus subtilis* contains a polysaccharide utilisation locus (PUL) encoding for three factors contributing to the uptake and utilisation of mannose towards glycolysis – these include a transcriptional factor, a phosphotransferase-system (PTS) mannose-specific enzyme and mannose-6-phosphatase (Dai et al., 2016; Suhaibani et al., 2021). Within the study of transcription analysis of *Streptococcus mutans,* it was observed that an operon (SMU.1956 to -1961) within the phosphoenolpyruvate-sugar PTS, was observed to contain inducible fructose and mannose sugar-specific multiprotein permeases ($EII^{Fru/Man}$) - which are transcribed in the presence of mannose (Ajdić et al., 2007; Morsy et al., 2019). The presence of mannose is, therefore, hypothesised to induce the production of $EII^{Fru/Man}$ in both the cytoplasm (EIIA and EIIB) and the membrane channel (EIIC). Mannose was observed to stimulate a response up to 37-fold higher than mannitol-grown cells (Ajdić et al., 2007; Morsy et al., 2019). The *Streptococcus aureus* strain was able to utilise MOS residues produced from the hydrolysis of SBM, with Morsy et al. (2019) supporting the results for *Streptococcus* species that have the capacity to utilise mannose. According to the literature, *Lactobacillus* species such as *Lactobacillus casei* possess the capability for mannose/fructose metabolism, a process regulated by the gene LSEI_0681 (Licandro-Seraut et al., 2014). The inhibition of mono-oligosaccharide utilisation will, however, occur within a nutrient-deficient

environment – resulting in the downregulation of LSEI_0681 (Kumar et al., 2012; Licandro-Seraut et al., 2014).

When referring to the probiotic bacteria: *Streptococcus*, *Bacillus*, and *Lactobacillus* – each maintains the capability to digest prebiotic MOS. Kango et al. (2022) state that the short-chain fatty acids and branched-chain amino acids produced are "disease-preventing." This raises the important question of whether MOS prebiotics and their probiotic digestion by-products can serve as an alternative to antibiotics. Antimicrobials from probiotic digestion can be classified as lactic acid, acetic acid, acetaldehyde, bacteriocins, bacteriocin-like compounds, and many others (Šušković et al., 2010). Bacteriocins are secondary metabolites commonly produced by bacteria, with a functionality debated to assist in the colonisation of the host bacteria, whilst also assisting in decreasing competition and host signalling via quorum sensing (Dobson et al., 2012). These peptides are produced ribosomally to supply protection according to the manufacturing bacteria's immunity (Šušković et al., 2010; Dobson et al., 2012). These antimicrobial compounds are commonly used by probiotics to compete with complex bacterial communities in the gastrointestinal tract – allowing a bacterial strain to amalgamate into a host's gut microbiome. *Lactobacillus* has been shown to possess antimicrobial activity – not only for its inhibition of pathogenic adhesion to cell walls and stimulation of the immune system, but also for its production of bacteriocin-like molecules (Jamalifar et al., 2011). Literature has also shown the presence of bacteriocins among *Bacillus* and *Staphylococcus* strains – indicating the potential for inhibition of pathogenic strains (Joseph et al., 2013).

This study focuses on the immobilisation of an endo-1,4-β-mannanase derived *A. niger* – with the goal to decrease production costs whilst enhancing enzyme stability, thermostability, and recyclability both in the presence of a simple soluble substrate and a complex insoluble substrate. Enzyme immobilisation is commonly employed to enhance an enzyme's capabilities. In addition, the study investigated the hydrolysis of ANFs in SBM – to break down the mannans detrimental to poultry health and replace these with prebiotic MOS.

### 1.5 Problem statement and justification for the study

Intensive poultry farming is becoming increasingly at risk due to the consistent use of Antibiotic Growth Promoters (AGPs) within the agricultural sector (Nkukwana, 2018; Arunrattanamook et al., 2020; Hedman et al., 2020). The rise of antibiotic-resistant organisms threatens the sustainable production of poultry, as well as consumers who require a healthy source of low-cost animal protein (Van der Poel et al., 2020). The Netherlands, the United

Kingdom and many more have banned the use of AGPs in poultry farming – seeking alternatives with a similar effect (Manyi-Loh, 2015). Antibiotic resistance is an ever-growing problem, influenced largely by the intensive use of antibiotics within the agricultural sector (Manyi-Loh, 2015; Arunrattanamook et al., 2020). Without alleviating the current stresses on the environment, the growth of antibiotic resistance is inevitable – with the capacity to threaten both the economic and health sectors (Abushaheen et al., 2020).

This study investigated the potential of enhancing the natural capabilities of poultry feed by using immobilised exogenous enzymes, seeking a cheap and accessible alternative to AGPs. The reusable enzyme employed also hydrolysed the ANFs of SBM, converting mannans detrimental to poultry health into beneficial prebiotics, MOS. MOS are classified as prebiotic compounds, which benefit the growth of probiotic flora within the gastrointestinal tract. The SBM-derived MOS function as a nutrient-rich food for the gastrointestinal tract's microbiome, which, in turn, alleviates the threat of colonisation by pathogenic bacteria while increasing nutrient availability and the overall health of poultry.

Linking AGPs and MOS, the use of AGPs has been shown to mitigate the adverse effects of ANFs in feed. However, the rise in antibiotic resistance has prompted the search for alternative strategies. By immobilising endo-1,4-β-mannanase onto solid matrices, the study aims to produce MOS from SBM hydrolysis effectively. These MOS not only replace AGPs by promoting probiotic growth and inhibiting pathogenic bacteria but also address the critical issue of antibiotic resistance in agriculture.

## 1.6 Research hypothesis, aims, and objectives

### 1.6.1 Hypothesis

The immobilisation of an *A. niger* Man26A will allow the repeated production of MOS from SBM with a consistent yield of MOS for each cycle compared to the use of the free enzyme.

### 1.6.2 Aims

The aim of the proposed project was to investigate the immobilisation of β-mannanases by a covalent reaction with glutaraldehyde-activated chitosan nanoparticles and glutaraldehyde-chitosan-coated magnetic $Fe_3O_4$ nanoparticles and to assess whether the immobilised enzyme will repeatedly produce a consistent MOS yield - when compared to a single dose of the free enzyme. A second aim of the project was to evaluate the prebiotic effect of MOS obtained from the hydrolysis of SBM with the immobilised enzyme.

### 1.6.3 Objectives

To achieve the above aims, the following objectives were addressed:

a) To immobilise β-mannanase on glutaraldehyde-activated chitosan-coated magnetic $Fe_3O_4$ nanoparticles and glutaraldehyde-activated chitosan nanoparticles;

b) To perform biochemical characterisation of the immobilised and free enzymes;

c) To evaluate the reusability (recyclability) of the immobilised β-mannanases;

d) To analyse the MOS obtained from the enzymatic hydrolysis of a mannan-rich substrate with free and immobilised enzymes;

e) To evaluate the effect of prebiotic MOS on probiotic bacteria.

## 1.7 Thesis Outline

The basic outline of this thesis concentrated initially on a general introduction (Chapter 1), progressing on to chapters on enzyme immobilisation (Chapter 2) and SBM hydrolysis (Chapter 3). Chapter 2 primarily focused on the strategies of immobilisation, validation of immobilisation, and characterisation of the various enzymes and their solid carriers. With optimised conditions and assurance of immobilisation with adequate activity yields (%), the immobilised enzymes were then tested against a more complex substrate, SBM. This analysis is presented in Chapter 3 – analysing the efficacy of hydrolysis and the various hydrolysis products. In this chapter, a prebiotic evaluation is completed, validating the SBM-produced sugars used as prebiotics within the poultry industry. The general discussion (Chapter 4) concluded this thesis - by summarising and discussing the overall findings of the study.

# CHAPTER 2: IMMOBILISATION OF AN ENDO-1,4-β-MANNANASE DERIVED FROM *ASPERGILLUS NIGER* FOR THE EFFECTIVE PRODUCTION OF MANNOOLIGOSACCHARIDES

## 2.1 Introduction

The immobilisation of enzymes is constantly employed to reduce operational costs and increase the stability of enzymes used industrially. There are various strategies of immobilisation, each with a varied effect on enzyme activity and reusability (Vaz and Filho, 2019; Alnadari et al., 2020; Arunrattanamook et al., 2020). These strategies include physical adsorption, entrapment in a matrix, cross-linking and covalent binding (Homaei et al., 2013). The covalent attachment of enzymes to solid carriers has shown potential, with evidence of high recyclability and enzyme activity (Homaei et al., 2013). Chitosan nanoparticles are ideal solid carriers for immobilisation, as they provide several advantages, such as a high surface area to volume ratio, facilitating high enzyme loading, as well as possessing various antimicrobial benefits (Raafat and Sahl, 2009; Thamilarasan et al., 2018; Divya and Jisha, 2018; Shoaib and Zhouping, 2020).

The immobilisation onto chitosan particles was attempted using two varying strategies. The first procedure used an initial preparation step of the chitosan by sonication and activation by glutaraldehyde to form glutaraldehyde-activated chitosan nanoparticles, subsequently referred to in this study as A-CTS. These particles were then washed and an endo-1,4-β-mannanase was immobilised via a covalent attachment - these were referred to as CTS – with the goal of being employed for reusable enzymatic hydrolysis. A second immobilisation approach used in this study looked at $Fe_3O_4$ nanoparticles, subsequently referred to as MAGS. To enable a similar process as described above, the MAGS were coated with chitosan, henceforth referred to as MAGS-chitosan. These newly formed particles were then activated via glutaraldehyde to form glutaraldehyde-activated chitosan-coated $Fe_3O_4$ nanoparticles, referred to as MAGS-A-CTS. The final step of this procedure was to wash the MAGS-A-CTS and complete an enzyme immobilisation step for the final product of enzyme immobilisation, chitosan coated $Fe_3O_4$ nanoparticles, designated as MAGS-CTS in this study. This procedure, in theory, therefore supports the easy recovery of the immobilised enzyme using an external magnet, which is a particularly desirable trait when hydrolysing insoluble substrates.

The activation of the chitosan was performed with a bi-functional agent known as glutaraldehyde, which binds the free aldehyde groups (CH=O) to the exposed amine ($NH_2$) groups of chitosan by an imine bond otherwise referred to as a Shiff's base formation (Collins et al., 2011; Klein et al., 2012; Gűr et al., 2018; Reshmy et al., 2022). This, in turn, revealed a free aldehyde group (CH=O) which could facilitate the covalent attachment of the enzyme's free amine groups ($NH_2$) by an imine bond formation (C=N) (Belowicha et al., 2012; Ciaccia et al., 2013; Morsy, et al, 2019). Two strategies of covalent attachment were employed within this study, both immobilisations were facilitated by glutaraldehyde activation, although one occured on plain chitosan nanoparticles, while the other was immobilised on $Fe_3O_4$ coated chitosan nanoparticles (Saravanakumar et al., 2014; Mohapatra, 2021).

Evaluation of enzyme immobilisation may be performed in many ways; common strategies include Fourier-transform infrared spectroscopy (FTIR) and X-ray powder diffraction (XRD). FTIR analyses the various surfaces obtained throughout the immobilisation procedure to investigate the change in surface adsorption of functional groups due to glutaraldehyde activation and enzyme immobilisation (Mohapatra, 2021; Sadaqat et al., 2022). This is a strategy commonly employed to confirm the addition of the enzyme to the solid carrier (Collins et al., 2011; Klein et al., 2012; Mahamed et al., 2013; Baroudi et al., 2018). XRD focuses specifically on the change in crystalline structure which can occur with immobilisation. Characteristic crystalline structures for chitosan at $2\theta = 10°$ and 20° should be observed (Kumar et al., 2012; Morsy et al., 2019; Galan et al., 2021) as well as a determination of the iron oxide phase (Hoa et al., 2009; Waifalkar et al., 2016; Gãmez et al., 2020). This investigates how the structure has changed, confirms the particle size, and confirms that the immobilisation was successful (Li et al., 2013; Garnica-Palafox et al., 2016; Sadaqat et al., 2022).

An effective immobilisation is one with high immobilisation yields (%) and high activity yields (%), when compared to the specific activity of the free enzyme (Saravanakumar et al., 2014; Mohapatra, 2021). The immobilisation yields (%) represent the quantity of protein immobilised onto the solid carrier relative to the total protein added during the immobilisation procedure. This was tested alongside activity yields (%), which showed the specific activity of the immobilised enzyme relative to the specific activity of the free enzyme (Blibech et al., 2011). This was established to assess the success of the immobilisation procedure, in terms of the quantity of enzyme being utilised within a reaction, as well as in terms of the ability of the immobilised enzyme to catalyse its reaction.

To efficiently validate the functionality of the immobilised enzymes compared to the free enzyme, as well as determine the optimum conditions for hydrolysis – the physicochemical characteristics of the immobilised enzyme should be established. Industrially used enzymes benefit from high reaction temperatures, low pH conditions, and short reaction times of the biocatalyst; these conditions lower the potential for microbial contamination, making them more favourable for industrial use (Liao et al., 2014). An important characteristic of the industrial use of enzymes, specifically for immobilised enzymes, is good thermostability and storage stability (Nigam, 2013). Thermostability is a principal aspect of enzyme immobilisation, describing the potential for long-term use after consecutive reactions at the optimum temperature (Guzik et al., 2014). Kinetic parameters are key factors for the use of enzymes in the food and agricultural industry, and these are commonly obtained using Michaelis-Menten kinetics (Choi et al., 2017). Kinetic parameters provide an accurate estimation of a biocatalyst's ability to convert substrate to product under optimum conditions (Galanakis et al., 2015). After enzyme immobilisation, a change in enzyme confirmation can occur, which can affect the catalytic abilities of the biocatalyst – comparing the kinetic capabilities of the free endo-1,4-β-mannanase versus the immobilised endo-1,4-β-mannanase should allow for an unbiased interpretation of whether the immobilised enzyme is efficient as a catalyst – and whether it would be preferred for industrial use over the free enzyme. The kinetic analysis of enzymes regarding Michaelis-Menten kinetics provides key data on $K_M$, $V_{max}$, $k_{cat}$, and $k_{cat}/K_M$, assigning values to substrate affinity, maximal reaction rate and catalytic efficiency of an enzyme (Galanakis et al., 2015; Bäuerle et al., 2017).

Visualisation of MOS products is an important aspect of comparing free and immobilised enzymes, ensuring that the immobilisation has not affected the enzyme's ability to randomly cleave the β-1,4-glycosidic linkages in the galactomannan backbone of the substrate (LBG). This can be determined in various ways, either by thin-layer chromatography (TLC) or by high-performance liquid chromatography (HPLC). TLC analysis is a qualitative analysis used to visualise components in a liquid, in this case, the hydrolysis products of LBG (Bele and Khale, 2011). This test is relatively quick and inexpensive, allowing for the identification of MOS products relative to the ($R_f$ values of) MOS standards: mannose (M1), mannobiose (M2), mannotriose (M3), mannotetraose (M4), mannopentaose (M5), mannohexaose (M6). TLC functions via the capillary action of a stationary and mobile phase, moving compounds of interest up the plate, with their migration distance depending on their molecular structure (Coskun, 2016). Regarding MOS, different-sized MOS will migrate at various rates – with

smaller molecules moving faster up the plate with the mobile phase. These compounds can then be identified after visualisation of the plate (Bele and Khale, 2011).

HPLC Refractive Index Detectors (HPLC-RID) are used to detect substances with no UV absorption, such as oligosaccharides (Swartz, 2010). HPLC-RID analysis compares the refractive light of a cell containing an analyte of interest compared to that of a reference cell – when a difference is picked up in the two cells, a peak is produced, providing evidence of a component in solution (Swartz, 2010). By comparing peak area and time, standard curves can be created to quantify components in a liquid. This gives both a qualitative and quantitative result as to how much of a given oligosaccharide there is in the solution.

The focus of this chapter is on the immobilisation of an endo-1,4-β-mannanase onto CTS and MAGS-CTS, with characterisation, optimisations and activity yields being determined with a model substrate – LBG. LBG is a soluble substrate and a source of galactomannans; the random cleavage of the β-1,4-glycosidic linkages present within LBG structure produces MOS; the desired product after hydrolysis of SBM (Liao et al., 2014; Phiwphech et al., 2019). LBG is well characterised as a substrate for the enzymatic hydrolysis by an endo-1,4-β-mannanase, with a galactose:mannose ratio of 1:4, and therefore, testing the efficiency of the free and immobilised enzymes can be conducted relatively effectively (Kashef et al., 2008; Malgas et al., 2015b; Surywanshi and Kango, 2021).

## 2.2 Hypothesis, aims and objectives

### 2.2.1 Hypothesis

Endo-1,4-β-mannanase derived from *A. niger* will be successfully immobilised onto the surface of glutaraldehyde-activated chitosan nanoparticles and chitosan-coated magnetic nanoparticles – allowing for the recyclable hydrolysis of LBG, the model substrate. The immobilised enzyme will outperform the free enzyme in terms of recyclability and physicochemical characteristics with no effect on the hydrolysis products themselves.

### 2.2.2 Aims

The aims of the project were to investigate the immobilisation of a β-mannanase by a covalent reaction with glutaraldehyde-activated chitosan nanoparticles and chitosan-coated magnetic nanoparticles and to test whether the immobilisation would affect the hydrolytic efficiencies of the enzymes to produce MOS.

### 2.2.3 Objectives

To achieve these aims, the following objectives were addressed:

a) To determine the specific activity of the free β-mannanase;
b) To immobilise the β-mannanase;
c) To compare the physicochemical properties of the immobilised and the free β-mannanase;
d) To analyse the recyclability of the immobilised enzyme;
e) To analyse the M S obtained from the enzymatic hydrolysis of β-mannan from LBG (in terms of MOS species diversity and composition).

## 2.3 Methods and Materials

### 2.3.1 Materials

Mannobiose, mannotriose, mannotetraose, mannopentaose, mannohexaose, galactosyl-mannotriose, di-galactosyl-mannopentaose, and endo-1,4-β-mannanase derived from *Aspergillus niger* were purchased from Megazyme (Bray, Wicklow, Ireland). The silica gel 60 $F_{254}$ thin-layer chromatography plates were purchased from Merck (Darmstadt, Hesse, Germany). The Carbosep CHO 411 HPLC column was purchased from Concise Separations (San Jose, CA, USA). All other chemicals used were of reagent grade and were purchased from Sigma Aldrich (St. Louis, MO, USA).

### 2.3.2 Determination of enzyme activity and protein concentration

#### 2.3.2.1 Protein concentration determination

A Bradford's assay was used to determine the protein concentration of endo-1,4-β-mannanase, by Bradford (1976). A standard curve was produced using bovine serum albumin (BSA) as a standard (0 – 2 mg/ml) as described by Blibech et al. (2011)(Appendices, Figure I). The BSA/unknown protein samples were combined with Bradford's working reagent in a 1:9.2 ratio, respectively. The readings were taken after 10 minutes on a Synergy MX microplate reader (BioTek, Winooski, USA) at a wavelength of 595 nm.

#### 2.3.2.2 Determination of reducing sugar concentration

The endo-1,4-β-mannanase activity was assayed by quantitatively measuring the amount of reducing sugars released after hydrolysis using the 3,5-dinitrosalicylic acid (DNS) method as described previously by Miller (1959), with slight modification. DNS reagent [1% (w/v) NaOH, 1% (w/v) 3,5-dinitro salicylic acid, 20% (w/v) potassium sodium tartrate tetrahydrate,

0.2% (w/v) phenol, and 0.05% (w/v) sodium metabisulphite] was combined with the reducing sugar sample in a 2:1 ratio. The samples were then incubated at 100°C for 6 minutes. The absorbance at 540 nm was read on a Synergy MX microplate reader (BioTek, Winooski, USA). A standard curve was prepared using mannose as a suitable standard (0.05 – 1 mg/ml)(Appendices, Figure H).

#### 2.3.2.3. Endo-1,4-β-mannanase activity assay

The activity of endo-1,4-β-mannanase was determined with the use of 0.5% (w/v) LBG, dissolved in 50 mM citrate buffer (pH 5.0), as described previously by Malgas et al. (2015b). The reaction was allowed to proceed at 55°C for 30 minutes. The enzymatic activity was terminated by incubation at 100°C for 5 minutes, followed by centrifugation at 16 060 ×*g* for 5 minutes. The enzyme activity was determined by measuring the amount of reducing sugars produced (according to section 2.3.2.2). One unit of enzyme activity was defined as the amount of enzyme that released 1 μmol of reducing sugars per minute under the assay conditions specified. All assays were performed in triplicate within a single trial, and the process was repeated. Values were reported as means ± standard deviations.

#### 2.3.2.4 Optimisation of enzyme loading for locust bean gum hydrolysis

The optimum enzyme loading for endo-1,4-β-mannanase was established at concentrations ranging from 0.0025 – 0.06 mg/ml. This was performed according to the previously stated method in section 2.3.2.3.

### 2.3.3 Immobilisation of endo-1,4-β-mannanase

#### 2.3.3.1 Enzyme immobilisation onto chitosan (CTS)

Glutaraldehyde activated chitosan nanoparticles were produced according to the method described by Mohapatra, (2021), with slight modification. Chitosan [0.25% (w/v)] was dissolved in 0.35 M acetic acid, 50 mM citrate buffer (pH 5.0), and 1% (v/v) Tween 80 and the mixture was stirred for 20 minutes at 30°C, with agitation at 150 rpm (B JPX-2008, Biobase, Shandong, China). Under sonication, using a Vibra-Cell™ (20 kHz at an amplification of 60), 1.4 M sodium sulphate solution was added dropwise and mixed with a magnetic stirrer (2 hours, 500 rpm). Particles were then collected via centrifugation using an 1.0R Megafuge (Heraeus Holding GmbH, Osterode, Germany) (3500 × *g*, 15 minutes, 4°C) and washed with deionised water (3500 ×*g*, 15 minutes, 4°C). The particles were activated under agitation by the addition of 1.25% (v/v) glutaraldehyde in 50 mM citrate buffer (pH 5.0) (30°C, 45 minutes). The activated chitosan nanoparticles were washed several times to remove excess glutaraldehyde

(3500 × *g*, 10 minutes, 4°C). The washed activated nanoparticles were then incubated (36 hours, 4°C) with a 0.1 mg/ml enzyme solution of endo-1,4-β-mannanase derived from *A. niger*. After incubation, the immobilised enzyme was washed several times. Washing was completed by combining the immobilised enzyme with buffer and then centrifuging (3500 × *g*, 10 minutes, 4°C) the sample. Each wash was assayed for protein concentration (section 2.3.2.1) and enzyme activity (section 2.3.2.3) to assist in the calculation of the immobilisation yield (section 2.3.3). The immobilised enzyme was stored at 4°C until further use.

#### 2.3.3.2 Enzyme immobilisation onto MAGS-CTS

This procedure was completed according to the method previously described by Saravanakumar et al. (2014) with slight alterations to the method of Nguyen, et. al. (2019) and Jonović et. al. (2022). Magnetic $Fe_3O_4$ was prepared by the co-precipitation of $Fe^{2+}$ and $Fe^{3+}$ ions.

##### 2.3.3.2.1 Preparation of magnetic $Fe_3O_4$ nanoparticles (MAGS)

Solutions of ferrous and ferric ions were prepared in a 1:1.029 ratio in 100 ml of deionised water. A 28% (v/v) ammonium hydroxide solution was added dropwise to the mixture and allowed to mix using a magnetic stirrer for 30 minutes. The solution was adjusted to pH 10 with 10 mM NaOH. The mixture was then heated to 80°C, for 30 minutes, in a water bath. The particles were allowed to cool to room temperature with stirring. Once cooled, the particles were collected with a permanent magnet and washed several times with deionised water.

##### 2.3.3.2.2 Preparation of chitosan-coated magnetic $Fe_3O_4$ nanoparticles (MAGS-chitosan)

To prepare the MAGS-chitosan nanoparticles, 1 g of chitosan was suspended in 100 ml of 1% (v/v) acetic acid. The chitosan, now in a soluble form, was combined with 25 ml of 1 mg/ml sodium tripolyphosphate (TPP). This solution was incubated for 10 minutes at 25°C, with shaking. The washed MAGS were then combined with the chitosan solution and stirred vigorously for 30 minutes. To precipitate the MAGS-chitosan out of solution, 25 ml of 1 M NaOH was added slowly into the solution under sonication. The particles were then washed with deionised water until a pH 7.0 was reached.

##### 2.3.3.2.3 Activation and immobilisation of MAGS-CTS

The newly formed MAGS-chitosan nanoparticles were activated by the addition of 1.25% (v/v) glutaraldehyde and incubation at 25°C for 12 hours. The newly formed glutaraldehyde-activated chitosan-coated Fe3O4 nanoparticles (MAGS-A-CTS) were then washed several times with deionised water. A 0.05 mg/ml enzyme solution was prepared with endo-1,4-β-

mannanase derived from *A. niger*. The enzyme solution was then added to the washed MAGS-A-CTS and left to incubate for 1 hour at 4°C.

### 2.3.3.3 Determination of immobilisation and activity yield (%)

The immobilisation yield (%) was determined by testing the protein concentration of the washes after immobilisation (sections 2.3.3.1 and 2.3.3.2), according to section 2.3.2.1. The activity yield (%) was determined by testing the enzyme activity of each immobilised enzyme, according to section 2.3.2.3, with slight modification. The CTS-immobilised particles were separated from the solution by centrifugation at 16060 $\times g$ for 5 minutes, and the MAGS-CTS immobilised particles were separated from the solution with the use of a permanent magnet.

The immobilisation yield was expressed as described previously by Blibech et al. (2011):

$$Immobilisation\ yield\ (\%) = \left(\frac{A-B}{A}\right) \times 100 \quad (1)$$

Where (A) is the quantity of enzyme loaded for the immobilisation procedure (mg), (B) is the unbound protein after immobilisation (mg), and (A-B) is the theoretical immobilised enzyme.

The activity yield was defined according to the following expression:

$$Activity\ yield\ (\%) = \frac{Total\ Activity\ of\ the\ Immobilised\ Enzyme}{Total\ Activity\ of\ the\ Free\ Enzyme} \times 100 \quad (2)$$

### 2.3.3.4 Optimisation of enzyme immobilisation procedure for CTS and MAGS-CTS

The following optimisation conditions were performed for the CTS (section 2.3.3.1) and MAGS-CTS (section 2.3.3.2) immobilisation procedures, regarding glutaraldehyde concentration, enzyme concentration and the duration (time) of the enzyme immobilisation. This was done to establish the optimal conditions under which the mannanase enzyme would bind and immobilise to the A-CTS and MAGS-A-CTS. The following parameters were optimised: optimum glutaraldehyde concentration (0 – 25% v/v), optimum enzyme loading concentration (0 – 0.1 mg/ml), and optimum enzyme incubation time with the activated carrier (0 – 12 hours).

### 2.3.3.5 FTIR analysis

A spectrum 100 FTIR system (Perkin Elmer, Wellesley, MA, USA) was used to characterise the chitosan, A-CTS, CTS, MAGS, MAGS-chitosan, MAGS-A-CTS, and MAGS-CTS. Each

sample dried (using critical point drying) was pressed uniformly against the sample spotting surface using a spring-loaded anvil. FTIR spectra were obtained from scans (32 per sample) ranging from 4000 to 600 $cm^{-1}$. Baseline and ATR corrections for penetration depth and frequency variations were carried out using Spectrum™ One software supplied with the equipment.

#### 2.3.3.6 XRD Analysis

Samples of chitosan, A-CTS, CTS, MAGS, MAGS-chitosan, MAGS-A-CTS, and MAGS-CTS were analysed via an X-ray diffractometer (XRD) (Bruker D2 Phaser, Karlsruhe, Germany). This was performed with a LYNXEYE XE-T detector using Cu radiation (wavelength λ = 0.154 A°) at a voltage of 30 kV on a current of 10 mA. The samples were scanned from 2θ of 5 to 60° with a step size of 0.02°. The determination time was 0.02° per second.

The crystalline size was determined for each of the particles according to Scherrer's equation, as expressed below:

$$D = \frac{K\lambda}{\beta Cos\theta} \quad (3)$$

*D* represents the crystallite size (nm); *K* represents the Scherrer constant, the shape factor of the particle, set at 0.9 ; λ represents the radiation wavelength; β represents the full width at half maximum (FWHM) of the diffraction peak; and θ represents the Bragg's angle in degrees, half of 2θ.

#### 2.3.3.7 SEM Analysis

Scanning Electron Microscopy (SEM) was employed to examine the surface morphology and structural details of the samples at high resolution. A-CTS and CTS were prepared according to section 2.3.3.1. The samples were then pre-treated with 2.5% (v/v) glutaraldehyde in 50 mM sodium phosphate buffer (pH 7.4) for 24 hours. The samples were then treated with a series of ethanol concentrations, each for 5 minutes (30%, 50%, 60%, 70%, 80%, 100%) and dried by critical point drying, using carbon dioxide. Samples were loaded onto a 1 x 1 cm conductive carbon adhesive tape and then onto an SEM specimen mount. The samples were then coated with gold and examined under vacuum using a SEM Tescan VEGA3 (Tescan Orsay Holding, Brno, The Czech Republic).

#### 2.3.3.8 Visual representation of MAGS-CTS magnetism

Visual representations of the MAGS-CTS particles separated from a solution of 50 mM citrate buffer (pH 5.0) with a permanent magnet were obtained using an iPhone 6 (Apple, California, U.S.) camera. A video was taken for 1 minute and 15 seconds at 25°C, where images were captured every 15 seconds.

### 2.3.4 Recyclability of immobilised endo-1,4-β-mannanase with LBG

Immobilised endo-1,4-β-mannanase was resuspended in 50 mM citrate buffer (pH 5.0). A reaction was then performed according to section 2.3.2.3., with slight modification. At the end of the reaction, the immobilised mannanase was not heated to 100°C but rather rinsed thrice with 50 mM citrate buffer (pH 5.0). Next, fresh 0.5% (w/v) locust bean gum was added, and the activity was tested again according to section 2.3.2.3. The reducing sugar concentration produced from the immobilised mannanase was analysed after each cycle according to section 2.3.2.2. All assays were performed in triplicate within a single trial, and the process was repeated. Values were reported as means ± standard deviations.

### 2.3.5 Comparison of physicochemical properties

#### 2.3.5.1 Temperature optima of the immobilised and free endo-1,4-β-mannanase

To determine the effect of temperature, the activities of the free enzyme (44.05 U/mg), CTS immobilised enzyme (9.14 U/mg), and MAGS-CTS immobilised enzyme (3.961 U/mg) were tested at temperatures ranging from 30°C - 80°C, using temperature intervals of 10°C. A mannanase activity assay with LBG was then completed (as described in section 2.3.2.3) and analysed by the DNS method (2.3.2.2). The maximal enzyme activity in each experiment was expressed as 100%, and the mannanase activity was expressed as a relative percentage of the maximal activity.

#### 2.3.5.2 pH optima of the immobilised and free endo-1,4-β-mannanase

The activities of the free enzyme (44.05 U/mg), CTS immobilised enzyme (9.14 U/mg), and MAGS-CTS immobilised enzyme (3.961 U/mg) were assayed at pH 2 – pH 9 using a universal buffer (Britton & Robinson, 1931). A mannanase activity assay with LBG was then completed (as described in section 2.3.2.3) and analysed by the DNS method (2.3.2.2). The maximal enzyme activity in each experiment was expressed as 100%, and the mannanase activity was expressed as a relative percentage of the maximal activity.

#### 2.3.5.3 Thermostability of the immobilised and free endo-1,4-β-mannanase

The effect of temperature on enzyme stability was determined at 55°C over a period of 72 hours. The free enzyme (44.05 U/mg), CTS immobilised enzyme (9.14 U/mg), and MAGS-CTS immobilised enzyme (3.961 U/mg) preparations were incubated in 50 mM citrate buffer (pH 5.0) at 55°C. The residual activity was measured at specific time intervals under the standard assay conditions (as described in section 2.3.2.3) and analysed by the DNS method (2.3.2.2). The maximal enzyme activity in each experiment was expressed as 100%, and the mannanase activity was expressed as a relative percentage of the maximal activity.

#### 2.3.5.4 Kinetic parameters of the immobilised and free endo-1,4-β-mannanase with locust bean gum

The kinetic parameters were determined using LBG as a substrate in the concentration range of 0.5 – 15 mg/ml in 50 mM citrate buffer (pH 5.0), with assay conditions as described in section in section 2.3.2.3 and analysed by the DNS method (2.3.2.2). The reactions were completed for free enzyme (44.05 U/mg), CTS immobilised enzyme (9.14 U/mg) , and MAGS-CTS immobilised enzyme (3.961 U/mg). The Michaelis–Menten constant, $K_M$, and maximum velocity, $V_{max}$, were determined from non-linear regression analysis using GraphPad Prism 9.0 software.

#### 2.3.5.5 Storage stability of immobilised and free endo-1,4-β-mannanase

The storage stabilities of the CTS and MAG-CTS enzyme preparations were determined according to the following standard procedure: several sample tubes containing the free enzyme (18.696 U/mg), CTS immobilised enzyme (6.631 U/mg), and MAGS-CTS immobilised enzyme (3.961 U/mg) were prepared, washed, and stored in 50 mM citrate buffer (pH 5.0) at 4°C. Samples were taken daily (over 10 days) and the hydrolytic efficiency was evaluated according to section 2.3.2.3.

### 2.3.6 Quantitative and qualitative analysis of MOS residues

#### 2.3.6.1 TLC analysis of MOS produced from LBG hydrolysis by immobilised and free endo-1,4-β-mannanases

The substrate of interest - 0.5% (w/v) LBG - was hydrolysed by the free enzyme (44.05 U/mg), CTS immobilised enzyme (9.14 U/mg), and MAGS-CTS immobilised enzyme (3.961 U/mg) preparations (as described in section 2.3.2.3). Aliquots were withdrawn upon completion of the hydrolysis reaction after heating at 100°C for 5 minutes in a Benchmark Scientific Digital heat block. The sugars present in the hydrolysates were quantified by the DNS method (as described

in section 2.3.2.2) and analysed by TLC, which was carried out with a solvent system of butanol: acetic acid: deionised water (2:1:1 (v/v)) using precoated silica gel 60 F254 plates. After the migration was repeated twice, the plate was air dried and sugar spots were visualised by spraying with a 0.3% (w/v) α-naphthol in 5% (v/v) sulphuric acid in methanol followed by heating in an oven at 110°C for approximately 5 minutes.

#### 2.3.6.2 HPLC analysis of MOS derived from immobilised and free endo-1,4-β-mannanase

The substrate of interest [0.5% (w/v) LBG] was hydrolysed by the free enzyme (44.05 U/mg), CTS immobilised enzyme (9.14 U/mg), and MAGS-CTS immobilised enzyme (3.961 U/mg) preparations (as described in section 2.3.2.3). Aliquots were withdrawn upon completion of the reaction after heating at 100° for 5 minutes in a Benchmark Scientific Digital heat block. The sugars present in the hydrolysates were measured by the DNS method (as described in section 2.3.2.2). Each sample was filtered (pore size: 22 μm) and placed in a clean and sterile 2 ml HPLC vial. The HPLC-RID Shimadzu system (Shimadzu Corp, Kyoto, Japan) was set up using a Carbosep CHO 411 column. Deionised water was used as the mobile phase in isocratic mode at a flow rate of 0.260 ml/min and the column temperature was set at 80°C. An injection volume of 20 μl was used for all samples. M S standards were prepared at 0.01 – 0.1% (w/v) concentrations for M1, M2, M3, M4, M5, and M6; and standard curves were constructed to allow the identification and quantification of the various MOS within the samples of interest.

### 2.3.7 Statistical analysis

All data were presented as the means and standard deviations (SD) of triplicates. A t-test was used to analyse all data using GraphPad Prism 9.0 software. A *p*-value of less than 0.05 indicated statistically significant differences between the compared data sets.

## 2.4 Results

### 2.4.1 Enzyme Immobilisation

#### 2.4.1.1 Immobilisation and activity yield

The immobilisation and activity yields (%) were determined for CTS and MAGS-CTS according to section 2.3.3.3; these results were accompanied by the specific activity (U/mg) values of the free, CTS and MAGS-CTS immobilised enzymes (Table 2.1). Immobilisation yields showed that CTS was highly successful for the attachment of the enzyme to the solid carrier – with binding of 81.14% of the total protein during the immobilisation procedure. MAGS-CTS was not as efficient in relation to enzyme immobilisation yield (%), with only

55.75% of the total protein being bound; this resulted in a large quantity of protein being detected in the enzyme wash after immobilisation. The specific activities (U/mg) of the different enzyme fractions varied quite significantly. The free enzyme displayed the highest specific activity of 18.70 U/mg, followed by the CTS enzyme fraction with a specific activity of 6.63 U/mg and MAGS-CTS with the lowest specific activity of 3.96 U/mg. The activity yields were expressed relative to the total activity of the free enzyme (0.075 U); and the free enzyme, CTS, and MAGS-CTS therefore displayed activity yields (%) of 100%, 35.45%, and 21.17%, respectively. This indicates that binding of the enzyme to the solid carrier is most probably inhibiting the enzyme activity in some way.

**Table 2.1: Immobilisation yield (%), specific activity (U/mg), and Enzyme activity yield (%) of free endo-1,4-β-mannanase, CTS and MAGS-CTS enzymes.**

| Immobilisation Parameters | Free Enzyme | CTS | MAGS-CTS |
|---|---|---|---|
| Immobilisation Yield (%) | N/A | 81.1 | 55.75 |
| Specific Activity (U/mg) | 18.70 | . 3 | 3.9 |
| Enzyme Activity (U) | 0.075 | 0.027 | 0.01 |
| Activity Yield (%) | 100 | 35. 5 | 21.17 |

#### 2.4.1.2 Optimisation of enzyme immobilisation

The optimisation of the immobilisation procedures for CTS and MAGS-CTS was completed according to section 2.3.3.4. This served to establish the optimal concentration of glutaraldehyde for activation of the solid carriers (Figures 2.1A and 2.1B), the optimal enzyme loading concentration (Figures 2.1C and Figure 2.1D), and the optimal time of immobilisation for attachment of the endo-1,4-β-mannanase to the solid carriers (Figures 2.1E and Figure 2.1F).

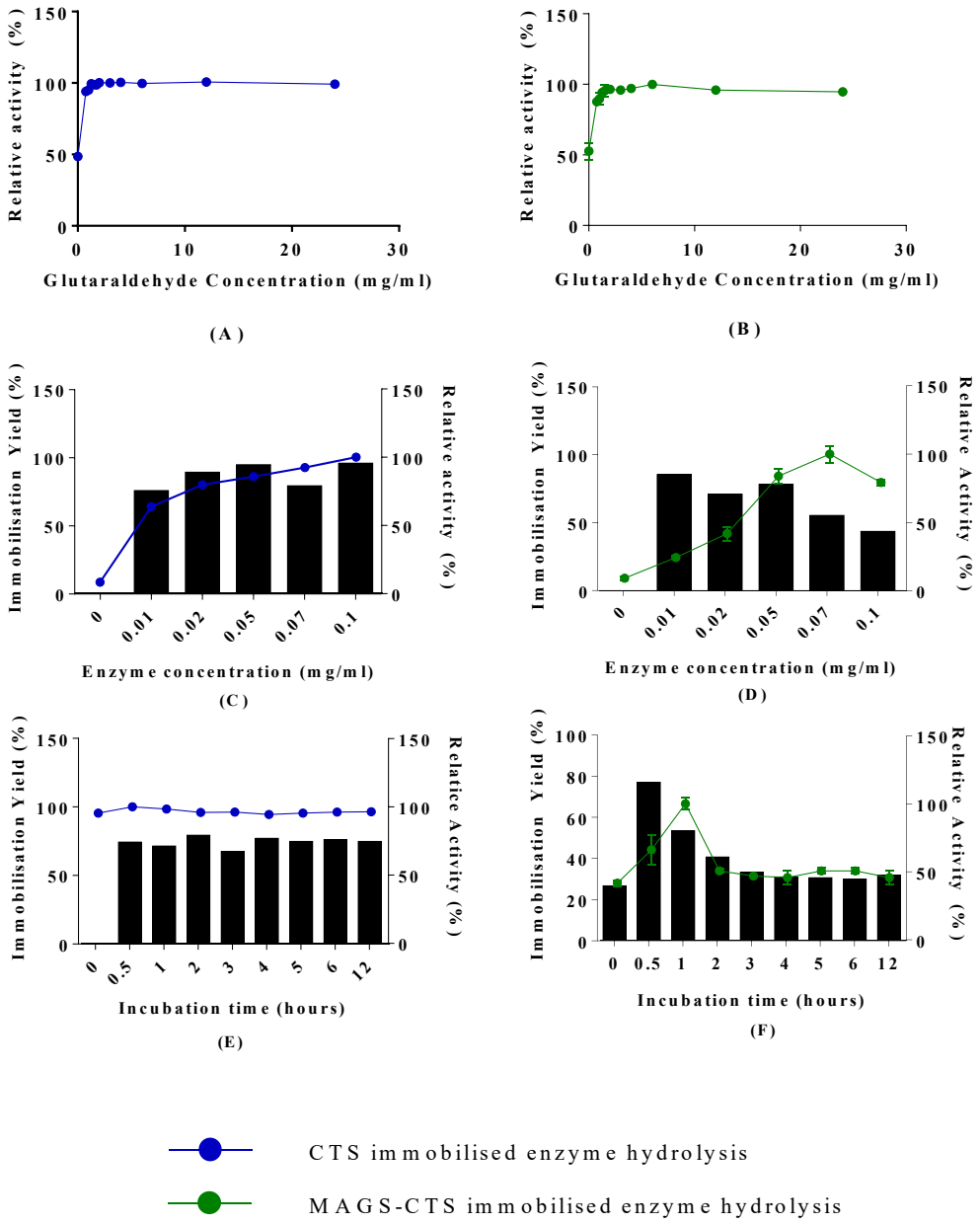


**Figure 2.1:** Optimisation of the (A and B) glutaraldehyde concentration (0 – 25% (v/v (%)), (C and D) endo-1,4-β-mannanase loading concentration (0 – 0.1 mg/ml), and (E and F) immobilisation time (0 – 12 hours) for the enzyme immobilisation procedure showing immobilisation and relative activity yield (%) of (A, C, E) CTS immobilised enzyme and (B, D, F) MAGS-CTS immobilised enzyme. Relative activity (%) was set as 100% for the highest activity obtained in the data set. For the glutaraldehyde concentration, enzyme loading concentration, and time of immobilisation for the CTS and MAGS-CTS, maximal activity was set as 6.273 U/mg, 5.96 U/mg, and 6.51 U/mg and 3.799 U/mg, 3.566 U/mg, and 3.479 U/mg, respectively.

Optimal glutaraldehyde concentration showed an exponential increase in relative activity, with a plateau being reached at 1.25% (v/v) for both the CTS and MAGS-CTS immobilisation procedures (Figure 2.1A and Figure 2.1B). The CTS particles showed that enzyme concentration (Figure 2.1C) had little effect and an 0.1 mg/ml enzyme loading concentration was therefore selected. The MAGS-CTS fraction showed more fluctuation with a variation in enzyme concentration (Figure 2.1D) - when the relative activity and immobilisation yield were considered, a 0.05 mg/ml enzyme concentration was selected for the immobilisation procedure. The time of immobilisation showed little fluctuation for the CTS immobilisation (Figure 2.1E) – with a consistent relative activity and immobilisation yield from 30 minutes of immobilisation. In contrast, the MAGS-CTS was more readily affected by the time of immobilisation (Figure 2.1F), with 1 hour of immobilisation being selected as the optimal time for maximal relative activity and immobilisation yield.

### 2.4.1.3 FTIR analysis

The FTIR spectra of chitosan, A-CTS, and CTS, MAGS, MAGS-chitosan, MAGS-A-CTS, and MAGS-CTS are shown in Figures 2.2A and 2.2B. The peaks were studied to identify the *in-situ* analysis of the various CTS and MAGS-CTS surfaces, in order to evaluate the shift in the surface adsorption of functional groups due to the enzyme immobilisation procedure.

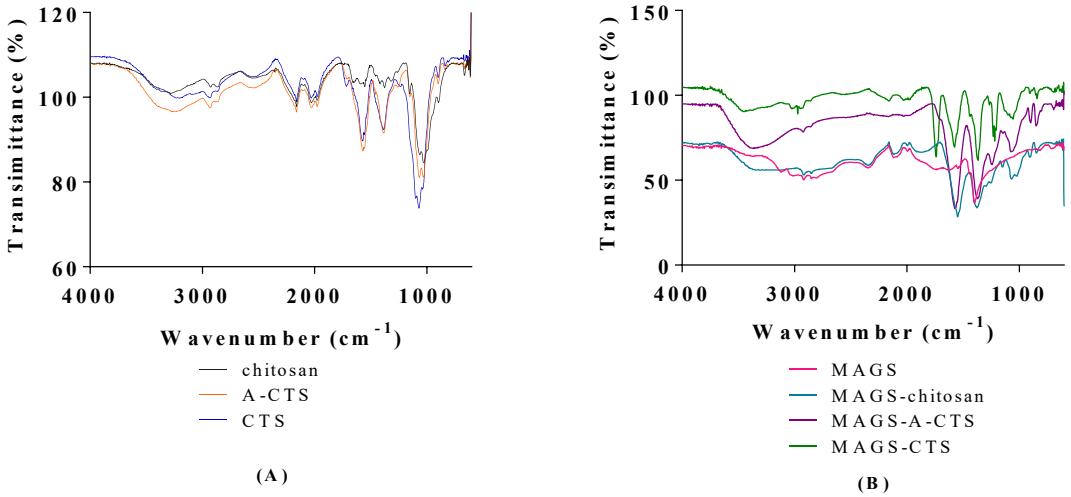


**Figure 2.2:** Comparison of FTIR spectra of (A) chitosan, A-CTS, and CTS and (B) MAGS, MAGS-chitosan, MAGS-A-CTS, and MAGS-CTS. FTIR spectra were obtained from scans from 4000 to 600 $cm^{-1}$. Baseline and Attenuated total reflection (ATR) corrections for penetration depth and frequency variations were carried out using the SpectrumTM One software supplied with the equipment.

The FTIR spectra of untreated chitosan, A-CTS, and CTS can be seen in Figure 2.2A. The identified peaks were studied to perform the *in-situ* analysis of the chitosan surface for investigating the surface adsorption of functional groups due to the glutaraldehyde activation and the enzyme immobilisation procedure. FTIR analysis of chitosan showed characteristic bands at 3276 $cm^{-1}$ (-OH and -NH stretching band), 2961 $cm^{-1}$ (-CH stretching region), and bands at 1642 $cm^{-1}$, 1604 $cm^{-1}$ ($-NH_2$) and, 1063 $cm^{-1}$ (C-O-C stretching vibrations). The A-CTS sample showed bands present at 3260 $cm^{-1}$ (-OH stretching vibration), 2967 $cm^{-1}$ (-CH stretching region), 2915 $cm^{-1}$ (-NH), 1730 $cm^{-1}$ (-C=O), 1681 $cm^{-1}$, 1687 $cm^{-1}$ (-C=N) and, 1077 $cm^{-1}$ (C-O-C stretching vibrations). The CTS sample experienced prominent bands at 3206 $cm^{-1}$ (-OH stretching vibrations), 2987 $cm^{-1}$ (-CH stretching region), 2910 $cm^{-1}$ (-NH), 1730 $cm^{-1}$ (-C=O), 1685 $cm^{-1}$, 1697 $cm^{-1}$ (C=N) and, 1082 $cm^{-1}$ (C-O-C stretching vibrations).

The FTIR spectra of the MAGS-CTS (Figure 2.2B) showed a large variety in their FTIR spectra with each step of immobilisation. The FTIR spectra of MAGS showed prominent bands at 3448 $cm^{-1}$ (OH-bending vibrations), 2389 $cm^{-1}$ ($CO_2$), and 1405 $cm^{-1}$ (-OH). The MAGS-chitosan showed characteristic bands at 3440 $cm^{-1}$ (OH and N-H stretching vibrations), 2972 $cm^{-1}$ (C-H stretching vibrations), 1565 $cm^{-1}$ (N-H bending vibrations), 1393 $cm^{-1}$ (C-N), 1080 $cm^{-1}$ (C-O-C stretching vibrations). The activation of the MAGS-chitosan to produce MAGS-A-CTS showed bands at 3448 $cm^{-1}$ (OH and N-H stretching vibrations), 2972 $cm^{-1}$ (C-H stretching vibrations), 2184 $cm^{-1}$ ($CH_2$), 1570 $cm^{-1}$ (N-H bending vibrations and $NH_2$ amino groups), 1094 $cm^{-1}$ (C-O-C stretching vibrations). After the immobilisation of the endo-1,4-β-mannanase to the MAGS-A-CTS, the FTIR spectra of MAGS-CTS produced characteristic bands at 3511 $cm^{-1}$ (OH and N-H stretching vibrations), 2973 $cm^{-1}$ (C-H stretching vibrations), 2194 $cm^{-1}$ ($CH_2$), 1745 $cm^{-1}$ (C=O), 1589 $cm^{-1}$ (N-H bending vibrations and $NH_2$ amino groups), 1102 $cm^{-1}$ (C-O-C stretching vibrations).

#### 2.4.1.4 XRD analysis

XRD was used to investigate the change in chitosan's structure after glutaraldehyde activation and enzyme immobilisation (Figure 2.3A).

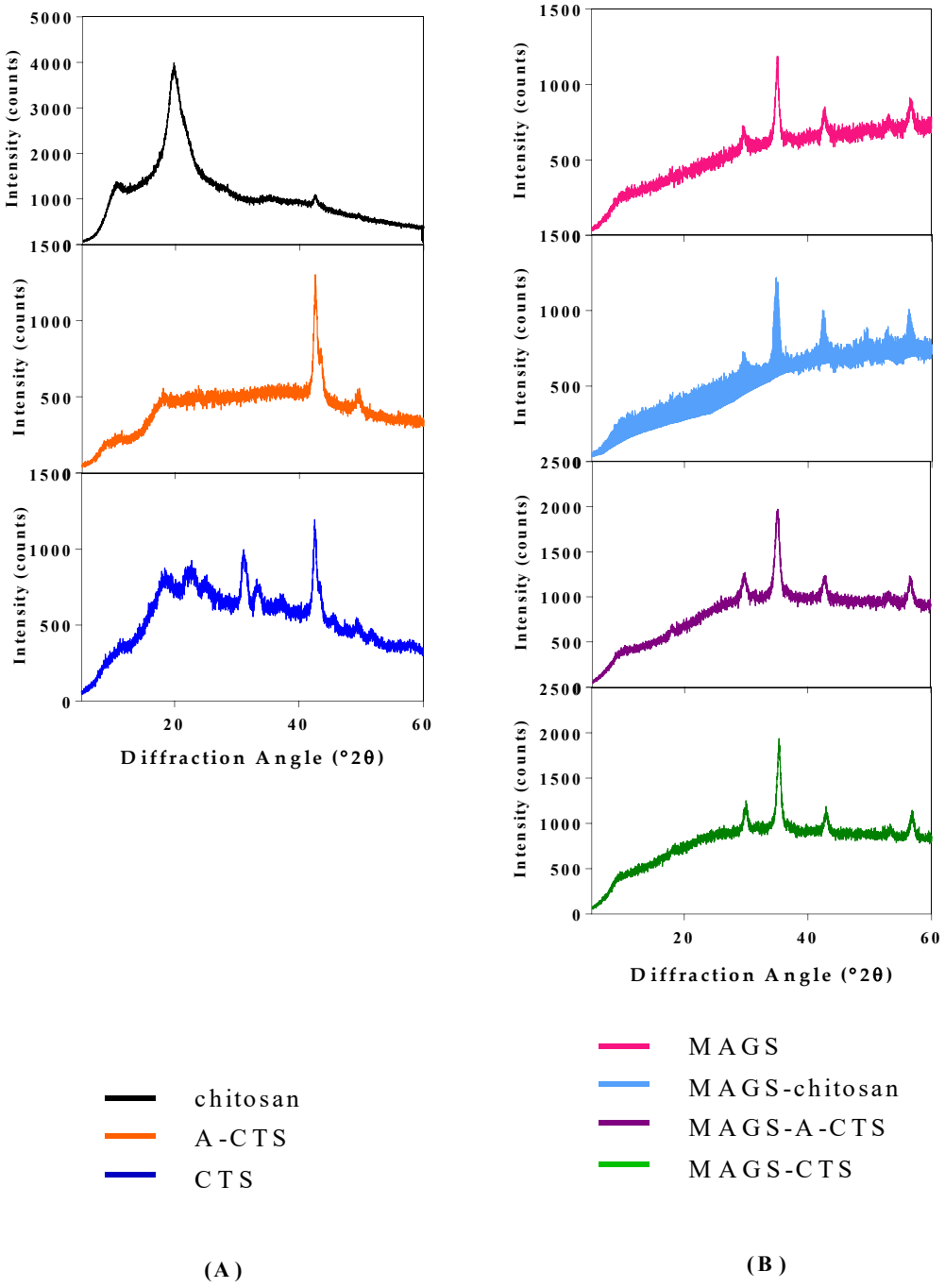


**Figure 2.3:** X-ray diffraction patterns of (A) chitosan, A-CTS, and CTS and (B) MAGS, MAGS-chitosan, MAGS-A-CTS, and MAGS-CTS. The samples were scanned from 2θ of 5 to 60° with a step size of 0.02°. The determination time was 0.02° per second.

The XRD pattern of chitosan showed two distinctive crystallinity peaks at 2θ = 10.558° and 19.661° associated with the 020 and 110 planes of the crystallite, respectively. The morphology of the chitosan was altered after activation with glutaraldehyde; this can be seen by the drastic

reduction in intensity with low peaks associated with the crystallinity of the biomass. Furthermore, the addition of Man26A to the surface of the glutaraldehyde-activated chitosan led to the re-emergence of the 2θ = 20° peak; however, it was broad, thus providing supporting evidence of immobilisation in an ordered amorphous manner. The sample's average crystallite size for chitosan, A-CTS, and CTS (Appendices, Table A), was analysed via Scherrer's equation to be 8.024 nm, 12.281 nm, and 10.071 nm, respectively – confirming the particles as nanoparticles.

The various magnetic particles were analysed via XRD (Figure 2.3B), showing the crystalline structure analysis of MAGS, MAGS-chitosan, MAGS-A-CTS, and MAGS-CTS. The XRD analysis for all analysed materials followed a similar pattern with few changes in peaks throughout testing. These patterns were found at 2θ = 29º, 3 º, 2º, and 5 º, with slight variation in the decimals (MAGS, MAGS-chitosan, MAGS-A-CTS, and MAGS-CTS). It was seen in the MAGS-chitosan sample that an additional peak became present at 2θ = 9 º, however, this peak disappeared in the MAGS-A-CTS and MAGS-CTS samples. When referencing the obtained peaks against that of magnetite and maghemite (Appendices, Figure AA and Figure AB) it was found that the peak patterns correlated closely with both materials. With these reference patterns in mind, it was determined the formed particles were magnetite – with this finding based primarily on the likeness of peaks between the reference sample and that of the synthesised MAGS (Appendices, Figure A). The crystallite size of MAGS, MAGS-A-CTS and MAGS-CTS were estimated as 8.38 nm, 8.15 nm, and 8.06 nm, respectively (Appendices, Table B).

#### 2.4.1.5 Visual analysis of CTS and MAGS-CTS

A-CTS (Figure 2.4 A-D) and CTS (Figure 2.4 E-H) were viewed via SEM analysis. This analysis showed small differences in surface morphology, but showing no effect on particle size. A roughening of the CTS surface (Figure E-H) compared with the A-CTS particles (Figure 2.4A-D) was visible, providing evidence of a change to the enzyme surface and, therefore, enzyme immobilisation.

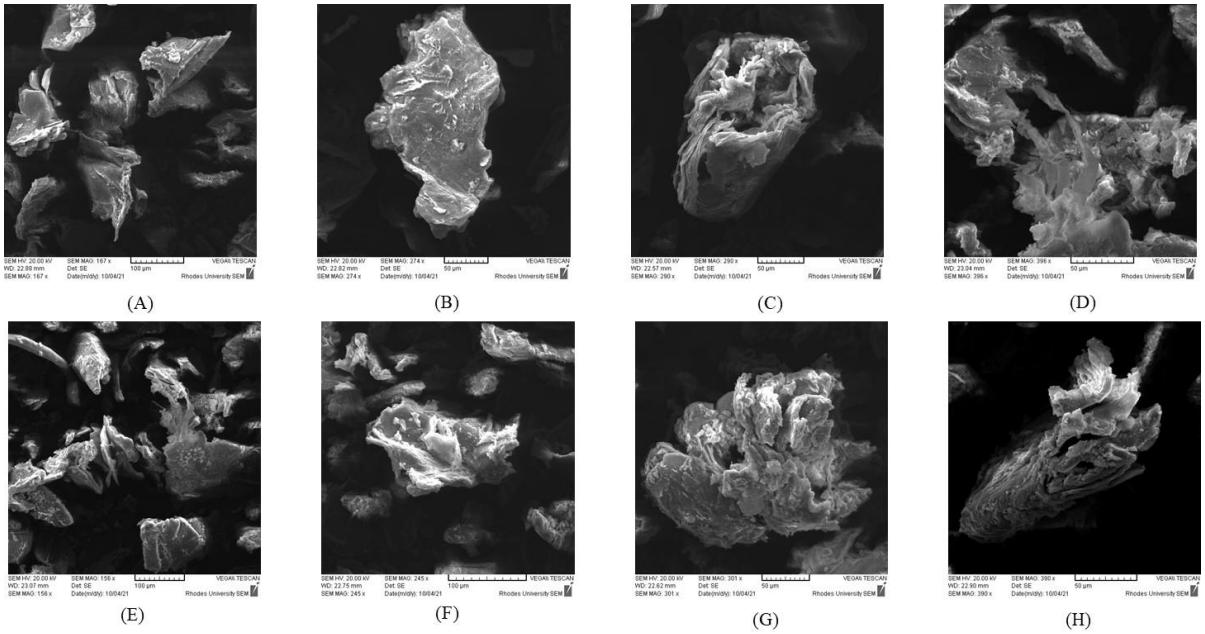


**Figure 2.4:** SEM images for characterising and visualising surface morphology of (A-D) A-CTS and (E-H) CTS. Magnification x150 – x300.

MAGS-CTS could be successfully separated from the aqueous solution with a permanent magnet, over 1 minute and 15 seconds at 25ºC (Figure 2.5). The particles had a blackish-brown tone, with the colour remaining uniform throughout the immobilisation procedures. Once the MAGS-CTS were separated from the solution, a clear solution of 50 mM citrate buffer (pH 5.0) remained.


**Figure 2.5:** Visual representation of the magnetic capabilities of the MAGS-CTS over 1 minute and 15 seconds at 25ºC by separation with a magnetic bar. The initial time of 0 seconds is represented on the far left where an image was taken every 15 seconds. The times of images captured are represented in seconds below the respective images.

### 2.4.2 Recyclability of immobilised endo-1,4-β-mannanase to produce reducing sugars

Endo-1,4-β-mannanase was immobilised on chitosan-activated nanoparticles, as stated in sections 2.3.3.1. The reusability of the immobilised enzyme was analysed using the model substrate 0.5% (w/v) LBG (30 minutes, 55°C), which produced 0.960 mg/ml of reducing sugars after cycle 1 (Figure 2.6A). Reducing sugar production showed its first significant drop at the 6$^{th}$ cycle. Wherein activity was maintained until a drop to 0.545 mg/ml at the 9$^{th}$ cycle. The second immobilisation of endo-1,4-β-mannanase on magnetic chitosan-coated $Fe_3O_4$ nanoparticles was completed and tested for recyclability (Figure 2.6B), with cycle 1 producing reducing sugars of 0.910 mg/ml. Thereafter, a major drop-in activity was displayed, illustrating that immobilisation in terms of activity retention was not successful. This study found that the MAGS-CTS immobilisation was not successful for recyclability, as a result of a significant drop in activity in subsequent cycles (0.33 mg/ml).

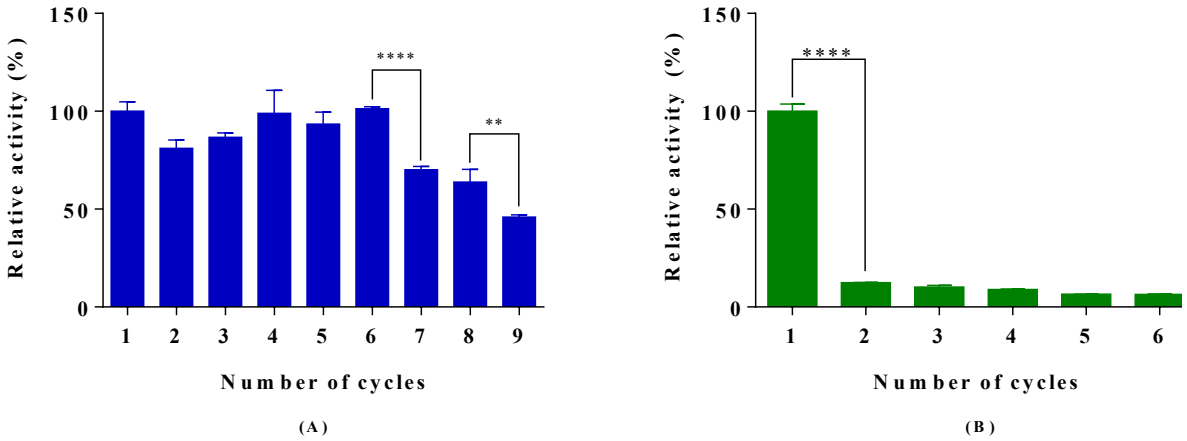


**Figure 2.6:** Recyclability test of endo-1,4-β-mannanase immobilised on (A) CTS (0.05 mg/ml) and (B) MAGS-CTS (0.05 mg/ml) using 0.5% (w/v) LBG as a substrate (30 minutes, 55°C) in 50 mM citrate buffer (pH 5.0). Each value in the panel represents the means ± SD (n = 3). Relative activity (%) was used, with the activity in cycle 1 set as 100%. Statistical analysis was conducted using *t*-test for cycles with respect to reducing sugar by the immobilised enzyme compared to previous cycle, key: ** ($p$ value ≤ 0.01), ****($p$ value ≤ 0.0001).

### 2.4.3 Comparison of physicochemical properties

#### 2.4.3.1 Effect of temperature on enzyme activity

The effect of temperature on the activities of the free and immobilised endo-1,4-β-mannanase was studied in 50 mM citrate buffer (pH 5.0) and 0.5% (w/v) LBG, according to section 2.3.5.1. The results showed that the free, CTS, and MAGS-CTS immobilised endo-1,4-β-mannanases had an optimum temperature of 60°C (Figures 2.7A, B and C, respectively). The temperature stabilities of the free, CTS and MAGS-CTS immobilised endo-1,4-β-mannanases were compared at 55°C in 50 mM citrate buffer (pH 5.0) from a period of 72 hours (Figures 2.7D, E and F, respectively). The free and CTS immobilised enzymes experienced no loss in activity after storage at 55ºC for 0 – 6 hours, after which a drastic decrease in activity was experienced. The MAGS-CTS enzyme experienced an immediate drop in activity after incubation at 55ºC for 30 minutes.

#### 2.4.3.2 Effect of pH on enzyme activity

The optimum pH was determined for the free, CTS, and MAGS-CTS immobilised enzymes, and presented in Figures 2.7G, H and I, respectively. The free enzyme displayed an optimum pH of 5 – 6; after immobilisation onto both the CTS and MAGS-CTS particles, the optimum pH shifted towards a more acidic pH of 3.0. These results showed that the immobilised enzymes preferred a more acidic pH of below pH 4.0, whilst the free enzyme was more active at a neutral pH above pH 5.0.

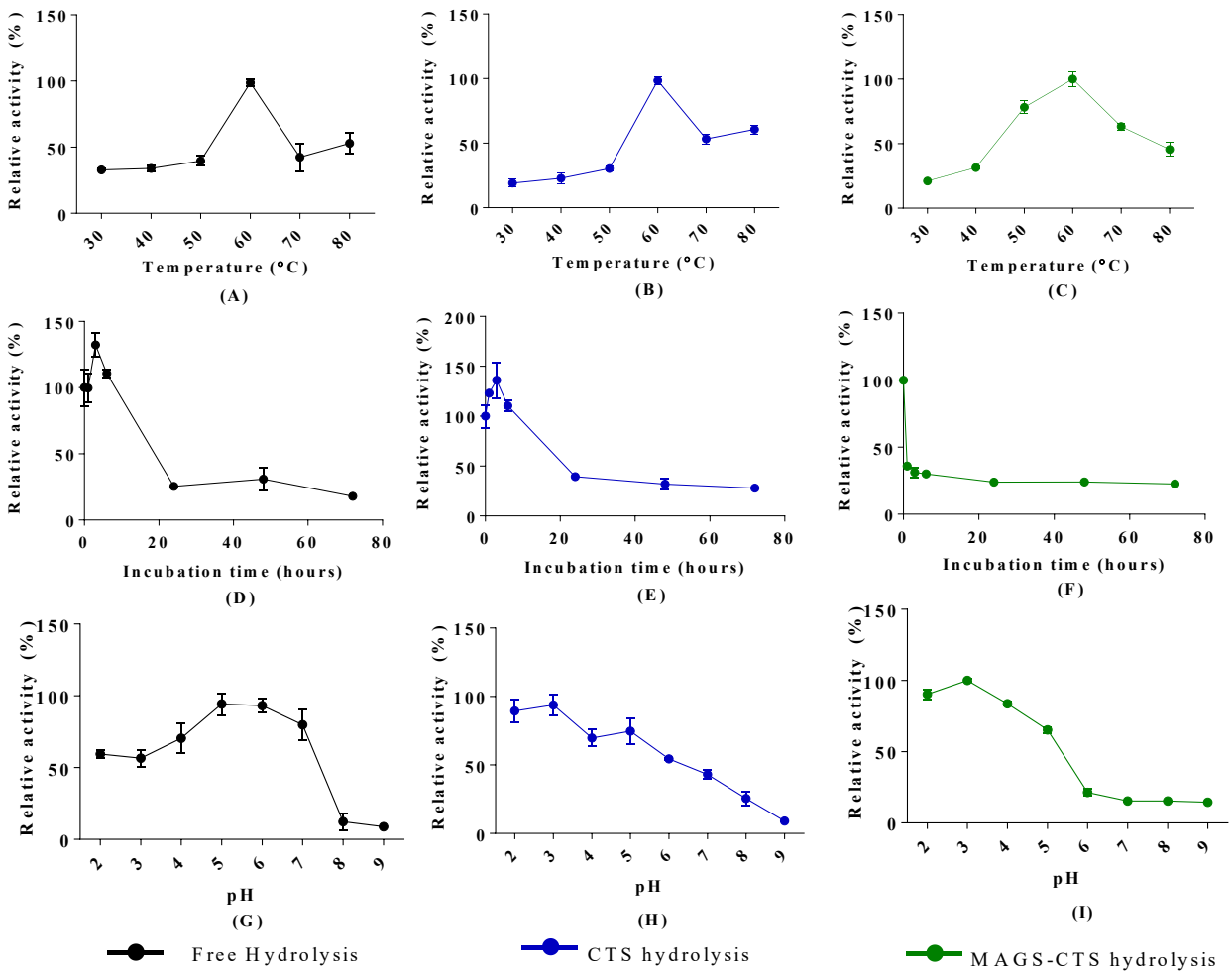


**Figure 2.7: (A, B, C)** Temperature optimum, **(D, E, F)** thermostability and (**G, H, I)** pH optimum study of the free (18.70 U/mg), CTS (6.63 U/mg), MAGS-CTS (3.96 U/mg) endo-1,4-β-mannanases under hydrolysis with 0.5% (w/v) LBG (30 min, 55°C). Each value in the graphs represents the means ± SD (n = 3).

### 2.4.3.3 Kinetic parameters

Under the optimal assay conditions, free and CTS and MAGS-CTS immobilised endo-1,4-β-mannanase were evaluated for kinetic parameters against LBG (Figure 2.8A – Figure 2.8C and Table 2.2). The LBG kinetics study for the free endo-1,4-β-mannanase (Figures 2.8A and Table 2.2) exhibited $K_M$ and $V_{max}$ values of 8.44 mM and 55.36 U/mg. A high $k_{cat}$ value of 5536 $s^{-1}$ indicated a high turnover number and high rate of product formation. The catalytic efficiency of the enzyme ($k_{cat}/K_m$) was 655.85 $s^{-1}$ $mM^{-1}$ , proving that the free enzyme is effective at hydrolysing LBG. The kinetic parameters of the CTS immobilised enzyme (Figure 2.8B and

Table 2.2) indicated $K_M$ and $V_{max}$ values of 7.74 mM and 12.10 U/mg, respectively. This shows that the immobilised enzyme had a lower catalytic rate; however, the immobilisation increased the catalyst's binding affinity to the substrate. The $k_{cat}/K_m$ values obtained showed that the immobilised enzyme was not as efficient at hydrolyzing the LBG substrate compared to the free enzyme. The MAGS-CTS immobilised enzyme (Figure 2.8C and Table 2.2) exhibited $K_M$ and $V_{max}$ values of 4.96 mM and 17.63 U/mg, respectively. This showed that the MAGS-CTS immobilised enzyme had the highest binding affinity to the substrate LBG with a $V_{max}$ value that outcompetes the CTS immobilised enzyme. However, the $k_{cat}$ of the MAGS-CTS (134.1 $s^{-1}$) revealed the hydrolysis was unproductive compared to the reactions with the free and CTS immobilised enzymes. This was determined as a result of MAGS-CTS displaying the lowest turnover rate. The $k_{cat}/K_m$ revealed that the MAGS-CTS was the least efficient at hydrolysing the soluble substrate LBG (27.04 $s^{-1}$ $mM^{-1}$ ).

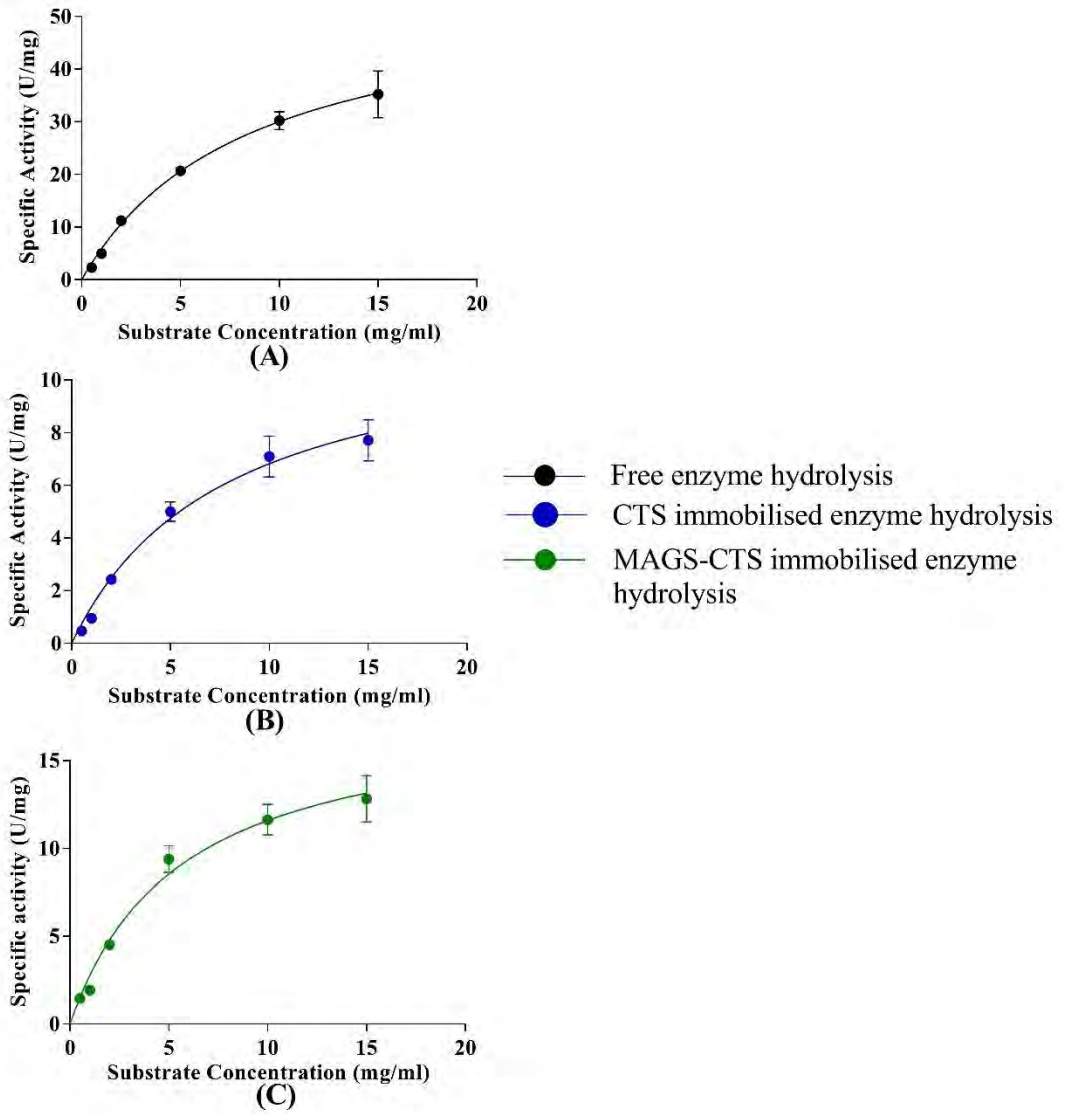


**Figure 2.8:** Michaelis-Menten kinetics of (A) free (B) CTS immobilised endo-1,4-β-mannanase and (C) MAGS-CTS immobilised endo-1,4-β-mannanase hydrolysing LBG (0.5 – 15 mg/ml) (30 min, 55°C). The kinetic parameters were determined at the optimal pH and temperature. The values were presented as means ± SD (n = 3).

**Table 2.2:** Kinetic parameters of free and immobilised endo-1,4-β-mannanases with LBG [0.05 – 0.15% (w/v)]

| Kinetic parameters | Free enzyme | CTS | MAG-CTS |
|---|---|---|---|
| $V_{max}$ (U/mg) | 55.36 | 12.10 | 17.63 |
| $K_m$ (mM) | 8.44 | 7.74 | 4.96 |
| $k_{cat}$ ($s^{-1}$) | 5536.0 | 322.6 | 134.1 |
| $k_{cat}/K_m$ ($s^{-1}$ $mM^{-1}$) | 655.85 | 41.67 | 27.04 |

### 2.4.3.4 Storage Stability

The storage stability for CTS and MAGS-CTS was determined according to section 2.3.5.5 and the results are presented in Figure 2.9. This analysis showed that the CTS and MAGS-CTS enzymes were both capable of being stored at 4°C for up to 120 hours. Both the immobilised enzymes followed a similar storage stability pattern, with 73% relative activity remaining after 120 hours.

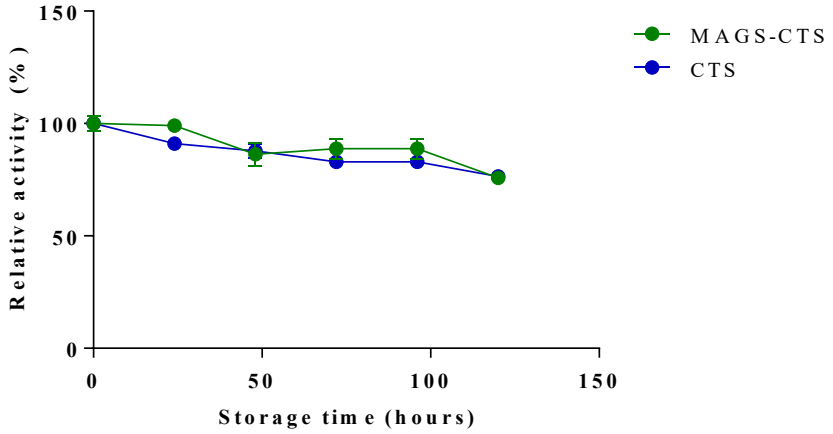


**Figure 2.9:** Storage stability analysis of CTS (6.63 U/mg) and MAGS-CTS (3.96 U/mg) stored at 4°C for 120 hours. The initial activity (at time t = 0 h) was taken as 100%, representing 1.07 mg/ml and 1.06 mg/ml of the CTS and MAGS-CTS immobilised enzymes, respectively. The values were presented as means ± SD (n = 3).

### 2.4.4 Quantitative and qualitative analysis of MOS

#### 2.4.4.1 TLC analysis of MOS derived from the hydrolysis of LBG with immobilised and free endo-1,4-β-mannanases

The hydrolysis products of the LBG substrate control, free enzyme, CTS immobilised enzyme, and MAGS-CTS immobilised enzymes were analysed via TLC (Figure 2.10). The LBG substrate control showed limited reducing sugars without enzyme hydrolysis, with two faint bands, located between M1 and M2, and between M2 and M3. After enzyme hydrolysis, four distinct bands were visible – with the free enzyme having a slightly darker bands than the CTS immobilised enzyme and MAGS-CTS immobilised enzyme. From these bands, M2, M3, M4, and M6 could confidently be identified from the MOS standards for all hydrolysis reactions. Low proportions of M1 were identified for the free and CTS immobilised enzymes. This result confirms that the immobilised and free enzymes could efficiently hydrolyse the galactomannan portion of LBG – producing a similar MOS pattern (and diversity of MOS species).

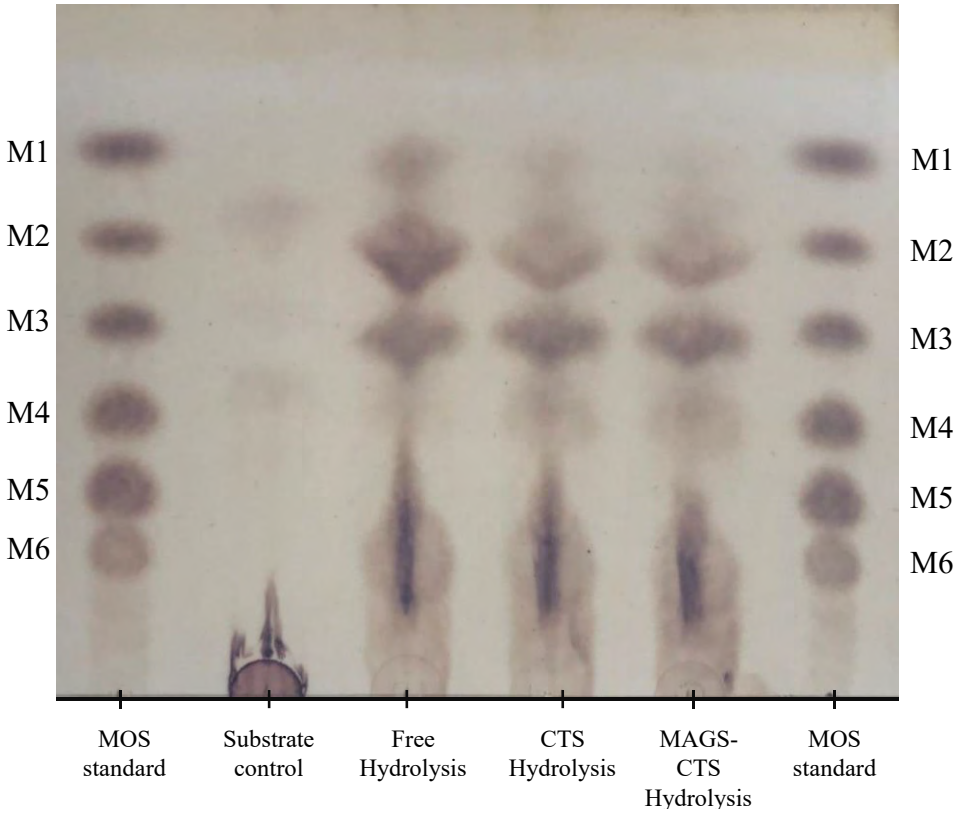


**Figure 2.10:** TLC plate of the reducing sugars produced by the free, CTS immobilised endo-1,4-β-mannanase, and MAGS-CTS immobilised endo-1,4-β-mannanase derived from *A. niger* in a reaction with 0.5% (w/v) LBG (30 minutes, 55°C). MOS standards were used to identify the bands of interest (M1-M6).

### 2.4.4.2 HPLC analysis of MOS derived from the hydrolysis of LBG with immobilised and free endo-1,4-β-mannanase

The untreated LBG (Figure 2.11A) was analysed for reducing sugars alongside the free, CTS, and MAGS-CTS hydrolysed substrate, according to section 2.3.6.2 (Figures 2.11B–D). The untreated LBG (Figure 2.11A) showed no oligosaccharides were present before hydrolysis. Comparing the obtained results with that of a MOS standard (Appendices, Figure B) showed that no MOS residues could be identified before enzyme hydrolysis. After hydrolysis with free and CTS enzymes, hydrolysis products of M1-M4 were visible, as illustrated in Figure 2.11B and Figure 2.11C. MAGS-CTS hydrolysis of LBG produced similar by-products however at lower intensities. It was also found that hydrolysis by MAGS-CTS was not capable of hydrolysing MOS to M1, unlike the free and CTS enzyme forms. This showed that the free and CTS enzyme forms, were able to hydrolyse the galactomannan portion of LBG to produce identical MOS residues – with MAGS-CTS producing similar yet weakened results.

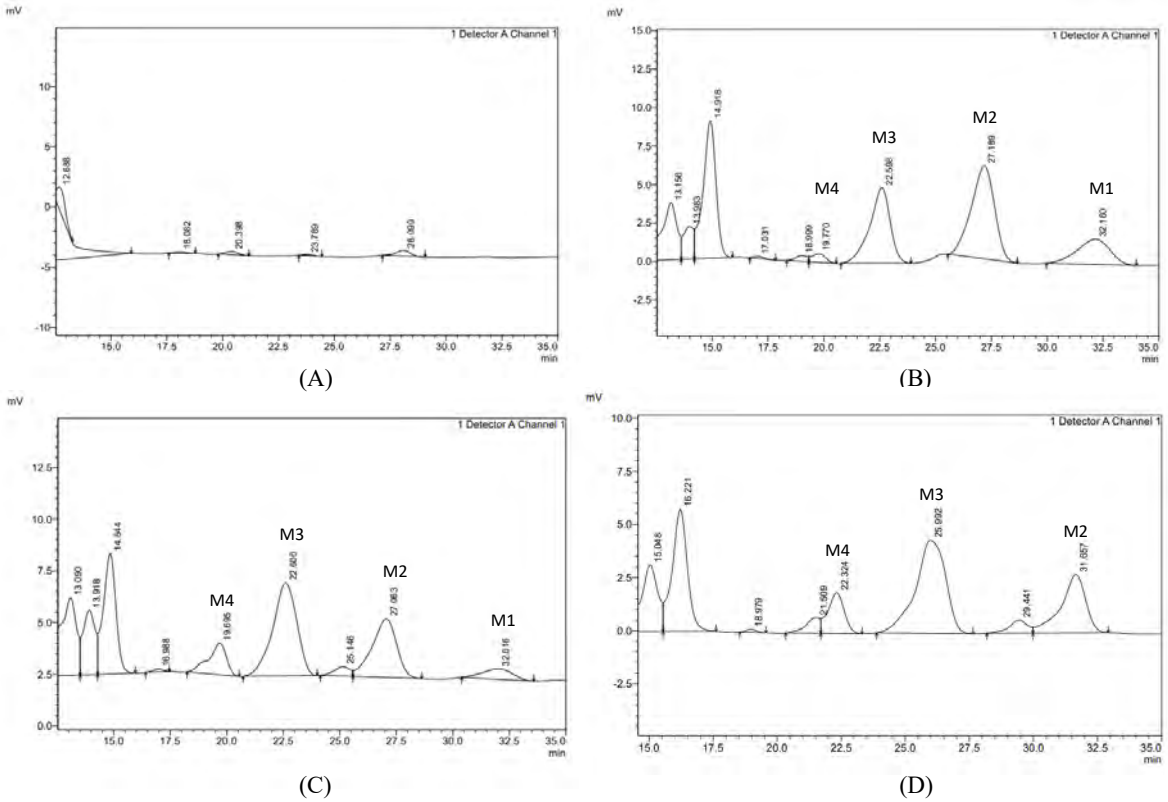


**Figure 2.11:** High-performance liquid chromatography (HPLC) analysis of (A) untreated LBG (B) free (C) CTS immobilised endo-1,4-β-mannanase and (D) MAGS-CTS immobilised endo-1,4-β-mannanase hydrolysing 0.5% (wv) LBG. Analysis was conducted using a Carbosep CHO 411 column, with a flow rate of 0.26 ml/min and a refractive index detector (RID). MOS standards were used to identify the peaks of interest (M1-M6).

## 2.5 Discussion

Enzyme immobilisation is an important aspect of ensuring practicality in terms of enzyme utilisation when relating to cost. The reusable nature of immobilised enzymes is only feasible if the enzyme is functioning at its highest efficiency; with increased thermostability, and storage stability, whilst maintaining a high level of activity.

A method of immobilising an enzyme should be tested for optimal conditions. This is achieved in literature by evaluating various immobilisation parameters such as glutaraldehyde concentration, enzyme concentration, and the duration of the immobilisation procedure. Literature has shown these parameters to be highly varied – as no study is identical (Collins et al., 2011; Klein et al., 2012; Saravanakumar et al., 201 ;  me  n et al., 201 ;  Gűr et al., 2018; Nguyen et al., 2019; Reshmy et al., 2022; Mohapatra, 2021; Sadaqat et al., 2022). Each study occupies a different immobilisation surface or technique of attachment, substrate, and/or application – influencing the methods parameters. A broad analysis of the results amongst literature indicates that a 0.25% - 25% (v/v) glutaraldehyde concentration can be utilised when activating chitosan (Klein et al., 2012; Saravanakumar et al., 201 ;  me  n et al., 201 ;  Gűr et al., 2018; Nguyen et al., 2019; Mohapatra, 2021; Sadaqat et al., 2022) as well as an immobilisation time (duration) of between one (1) and 20 hours (Klein et al., 2012; Nguyen et al., 2019; Najavand et al., 2020; Mohapatra, 2021; Jonović et al., 2022; Sadaqat et al., 2022). Information in literature regarding the preferred concentration of endo-1,4-β-mannanase used is limited, but when comparing reports in literature it was found that this parameter was linked to the type of enzyme utilised, the purity of the enzyme sample, as well as the surface utilised for immobilisation – with examples reported in specific activity or volume rather than concentration (  nem et al., 201 ;  Mohapatra, 2021; Jonović et al., 2022; Sadaqat et al., 2022).

Among the *Aspergillus* species of endo-1,4-β-mannase, there are large variations in specific activity (U/mg) reported, with results ranging from 34.44 U/mg to 2290.5 U/mg (Bien-Cuong et al., 2009; Zyl et al., 2010; Liao et al., 2014; Chai et al., 2016; Xie et al., 2020). Table 2.1 illustrates the specific activities of the free (18.70 U/mg), CTS (6.63 U/mg), and MAGS-CTS (3.96 U/mg) enzymes against LBG which was completed within this study. A decrease in specific activity after immobilisation is frequently seen in literature, where it is attributed to a conformational change in the enzyme upon binding (Mohapatra, 2021). Activity yields for CTS and MAGS-CTS were calculated as 35.45% and 21.17%, respectively. The immobilisation yields of a β-mannanase onto CTS and MAGS-CTS range between 38.3% and 98.8% across

literature, with high variations likely caused by differences in the immobilisation protocols (Klein et al., 2012; Saravanakumar et al., 201 ; Nguyen et al., 2019; Mohapatra, 2021; Jonović et al., 2022; Sadaqat et al., 2022).

Immobilisation yields for CTS and MAGS-CTS vary across literature, with higher success shown by endo-1,4-β-mannanase immobilised on MAGS-CTS with yields of between 81.7% and 98.8% (Klein et al., 2012; ne m et al., 201 ; Nguyen et al., 2019; Jonović et al., 2022; Sadaqat et al., 2022). Although MAGS-CTS was more successful in literature, the results obtained in this study were lower – with CTS results showing the most successful immobilisation with 81.14%. There are various reasons for this, one being insufficient activation of the chitosan leading to less locations for covalent attachment.

Although the immobilisations of CTS and MAGS-CTS were deemed successful, based on the immobilisation and activity yields – further validation was required to confidently state that a covalent immobilisation occurred. This can be conducted in various ways, with FTIR analysis and XRD analysis being employed in this study.

The chemical structure of chitosan, when analysed via FTIR, has been documented via literature to have five characteristic bands – each representing a key component of the polymer's structure ( suna et al., 2012). Of these characteristic functional groups, the CTS (Figure 2.2A) and MAGS-CTS (Figure 2.2B) immobilised enzymes possessed: OH and N-H stretching vibrations (±3400 $cm^{-1}$), C-H stretching vibrations characteristic of the pyranose ring of chitosan (±2900 $cm^{-1}$) (Mahamed et al., 2013; Baroudi et al., 2018), N-H bending vibrations (±1600 $cm^{-1}$), C-N stretching vibrations (±1400 $cm^{-1}$), and C-O-C stretching vibrations (±1070 $cm^{-1}$) (Osuna et al., 2012; Nadaroglu and Sonmez, 2016; Sadaqat et al., 2022). Slight shifts between compounds indicate a change in quantity, or a change in confirmation of the sample under analysis (Osuna et al., 2012; Mohapatra, 2021). Confirmation of the C-O-C stretching vibrations within all samples, excluding MAGS, provided sufficient evidence that the MAGS-CTS were coated with chitosan. It should be noted that with the co-precipitation method utilised for production of MAGS, $Fe(OH)_3$ (magnetite) and $Fe_2O_3$ (maghemite) could also be formed as a by-product. Thus, it could not be assumed that $Fe_3O_4$ was the major product, which necessitated further confirmation by XRD (Hoa et al., 2009).

With chitosan present in both samples, the surfaces were then activated with glutaraldehyde (Collins et al., 2011; Klein et al., 2012; Gűr et al., 2018; Mohapatra, 2021). The band located at ±1630 $cm^{-1}$ indicates an imine bond (C=N), with the method of formation often described as

a Shiffs base formation (Collins et al., 2011; Klein et al., 2012; Gűr et al., 2018; Mohapatra, 2021), illustrating the binding of glutaraldehyde to chitosan. The band at ±1730 $cm^{-1}$ provides evidence of a C=O structure, representing free aldehyde groups across the chitosan structure (Belowicha et al., 2012; Ciaccia et al., 2013; Dai et al., 2016; Klein et al., 2012; Mohapatra, 2021), illustrating chitosan's activation by glutaraldehyde.

Endo-1,4-β-mannanase was successfully immobilised to form CTS. This was described by a shift in wavenumber from approximately 1630 $cm^{-1}$ to 1680 $cm^{-1}$, representing the binding of an amine and an aldehyde to form an imine bond with covalent characteristics (Collins et al., 2011; Belowicha et al., 2012; Klein et al., 2012; Ciaccia et al., 2013; Dai et al., 2016; Morsy et al., 2019; Mohapatra, 2021). MAGS-CTS showed evidence of free aldehyde groups within its structure, however, gave no indication of an imine bond formation. This could suggest various outcomes, such as an insufficient quantity of chitosan coating the MAGS or an in sufficient activation. Both of these scenarios suggested that the reaction was not efficient with regards to preparing the solid carrier for immobilisation – thus producing less binding sites for the enzyme to attach to. The appearance of additional bands in the FTIR spectra with each immobilisation step does suggest that alterations to the surface were made – with these possibly contributing to the immobilisation of endo-1,4-β-mannanase.

The crystalline structure of untreated chitosan (Figure 2.3A), showed characteristic peaks of chitosan at 2θ = 10.558° and 19. 1 ° –frequently referenced in literature as prominent peaks for 95% deacetylated chitosan (Kumar et al., 2011; Kumar et al., 2012; Morsy et al., 2019; Galan et al., 2021; Sadaqat et al., 2022). An additional peak at 2θ = 2.531º was also identified, although it is usually allocated to a peak of untreated chitosan (Garnica-Palafox et al., 2016; Galan et al., 2021). After activation (A-CTS) and immobilisation (CTS), results showed a drastic drop in the intensity counts for the crystallinity peaks, with a slight shift in 2θ = 19. 1° peak to 2θ = 18.032°. With the attachment of glutaraldehyde's free aldehydes to chitosan's surface, hydroxyl and amino groups are displaced, leading to the deformation of hydrogen bonds and the formation of an amorphous structure (Li et al., 2013; Galan et al., 2021). Along with the above-mentioned peaks, CTS XRD spectra showed several new peaks (2θ = 18.032°, 22.631°, 24.739°, 31.064°, 33.363°, 37.005°, 42.531°, 45.533°, 49.469°, and 51.569°) – a result mentioned by Sadaqat et al. (2022) to indicate successful immobilisation.

The XRD analysis of the MAGS-CTS analysed the immobilised enzyme at various stages of immobilisation (MAGS, MAGS-chitosan, MAGS-A-CTS, and MAGS-CTS). These results

showed great similarity, with slight shifts to prominent peaks at 2θ = 29º, 3 º, 2º, and 5 º . The XRD spectra of magnetite and maghemite (Appendices Figure A and Figure B, respectively) were analysed to identify the major by-product of the co-precipitation method (Figure 2.3B). Four prominent common peaks supported the conclusion that the co-precipitation of $Fe^{+2}$ and $Fe^{+3}$ ions produced magnetite as a by-product (Patrikiadou et al., 2015; Gãmez et al., 2020), further supported by the blackish-brown colour of the sample (Peternele et al., 2014; Samrot et al., 2018; Gãmez et al., 2020). The results for MAGS-CTS are characteristic of a material with a spinel structure, with literature indexing the observed peaks at 2θ = 29º, 3 º, 2º, and 5 º to correspond to (220), (311), (400), and (422) hkl planes (Hoa et al., 2009; Gãmez et al., 2020). It was expected that with the addition of chitosan, new peaks would become visible within the XRD structure. Samrot et al. (2018), produced a similar result, showing peaks with only slight shifts upon addition of chitosan to the magnetic particles.

The average crystalline size was estimated through the Scherrer equation (*Eq. 3*), as stated in section 2.3.3.6. CTS and MAGS-CTS results estimate the crystallite size of the particles at between 8 and ±12 nm – classifying both CTS and MAGS-CTS as nanoparticles (Thamilarasan et al., 2018; Eddya et al., 2020).

XRD analysis of CTS confirmed that chitosan was activated by glutaraldehyde and that a successful enzyme immobilisation occurred to produced nanoparticles. The MAGS-CTS result was less conclusive regarding validation of the immobilisation procedure – with no major shifts in intensity or peak patterns to confidently state that the enzyme immobilisation was successful.

SEM imagery facilitated the visual confirmation of changes in the surface morphology for CTS immobilisation (Wang et al., 2006; Kulkarni et al., 2007; Li et al., 2013). SEM based imagery of CTS have reported varied results, ranging from rough and porous to spherical and smooth (Wang et al., 2006; Kulkarni et al., 2007; Li et al., 2013). A rough morphology was observed within this study, increasing with each immobilisation step, potentially an outcome of the addition of free aldehyde groups by glutaraldehyde and subsequent enzyme attachment (Li et al., 2013; Kim and Lee, 2019).

After immobilisation, CTS showed successful reusability for six cycles, with a 43.23% decrease observed after cycle 9. MAGS-CTS experienced a 63.74% decrease after cycle 1. There are various possible reasonings for this, but one could be that the binding of the enzyme was not sufficient to support a second cycle. Various results of recyclability are depicted in literature, with CTS and MAGS-CTS tested on average to between 6 and 16 cycles (Sànchez-

Ramírez et al., 2017; Nguyen et al., 2019; Podrepšek et al., 2020; Mohapatra, 2021; Jonović et al., 2022; Sadaqat et al., 2022). The success of reusability has been largely allocated to the immobilisation procedure utilised, with further variation possibly being a result of changes in immobilisation procedure (Kim and Lee, 2019; Nguyen et al., 2019; Jonović et al., 2022). These can be small changes such as a thorough washing procedure for clearing catalytic sites – a possible cause for the fluctuation at cycle 4 for the CTS (Figure 2.6A) (Kim and Lee, 2019). Possible causes for the lack of reusability for MAGS-CTS could be allocated to insufficient binding of the enzyme to the solid carrier, an insufficient chitosan coat, or magnetite inhibiting the enzymatic activity of the enzyme (Zucca and Sanjust, 2014), the above reasons were supported by FTIR (Figure 2.2B) and XRD (Figure 2.3B).

Temperature optimum studies (section 2.3.5.1) with the free (Figure 2.7A), CTS (Figure 2.7B), and MAGS-CTS (Figure 2.7C) enzymes indicated an identical optimum temperature of 60ºC. This result was in agreement with the literature, as both the free and immobilised forms of endo-1,4-β-mannanase typically function optimally between 50ºC and 75ºC (Lisboa et al., 2006; Van Zyl et al., 2009; Ariandi et al., 2015; Liu et al., 2018; Mohapatra, 2021). It is possible for immobilised enzymes to maintain enhanced stability with regards to changes in pH and temperature; however, this study showed optimum temperature remained unaffected after immobilisation (Guzik et al., 2014; Nadaroglu, and Sonmez, 2016; Shalaby et al., 2017; Mohapatra, 2021; Jonović et al., 2022; Sadaqat et al., 2022).

Endo-1,4-β-mannanase derived from *A. niger* has been previously described as a thermostable enzyme (Harnpicarnchai et al., 2016), with literature suggesting that the covalent immobilisation of an enzyme facilitates an increase in thermostability (Blibech et al., 2011; Sadaqat et al., 2022). This study showed that the free (Figure 2.7D) and CTS (Figure 2.7E) enzymes displayed no difference in thermostability, maintaining a high relative activity with storage up to 6 hours – similar to what is seen in literature (Harnpicarnchai et al., 2016). The MAGS-CTS (Figure 2.7F) was less thermostable, losing more than 50% of the relative activity after the first 30 minutes. This could have possibly been caused by the immobilisation altering the structural characteristics of the enzyme (Arunrattanamook et al., 2020). Immobilisation of CTS failed to enhance the thermostability of the enzyme, illustrating a thermostability similar to the free enzyme. This was unlike the results of MAGS-CTS, which showed a decrease in the enzymes thermostability.

Investigating the optimal pH for enzymatic hydrolysis (section 2.3.5.2, Figures 2.8G – H), it was established that the CTS (Figure 2.7H) and MAGS-CTS (Figure 2.7I) preferred more acidic conditions (pH 3.0), with the free enzyme (Figure 2.7G) favouring a pH of 5.0 – 6.0. Endo-1,4-β-mannanases typically prefer acidic conditions, with literature showing the free enzyme functions optimally between pH 3.0 and 5.5 (Lisboa et al., 2006; Van Zyl et al., 2009; Yoo et al., 2015; Sadaqat et al., 2022). The reduced pH benefits industrial use - decreasing the potential for microbial contamination (Rebroš et al., 2007). A change in optimal pH after immobilisation is well documented in the literature (Panwar et al., 2017; Jonović et al., 2022; Sadaqat et al., 2022).

The kinetic analysis of the free enzyme, CTS and MAGS-CTS (Figure 2.8A-C and Table 2.2) showed that the immobilisation both positively and negatively affected the enzymes catalytic efficiency. The positive attributes were visualised through the $K_M$ of the CTS (7.74 mM) and MAGS-CTS (4.96 mM) being lower than that of the free enzyme (8.44 mM), illustrating an increased affinity for the substrate for the enzymes' active sites.

Adverse kinetic attributes, such as a subsequential decrease in the $V_{max}$, $k_{cat}$, and $k_{cat}/K_M$ values after immobilisation, described the catalysis as unproductive. The activity of free enzyme was more in line with what is reported in literature, describing a more productive hydrolysis reaction and product formation with LBG as a substrate (Bien-Cuong et al., 2009; Liao et al., 2014; Yoo et al., 2015; Zhou et al., 2018; Ratnakomala et al., 2022). The success of hydrolysis was reflected in the $k_{cat}$ of the free enzyme (5536.0 $s^{-1}$). The above results, with regard to physicochemical characteristics and kinetic parameters, are likely caused by a shift in enzyme shape after binding and/or the influence of the surface it binds to (Rebroš et al., 2007; Blibech et al., 2011, Panwar et al., 2017; Neira and Herr, 2018; Dhiman, et al, 2019; Mohapatra, 2021; Ramírez-Ramírez et al., 2022; Sadaqat, et al., 2022). This, in turn, confirmed that the free enzyme is the most efficient when hydrolysing LBG, followed by CTS.

The storage stabilities of the CTS and MAGS-CTS were assessed and showed that 27% relative activity was lost after 120 h of storage at 4°C. The immobilisations of CTS and MAGS-CTS were based on covalent interactions, as confirmed previously by FTIR analysis (Figure 2.2A and Figure 2.2B). These are strong interactions which prevent detachment or shifting that might affect enzyme activity (Lee et al., 2020). In previously conducted studies, long-term storage of an immobilised enzyme was achievable, maintaining 80% relative activity after 20 days of storage – far outcompeting the free enzyme (Jankowska et al., 2019).

TLC analysis of the free, CTS, and MAGS-CTS enzymes confirmed the production of M2, M3, M4, and M6; with low quantities of M1 produced for the free and CTS enzymes – which correlated with results stated in the literature (Zahura et al., 2010; Kim et al., 2018; Ratnakomala et al., 2022; Sadaqat et al., 2022). The production of M1 requires 1,4-β-mannosidase activity, allowing the enzyme access to internal glycosidic bonds of the mannan backbone (Liao et al., 2014; Kim et al., 2018; Sadaqat et al., 2022). From the results obtained in Figure 2.10, it could not be concluded with confidence that mannose was a product. However, this could perhaps be confirmed with the assistance of HPLC.

HPLC analysis confirmed the presence of M2, M3, and M4, with no evidence of M6 being present within the sample. This result illustrates that the M6 detected in the TLC analysis could have been a mannooligosaccharide with galactose branches – however, it could be confirmed that it was not M6. It was also confirmed that M1 was present after hydrolysis at low levels for the free enzyme and CTS hydrolysis (Liao et al., 2014; Kim et al., 2018). Although this activity is not commonly observed, it has been described by Soni et al. (2016) in regard to a mannanase from an *Aspergillus* species – supporting the results of M1 production within this study. *Saccharomyces cerevisiae,* expressing the gene for β-mannanase from *A. sulphureus*, was also shown to be successful in the hydrolysis of mannan substrates, with hydrolysis products of M1-M6 (Liu et al., 2018). A study by Liu et al. (2018) showed that M1 and M5 were present at the lowest concentrations after hydrolysis.

## 2.6 Conclusion

The endo-1,4-β-mannanase derived from *A. niger* was successfully immobilised onto A-CTS, with confirmation of a covalent immobilisation by FTIR and XRD analysis. The MAGS-CTS was partially immobilised, although we could not provide evidence of a covalent attachment in this study. The immobilised and free enzymes displayed identical thermostability and temperature optima to those displayed by the free enzyme at 60°C. However, an optimum pH in the acidic range for the CTS and MAGS-CTS enzymes suggests a change in conformation after immobilisation. The results from the reusability and storage stability analysis supported the use of the CTS-immobilised enzyme within an industrial setting. Poor retention of catalytic activity suggests that further optimisation experiments should be conducted for the MAGS-CTS enzyme. The qualitative and quantitative analysis of MOS showed that the CTS and free enzymes displayed no difference in catalytic activity in terms of products produced, with a

slight differentiation with regard to MAGS-CTS. The immobilised enzymes differed with regards to their kinetic parameters and their ability to produce high concentrations of MOS - compared to the free enzyme. The CTS and MAGS-CTS enzymes were analysed for potential use against SBM in Chapter 3, with the preliminary results in this chapter suggesting that the CTS immobilised enzyme is the more suitable option.

# CHAPTER 3: THE HYDROLYSIS OF SOYBEAN MEAL FOR THE EFFECTIVE PRODUCTION OF PREBIOTIC MOS BY IMMOBILISED AND FREE ENDO-1,4-β-MANNANASE

## 3.1 Introduction

SBM is an essential additive to agricultural feedstocks, mainly for its delivery of essential amino acids and high protein content (Frempong et. al., 2019). Although nutritionally beneficial, SBM contains various ANFs, which have been found to adversely affect the health and weight of poultry (Choct et. al., 2010; Vangroenweghe et al., 2021). The ANFs present within SBM appear in various forms; and although they are detrimental to poultry health, many methods have been investigated to mitigate their negative effect (Sinha and Khare, 2017; White et al., 2021). An ANF termed β-mannan has become a topic of increasing interest due to its presence in animal feed, but, unlike many other ANFs, this compound cannot be easily denatured with heat treatment (White et al., 2021). It is for this reason that employing the use of exogenous enzymes is being investigated in this study.

The hemicellulosic portion of SBM contains various proportions of soluble and insoluble polysaccharides (Choct et al., 2010; Karr-Lilienthal, et. al., 2005). The sugar composition of SBM differs between regions – due to soil quality and climate (Ibáñez et al., 2020). For this reason, a sugar composition analysis is important to validate that the SBM being analysed possesses a sufficient quantity of sugars, which, in this case, are the ANF, β-mannan. This analysis can be achieved by acid hydrolysis using various strategies, such as the trifluoracetic acid (TFA) method or the hydrochloric acid (HCl) method. These treatments break the structures down into monosaccharides, facilitating accurate carbohydrate determination via assay kits or high-performance liquid chromatography equipped with a refractive index detector (HPLC-RID).

Increasing evidence has suggested that the application of enzymes such as endo-1,4-β-mannanases can improve the nutritional value of SBM-based diets – to break down the ANFs (such as mannans) and release prebiotic compounds (Saeed, et, al., 2019: White, et. al., 2021). These enzymes are endo-hydrolases, responsible for the random cleavage of internal β-1,4-glycosidic bonds in the backbone of galactomannans to produce MOS – short chain residues with prebiotic characteristics. Galactomannans are located in the cell walls of the SBM

structure (Wang et al., 2013; Erdaw, et, al., 2016; Sharma et al., 2020). It is therefore expected that effective hydrolysis of the mannan portion of SBM result in the effective breakdown of SBM cell walls. To ensure that this is the case, SEM and FTIR techniques can be employed to analyse the change in structure both physically and chemically. SEM analysis attempts to validate hydrolysis visually, investigating various hydrolysis forms of SBM and how a change in structure could have been caused by the hydrolysis of the galactomannans within the cell walls. FTIR analysis provides a more in-depth view of how the structure of the SBM changes with regards to shifts in functional groups throughout the hydrolysis procedure.

For an enzymatic process to be practical for industrial use, it is important to determine the kinetic parameters of the hydrolysis reaction. SBM contains galactomannan in an insoluble form, a characteristic likely to have a negative effect on the catalytic capabilities of the free and immobilised enzymes (Singh et al., 2013; Vaghari et al., 2015). Recyclability is another essential parameter to ensure that enzyme reactions are cost-effective for long-term use within the agricultural industry. For effective recyclability within a reaction utilising SBM as a substrate, a practical method is required to remove the enzyme from the reaction mixture (Puri and Abraham, 2016). This will allow the enzyme to be washed and reused, increasing the quantity of reducing sugars typically produced from a single dose of the enzyme during a reaction (Bilal et al., 2018). This removal may be facilitated via various methods, such as centrifugation or a permanent magnet, however this is dependent on the matrix.

With the hydrolysis of the galactomannan portion of SBM, there is potential for varying forms of MOS to be synthesised. This is as a result of the random hydrolysis of the β-1,4-glycosidic linkage of the galactomannan backbone (Malgas et al., 2015a; Malgas et al., 2015b; Sharma et al., 2018). This can be evaluated using techniques such as TLC and HPLC, for determining and quantifying MOS residues originating from LBG. It has been reported in literature that some forms of mannooligosaccharides (M2-M5) are more effective for prebiotic utilisation (Srivastava and Kapoor, 2017; Tiwari et al., 2020; Zhang et al., 2021). SBM is a complex substrate, comprised of various sugars which can promote the growth of probiotic bacteria (Hazrati et al., 2019). Therefore, along with the testing of MOS residues, it is important to establish whether the SBM-produced sugars are effective prebiotics. This can be established by analysing the cell viability and density of various probiotics exposed to SBM-produced sugars, relative to a positive and negative control (Magengelele et al., 2021). The probiotics *Lactobacillus bulgaricus, Streptococcus thermophilus*, and *Bacillus subtilis*, have each been established to utilise M S, to varying extents (Šušković et al., 2010; Dobson et al., 2012), with

evidence of antimicrobial production after MOS digestion (Jamalifar et al., 2011; Joseph et al., 2013). The utilisation of prebiotics with the goal to produce antimicrobials from probiotic bacteria is a major strategy for finding antibiotic alternatives to defend poultry from pathogenic bacteria (Markowiak and Śliżewska, 2018). This would create a healthier gut microbiome, promoting nutrient uptake whilst preventing the colonisation of pathogenic bacteria (Hazrati et al., 2019; Kango et al., 2022).

Probiotics utilise compounds such as MOS, releasing short-chain fatty acids and branched amino acids as by-products (Kango et al., 2022). These are secondary metabolites with the potential to increase the overall health of the poultry gastrointestinal tract by inhibiting the growth of pathogenic bacteria (Šušković et al., 2010; Dobson et al., 2012; Kango et al., 2022). With the demand for South Africa to seek alternatives to AGPs, the search for a sustainable replacement to promote the health and growth of poultry is of vital importance. The effect of probiotic secondary metabolites on the growth of pathogenic bacteria be established according to the Resazurin antibacterial assay, previously described by Elshikh, et al, (2016). This study entails inoculating pathogenic bacteria (*Escherichia coli, Staphylococcus aureus* and *Klebsiella pneumoniae*); in their growth phase, with filtered probiotic extract. Under defined growth parameters, relative to a positive and negative control, it can then be established if the viability of pathogenic bacterial cells is affected after exposure to secondary metabolites produced from probiotics fed SBM-produced sugars (Elshikh, et al, 2016).

Chapter 3 focused on utilising an immobilised and free endo-1,4-β-mannanase for the effective hydrolysis of SBM. This investigated the catalytic capabilities of the enzymes against the complex, insoluble substrate, and the potential for industrial application in terms of recyclability. This study explored the benefits of an SBM-hydrolysis reaction, specifically examining whether sugars produced from SBM can stimulate probiotic growth to a level that results in antimicrobial production.

## 3.2 Hypothesis, aims and objectives

### 3.2.1 Hypothesis

The immobilised β-mannanase produces MOS of similar quantity and type (diversity) as the free enzyme after hydrolysis of β-mannans from SBM; these MOS have a prebiotic effect in stimulating probiotic growth.

### 3.2.2 Aims

This part of the project compared the prebiotic effects of the MOS produced from immobilised β-mannanases to those of the MOS produced using a free enzyme.

### 3.2.3 Objectives

To achieve this aim, the following objectives were addressed:

a) To generate M S via the enzymatic hydrolysis of β-mannan from SBM using free and immobilised endo-1,4-β-mannanases;
b) To evaluate the recyclability of the immobilised enzyme with SBM;
c) To analyse the M S obtained from the enzymatic hydrolysis of β-mannan from SBM (in terms of the diversity and composition of the MOS species); and
d) To evaluate the potential prebiotic effects of the MOS generated.

## 3.3 Methods and Materials

### 3.3.1 Materials

SBM was purchased from Rayner General Agencies (Makhanda, EC, South Africa). All other chemicals used were purchased from Sigma Aldrich (St. Louis, MO, USA).

### 3.3.2 Mannanase activity assay

#### 3.3.2.1 Endo-1,4-β-mannanase activity assay with SBM

The activity of endo-1,4-β-mannanase was determined with 50 mM citrate buffer (pH 5.0) and 6% (w/v) SBM that was prewetted for 2 hours at 90°C. The reaction was conducted at 55°C for 48 hours. The enzymatic activity was terminated by incubation at 100°C for 5 minutes, followed by centrifugation at 16 060 ×*g* for 5 minutes. The enzyme activity was determined by measuring the amount of reducing sugars produced (according to section 2.3.2.2). One unit of enzyme activity was defined as the amount of enzyme that released 1 μmol of reducing sugars per minute under the assay conditions specified. All assays were performed in triplicate, and each reaction was repeated. Values were reported as means ± standard deviations.

### 3.3.3 Examination of SBM

#### 3.3.3.1 SBM substrate composition analysis

The total carbohydrates of SBM were determined using a 2 M TFA hydrolysis protocol as described previously by Daub et al. (2020). A 1% (w/v) SBM sample and a positive control

(Avicel) was prepared and hydrolysed at 100ºC for 4 hours, and, thereafter, evaporated in a FreeZone 2.5, CentriVap trap and CentriMap DNA concentrator (Labconco, Limassol, Cyprus) at 80ºC for 6-hours. The monosaccharides were quantified enzymatically according using Megazyme$^{TM}$ sugar kits (GOPOD, K-GLUC, K-XYLOSE, K-ARGA and K-MANGL).

#### 3.3.3.2 Optimisation of endo-1,4-β-mannanase activity assay with SBM

The activity of endo-1,4-β-mannanase (0.025-0.6 mg/ml) was determined in 50 mM citrate buffer (pH 5.0) and 0.5-8% (w/v) SBM that was prewetted for 0.5-6 hours at 90°C. Hydrolysis was conducted at 55°C for 0 - 96 hours; thereafter, the enzymatic activity was terminated by incubation at 100°C for 5 minutes. SBM-produced sugars were collected by centrifugation at 16 060 ×*g* for 5 minutes. The enzyme activity was determined by quantification of the reducing sugars (according to section 2.3.2.2). One unit of enzyme activity was defined as the amount of enzyme that released 1 μmol of reducing sugars per minute under the assay conditions specified. All assays were performed in triplicate, and each reaction was repeated. Values were reported as means ± standard deviations.

#### 3.3.3.3 FTIR analysis of SBM

FTIR analysis was conducted for ground SBM, prewetted SBM, and hydrolysed SBM, under the optimum conditions determined in section 3.3.3.2. This method was conducted as described in section 2.3.3.5, with slight modifications in accordance with the analysed samples.

#### 3.3.3.4 SEM analysis of SBM

SEM analysis was conducted for prewetted SBM and hydrolysed SBM, according to the method previously described in section 2.3.3.7.

### 3.3.4 Immobilisation of endo-1,4-β-mannanase

The immobilisation procedure of CTS and MAGS-CTS was performed as previously described in sections 2.3.3.1 and 2.3.3.2, respectively.

### 3.3.5 Kinetic parameters of immobilised and free endo-1,4-β-mannanases with SBM

The kinetic parameters were determined for the free, CTS, and MAGS-CTS immobilised enzymes using SBM as a substrate in a concentration range of 30 - 80 mg/ml in 50 mM citrate buffer (pH 5.0), with assay conditions as described in section in 3.3.2.1. The Michaelis–Menten constant, $K_M$, and maximum rate, $V_{max}$, were determined from non-linear regression analysis, performed using GraphPad prism 9.0 software.

### 3.3.6 Recyclability of immobilised endo-1,4-β-mannanase with SBM

CTS and MAGS-CTS immobilised endo-1,4-β-mannanases were resuspended in 50 mM citrate buffer (pH 5.0). A reaction was then conducted according to section 3.3.2.1, with slight modification. At the end of the reaction, the immobilised mannanase was not heated to 100°C but rather washed thrice with 50 mM citrate buffer (pH 5.0). Next, a fresh 6% (w/v) SBM was added, and the activity was tested again according to section 3.3.2.1. The reducing sugar concentration produced from the immobilised mannanase was analysed after each cycle according to section 2.3.2.2. All assays were performed in triplicate within a single trial, and the process was repeated. Values were reported as means ± standard deviations.

### 3.3.7 Quantitative and qualitative analysis of MOS residues with SBM

#### 3.3.7.1 TLC analysis of MOS produced from SBM derived from immobilised and free endo-1,4-β-mannanases

The substrate [6% (w/v) SBM] was hydrolysed by the free, CTS, and MAGS-CTS immobilised endo-1,4-β-mannanases derived from *A. niger* (the commercial enzyme, as described in section in 3.3.2.1). The samples were then analysed on TLC, according to the previously described method in section 2.3.6.1.

#### 3.3.7.2 HPLC analysis of MOS derived from immobilised and free endo-1,4-β-mannanases

The substrate [6% (w/v) SBM] was hydrolysed by the free, CTS, and MAGS-CTS immobilised endo-1,4-β-mannanases derived from *A. niger* (as described in section in 3.3.2.1). The samples were then analysed via HPLC analysis according to the previously described method in section 2.3.6.2.

### 3.3.8 Evaluation of the prebiotic potential of SBM-derived MOS

The prebiotic activity of SBM-produced MOS generated by free and CTS immobilised endo-1,4-β-mannanases was evaluated according to the method by Magengelele et al. (2021). *In vitro* fermentation of these prebiotics was carried out by probiotic bacteria (*S. thermophilus, B. subtilis* and *L. bulgaricus*) grown in M9 media (2.5 g/L NaCl, 5 g/L $NH_4Cl$, 15 g/L $KH_2PO_4$ at pH 7.4). Each strain was inoculated to an initial absorbance ($OD_{600}$) of 0.1 and cultivated at 37°C for 7 hours. Batch fermentation was carried out in M9 media which was supplemented with 0.05% MOS derived from the hydrolysis of SBM with immobilised and free endo-1,4-β-mannanases. Negative controls were prepared (bacteria and deionised water) and positive

controls (Bacteria and Glucose) were prepared, and all experiments were completed as biological duplicates, in triplicate.

#### 3.3.8.1 Effects of MOS on cell growth

The viability of the cultured bacterial cells was determined by adding 50 µl of 0.02% (w/v) of *p*-iodonitrotetrazolium chloride (INT) into a 96-well microtiter plate (Lasec, Cape Town, WC, South Africa) containing 200 µl of the cultured bacterial sample. INT is hydrolysed by metabolically active cells to formazan, indicating the proportion of viability by a change in colour. The plate was incubated for 1 hour at 27°C and the absorbance was measured at 490 nm using a Synergy MX microplate reader (Biotek, Winooski, VT, USA).

#### 3.3.8.2 Effects of MOS on cell density

Cell density was established by centrifuging (16 050 ×*g*, 3 minutes) 1 ml of bacterial sample, removing the supernatant, and resuspending in 250 µl of phosphate buffer (pH 7.4). These were completed to evaluate bacterial cell growth. The samples were placed in a 96-well microtiter plate (Lasec, Cape Town, WC, South Africa) and the absorbance (OD600) was measured using a Synergy MX microplate reader (Biotek, Winooski, VT, USA).

### 3.3.9 Resazurin antibacterial assay

The resazurin antibacterial assay was completed according to the method by Elshikh, et. al. (2016). This method evaluated the inhibitory effect of secondary metabolites produced from the probiotic digestion of SBM-produced sugars. Before the method could be attempted, the bacterial log phases of *E. coli*, *S. aureus*, and *K. pneumonia* were established (Appendices, Figure G).

#### 3.3.9.1 Determination of bacterial log phase

Using a sterile method, bacterial strains were plated on Luria Broth (LB) Agar (13 g/L Agar, 10 g/L Tryptone, 10 g/L NaCl, 5 g/L Yeast) for 16 hours at 37°C. A single colony from each bacterium was chosen and inoculated into 5 mL of LB broth (10.5 g/L Tryptone, 10.5 g/L NaCl, 5.25 g/L Yeast Extract) and incubated with agitation (16 hours, 160 rpm, 37°C). Of the overnight culture, 1 mL was inoculated into 100 mL of sterile LB broth and incubated for 7-hours (160 rpm, 37°C), taking the $OD_{600}$ readings every hour. The $OD_{600}$ readings were then plotted against incubation time (minutes); where the most linear portion of the graph was used to indicate the exponential growth phase (Log phase) of the bacteria.

### 3.3.9.2 Preparation of bacterial cultures and extracts for antimicrobial analysis.

Bacterial cultures were prepared as described above (section 3.3.9.1) and grown to log phase. The log phase bacterial cultures were then diluted 1:50 in LB broth. Resazurin was prepared in a 0.135 mg/ml concentration in 50 mM PBS buffer (pH 7.4) and covered to protect from light exposure. All samples were obtained from the experiment in section 3.3.7, where samples were centrifuged and stored at -20°C. All samples and resazurin were filter sterilised and stored at 4°C before use. The assay was performed by combining 20 µL of sample extract, 20 µL of diluted bacterial culture and 160 µL of LB Broth into a 96-well plate. Three controls were employed: a positive control of untreated bacterial cells, a negative control of bacterial cells treated with 50µg/ml kanamycin and a contamination control of LB broth. The plates were covered and incubated at 37°C for 24 hours with agitation (70 rpm). After incubation, the cells were combined with 20 µL of resazurin and incubated for 15 minutes. The fluorescence was read at an excitation wavelength of 560 nm and an emission wavelength of 590 nm. The equation below was used to calculate percentage viability, with a decrease in cell viability indicating antibacterial potential:

(4) $$Percentage\ Viability\ (\%) = 100[(A_i - A_f)/(A^+ - A_f)]$$

($A_i$): Absorbance of sample; ($A_f$): Absorbance of the background reading; ($A^+$): Absorbance of the positive control. All experiments were completed in biological replicate and in technical triplicate.

## 3.4 Results

### 3.4.1 SBM composition analysis and enzymatic hydrolysis

#### 3.4.1.1 Sugar composition of SBM

In order to confirm the presence of mannan in SBM, a substrate composition analysis was completed, as described in section 3.3.3.1 and is displayed in Table 3.1 below.

**Table 3.1: Chemical composition analysis of SBM (percentage dry mass (%))**

| Sugar Composition | Proportion of sugars (%) |
|---|---|
| **Total Reducing Sugars[a]** | 10.153 ± 0.010 |
| **D-Xylose[b]** | 0.056 ± 0.0001 |
| **L-Arabinose[b]** | 2.643 ± 0.04 |
| **D-Galactose[b]** | 0.265 ± 0.04 |
| **D-Fructose[b]** | 0.484 ± 0.002 |
| **D-Mannose[b]** | 0.366 ± 0.002 |
| **D-Glucose[b]** | 4.116 ± 0.03 |

*[a]-DNS method, [b]-Megazyme sugar kits. The data is represented as the means ± SD (n=3).*

The total composition of reducing sugars in 1 mg/ml of SBM was 10.153% ± 0.010. These results showed that D-mannose constituted 0.366% ± 0.002 (Table 3.1) of the total composition in SBM. The bulk of the sugars comprised D-glucose and L-arabinose, taking up 4.116% ± 0.03 and 2.643% ± 0.04, respectively (Table 3.1). D-xylose possessed the lowest percentage composition with 0.056% ± 0.0001. The proportions of D-mannose in SBM were relatively low but considered to be sufficient to proceed with further enzymatic experimentation.

### 3.4.1.2 Optimisation of SBM hydrolysis by endo-1,4-β-mannanase derived from *A. niger*

To ensure that the enzymatic hydrolysis of SBM and the endo-1,4-β-mannanase was functioning optimally, the optimum enzyme reaction conditions were established for the free enzyme according to section 3.3.3.2. Assay optimisation confirmed the optimal conditions for time of hydrolysis (Figure 3.1A), prewetting duration (Figure 3.1B), substrate concentration (Figure 3.1C), and enzyme concentration (Figure 3.1D).

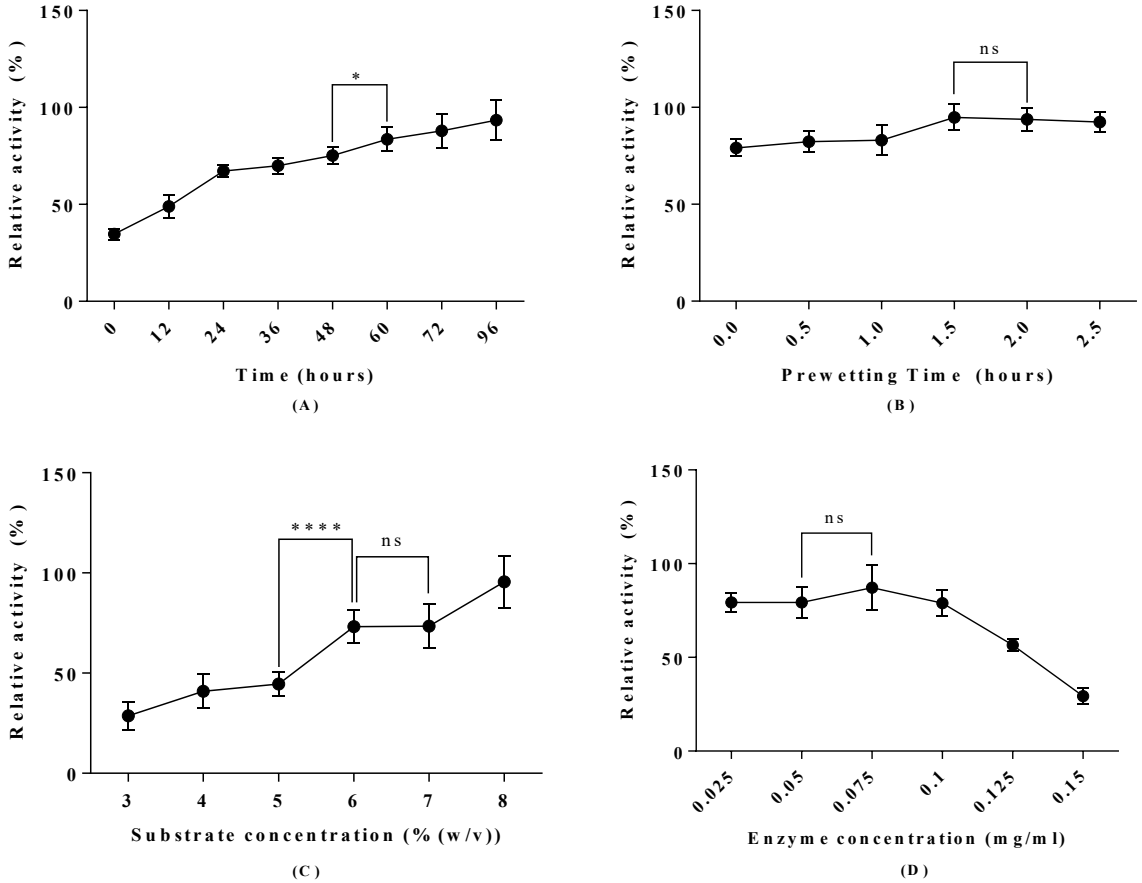


**Figure 3.1:** Optimisation of (A) hydrolysis time (0 – 9 hours), (B) prewetting conditions (0 – 2.5-hours, 90°C), (C) SBM concentration (3-8% (w/v)) and (D) enzyme concentration analysis (0.025 mg/ml – 0.15 mg/ml). A relative activity of 100% represented ±0.48 mg/ml of reducing sugars. Statistical analysis was conducted using *t*-test to compare the relative activity (%) of the various optimisation conditions, key: ns ($p > 0.05$), * ($p \leq 0.05$), **** ($p \leq 0.0001$).

A study of the effect of hydrolysis time (Figure 3.1A) showed that 48 hours was adequate time for producing a sufficient quantity of reducing sugars. The duration of substrate prewetting

(Figure 3.1B) was used to enhance the accessibility of the enzyme to the galactomannan portion of SBM; from this analysis, it was seen that 1.5 hours of exposure to 90°C was sufficient to promote the release of reducing sugars. Increasing the substrate concentration to 6% (w/v) SBM (Figure 3.1C) produced a sufficient quantity of reducing sugars - at higher substrate concentrations, the increase in reducing sugars was due to leaching from the substrate and not enzymatic hydrolysis. A concentration of *A. niger* endo-1,4-β-mannanase (Figure 3.1D) of 0.05 mg/ml was shown to be optimal. This was determined after statistical analysis to be a 0.05 mg/ml concentration of enzyme, as it was found to be not significantly different to the results obtained for hydrolysis with a 0.075 mg/ml enzyme concentration ($P = 0.2672$).

### 3.4.1.3 FTIR analysis of SBM

The ground SBM, prewetted SBM, and hydrolysed SBM were analysed via FTIR to investigate whether there were any changes in functional groups throughout the hydrolysis procedure (Figure 3.2). This analysis showed prominent bands at 3342 $cm^{-1}$ (OH and N-H stretching vibration), 2954 $cm^{-1}$ (C-H stretching vibrations), 1760 $cm^{-1}$ (COOH), 1581 $cm^{-1}$ (amide II, C-N stretching vibration), 1268 $cm^{-1}$ (amide III, C-N stretching and N-H bending vibrations), 1040 $cm^{-1}$ (C-O stretching vibrations) and 931 $cm^{-1}$ (β-1,4-glycosidic linkages).

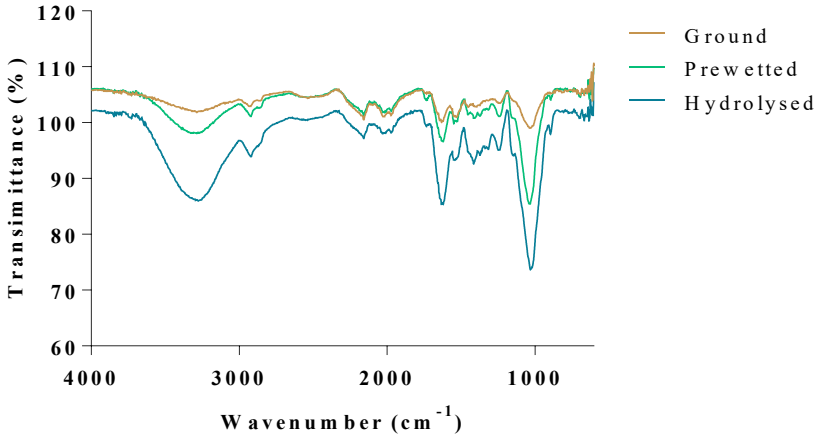


**Figure 3.2:** Comparison of FTIR spectra of ground, prewetted, and hydrolysed SBM were obtained from scans from 4000 to 600 $cm^{-1}$. Baseline and ATR corrections for penetration depth and frequency variations were carried out using Spectrum™ One software supplied with the FTIR equipment.

### 3.4.1.4 SEM analysis of SBM

The qualitative analysis of SBM cell wall structures after grinding (Figure 3.3A and Figure 3.3B), prewetting (Figure 3.3C and Figure 3.3D), and hydrolysis by endo-1,4-β-mannanase derived from *A. niger* (Figure 3.3E and Figure 3.3F) was evaluated using SEM imaging (Figure 3.3).

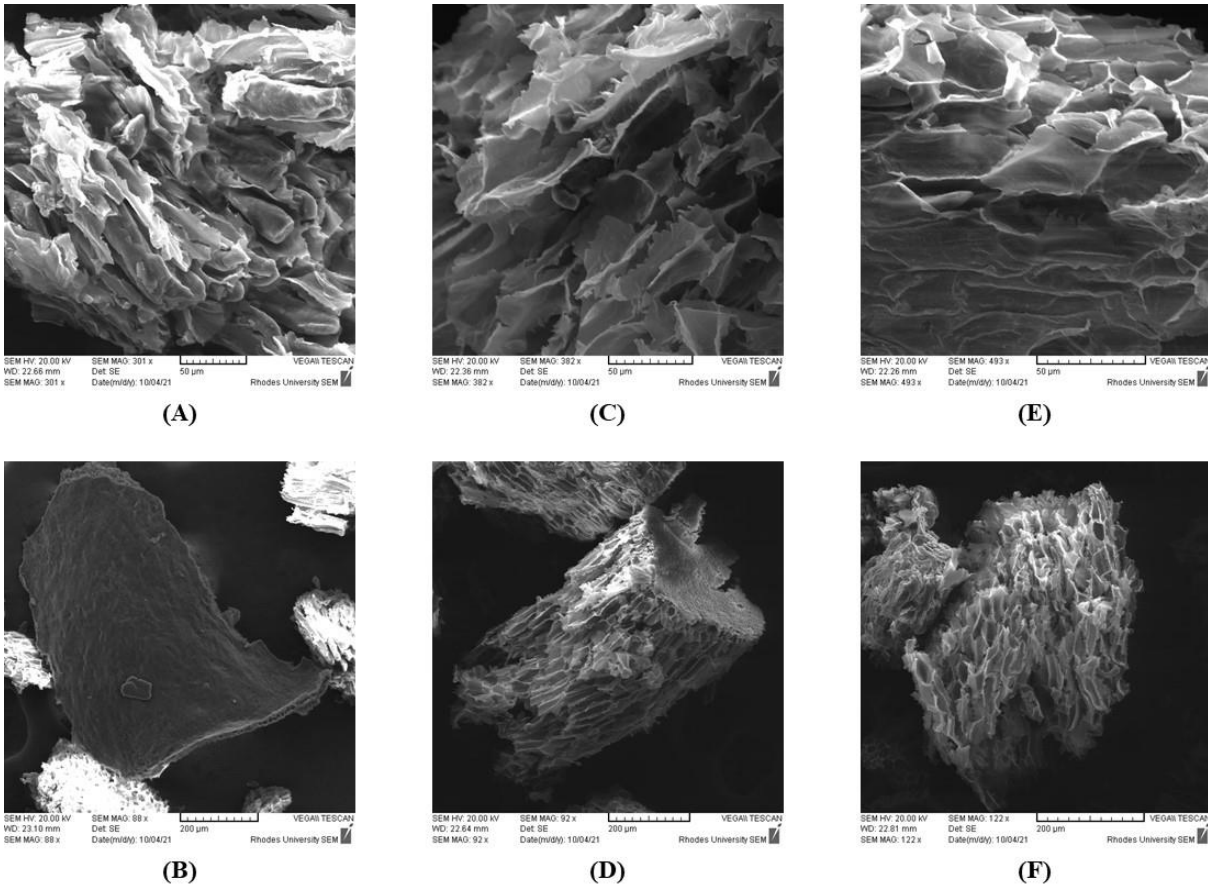


**Figure 3.3:** Scanning electron microscopy (SEM) of (A and B) ground SBM, (C and D) prewetted SBM in 50 mM citrate buffer (pH 5.0) and (E and F) hydrolysed SBM with endo-1,4-β-mannanase derived from *A. niger*. The CTS immobilised enzyme biomass was coated in gold and fixed on Quanta holders, after which the surfaces were scanned on a SEM Tescan VEGA3 working at 20 kV.

An increase in cell wall degradation in the SBM structure was experienced after each step in the hydrolysis procedure. In the ground SBM (Figure 3.3A and Figure 3.3B), cell wall compartments can be visualised, with these structures becoming broken and exposed after grinding (Figure 3.3C and Figure 3.3D) and hydrolysis (Figure 3.3D and Figure 3.3E). It should be noted that there is little difference between the imagery of the prewetted (Figure 3.3C and Figure 3.3D) and the hydrolysed (Figure 3.3E and Figure 3.3F) samples. This suggests that grinding of the SBM allowed sufficient destruction of the cell wall to allow the enzyme access to the mannan residues within.

### 3.4.2 Kinetic parameters of SBM with immobilised and free enzymes

The kinetic parameters for the free, CTS, and MAGS-CTS enzymes with SBM (Figure 3.4, Table 3.2) were determined. $K_M$ and $V_{max}$ values of 53.43 mM and 0.03099 U/mg, 10.26 mM and 0.02672 U/mg, and 21.80 mM and 0.01517 U/mg, were reported for the free, CTS and MAGS-CTS enzymes, respectively. This indicated that CTS showed the highest affinity for the substrate, while the free enzyme displayed the highest reaction velocity.

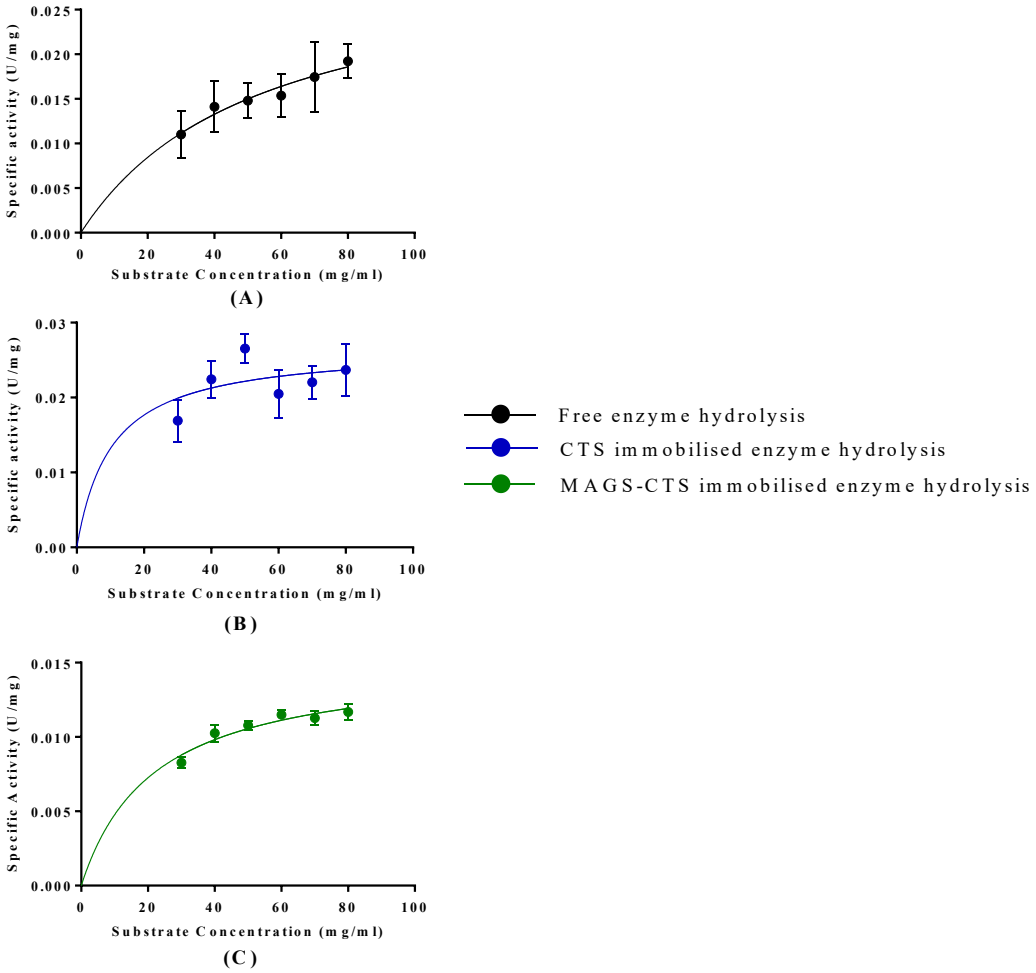


**Figure 3.4:** Michaelis-Menten kinetics of **(A)** free **(B)** CTS immobilised endo-1,4-β-mannanase and **(C)** MAGS-CTS immobilised endo-1,4-β-mannanases hydrolysing SBM (30 – 80 mg/ml) (2 hours prewetting at 90°C, 48 hours hydrolysis at 55°C). The kinetic parameters were determined at the pH and temperature optima for the free and immobilised enzymes. The values were presented as means ± SD (n = 3)

**Table 3.2:** Kinetic parameters of free and immobilised endo-1,4-β-mannanase with SBM

| **Kinetic parameters** | **Free enzyme** | **CTS** | **MAGS-CTS** |
|---|---|---|---|
| $V_{max}$ (U/mg) | 0.03099 | 0.02672 | 0.01517 |
| $K_m$ (mM) | 53.43 | 10.26 | 21.80 |
| $k_{cat}$ ($s^{-1}$) | 0.6199 | 1.006 | 0.1517 |
| $k_{cat}/K_m$ ( $s^{-1}$ $mM^{-1}$ ) | 0.0116 | 0.0981 | 0.00696 |

The $k_{cat}$ and $k_{cat}/K_m$ favoured the CTS reaction (1.006 $s^{-1}$ and 0.0981 $s^{-1}$ $mM^{-1}$ , respectively) when hydrolysing SBM as the substrate.

### 3.4.3 Recyclability analysis of immobilised enzymes

The immobilised enzymes, CTS and MAGS-CTS were analysed for their reusability (recyclability) against the 6% (w/v) SBM substrate (Figure 3.5).

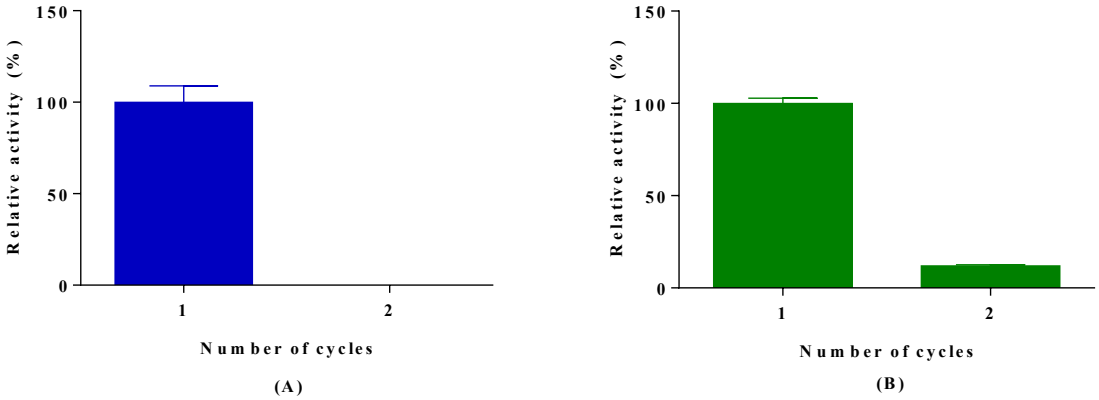


**Figure 3.5:** Recyclability of endo-1,4-β-mannanase immobilised on (A) CTS (100% set as 0.489 mg/ml) and (B) MAGS-CTS (100% set as 0.361 mg/ml) using 6% (w/v) SBM as substrate (hydrolysis parameters as described in section 3.3.6). Each value in the panel represents the means ± SD (n = 3). Relative activity (%) was used, with cycle 1 set as 100%.

The study showed that 0.489 mg/ml and 0.361 mg/ml of net reducing sugars were produced after cycle 1 of CTS reactions (Figure 3.5A) and MAGS-CTS (Figure 3.5B) reactions, respectively. After cycle 1, the CTS enzyme could not be separated from the insoluble SBM and, therefore, could not be tested for cycle 2. The MAGS-CTS enzymes, however, were recovered from the reaction mixture, washed, and reused. However, these enzyme had lost a significant amount of activity and could not be reused. The reusability of the MAGS-CTS enzyme therefore proved unsuccessful.

### 3.4.4 Qualitative and quantitative analysis of MOS residues from SBM

#### 3.4.4.1 TLC analysis of MOS derived from the hydrolysis of SBM

Thin layer chromatography was used to qualitatively analyse the MOS products from the hydrolysis of SBM via free, CTS immobilised, and MAGS-CTS immobilised endo-1,4-β-mannanases (Figure 3.6). A MOS standard containing M1, M2, M3, M4, M5, and M6 were used to identify the MOS residues produced with hydrolysis. The total sugars run on the TLC plate were quantified as 0.65 mg/ml, 0.61 mg/ml, and 0.59 mg/ml for the free, CTS, and MAGS-CTS enzymes, respectively.

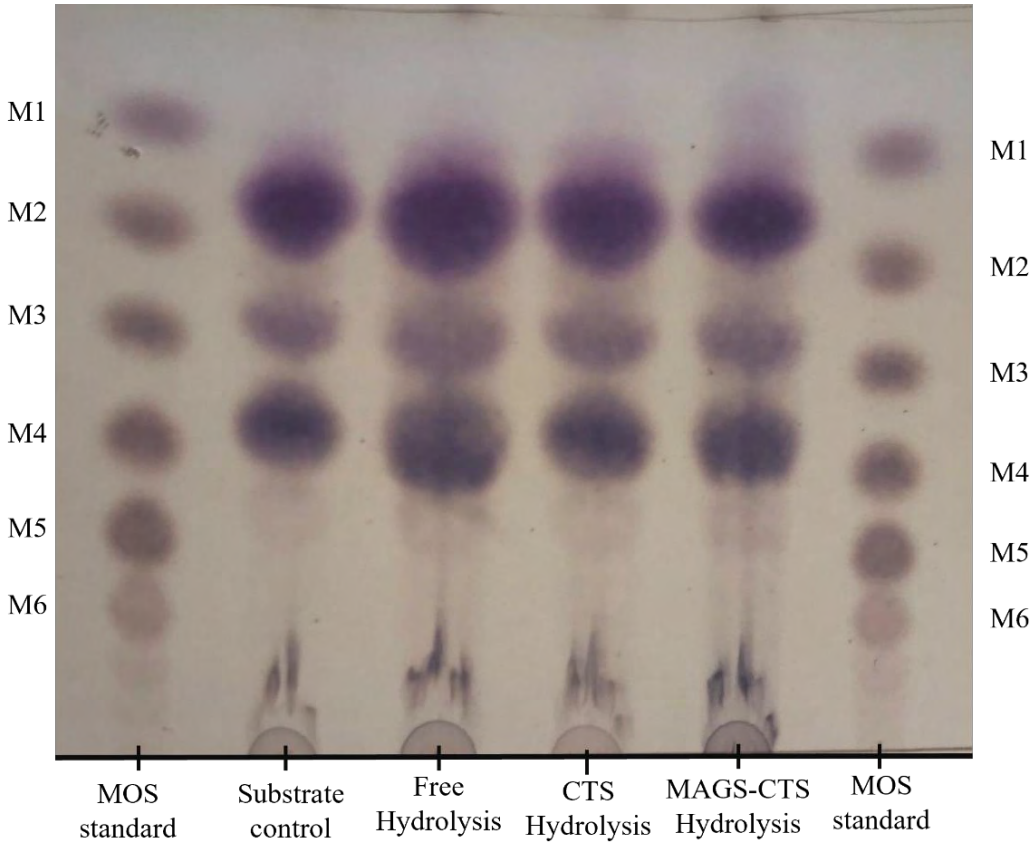


**Figure 3.6:** TLC plate of the reducing sugars produced by the free, CTS, and MAGS-CTS immobilised *A. niger* endo-1,4-β-mannanase in a reaction with 6% (w/v) SBM (48-hours, 55°C). The MOS standards represent M1 – M6 (indicated and labelled on the ladders).

The analysis of the MOS via TLC was inconclusive. Prominent bands could be seen between M1 and M2, M2 and M3, M3 and M4, and a faint band between M4 and M5. It was hypothesised that the bands indicated the presence of glucose, galactose as well as structures

composed of galactose and mannose, i.e. galactomannans (GM2 and GM3). However, the bands in the hydrolysates were all similar to that of the substrate control, indicating that little to no enzymatic hydrolysis had taken place.

### 3.4.4.2 HPLC analysis of MOS derived from the hydrolysis of SBM

HPLC was used to analyse the hydrolysis products of SBM, both qualitatively and quantitatively (Figure 3.7). HPLC standards were used to identify the MOS residues within the samples. These standards were as follows: M1 (33.601 minutes), M2 (27.919 minutes), M3 (23.254 minutes), M4 (19.946 minutes), M5 (17.481 minutes), and M6 (15.625 minutes). Standard curves (Appendices, Figure C) were constructed for each MOS standard to assist in the determination of the MOS residues.

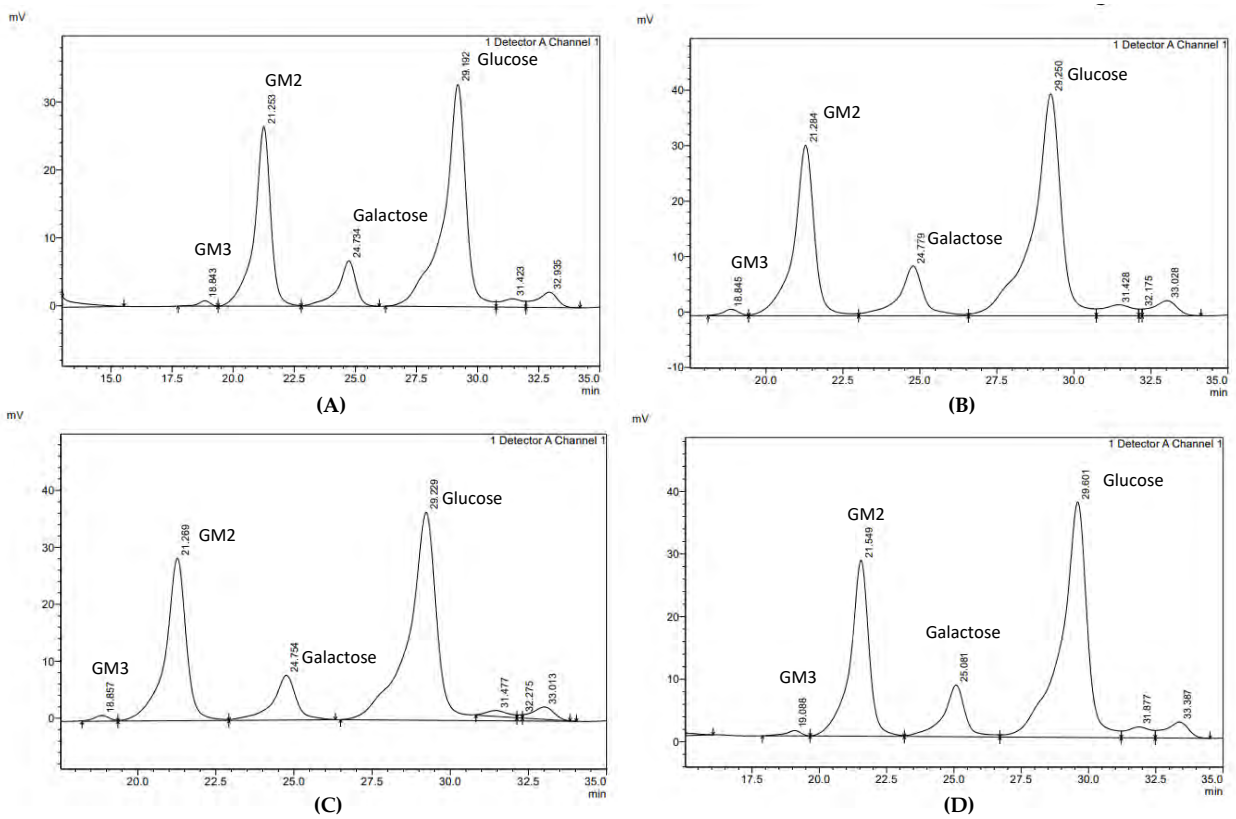


**Figure 3.7:** High-performance liquid chromatography analysis of (A) untreated 6% SBM, hydrolysed 6% (w/v) SBM (0.39 mg/ml) by (B) free (0.81 mg/ml)(Appendices, Figure D), (C) CTS (0.77 mg/ml)(Appendices, Figure E), and (D) MAGS-CTS (0.72 mg/ml)(Appendices, Figure F), endo-1,4-β-mannanase. Analysis was carried out on a Carbosep CHO 411 column, flow rate (0.26 ml/min), and a refractive index detector (RID). MOS standards were used to identify the peaks of interest (M1-M6).

An in-depth analysis of the reducing sugar content within each sample showed that no mannose residues could be identified confidently from the HPLC standards. This confirms a similar conclusion to that of the TLC plates. Three prominent peaks are distributed throughout the chromatographs, at approximately 21.5-minutes, 25-minutes, and 29.3-minutes – present in both the untreated and hydrolysed samples. These peaks were not identifiable from the MOS standards - it is suspected that these oligosaccharides may be mixtures of galactose and mannose., e.g. galactomannan as well as glucose and galactose.

### 3.4.5 The prebiotic effects of SBM-produced sugars.

The prebiotic potential of the sugars produced by the hydrolysis of SBM with free and CTS immobilised mannanases was evaluated. Figure 3.8 shows the cell viability (Figure 3.8A) and cell density (Figure 3.8B) of the probiotics because of cultivation in MOS; as well as positive (glucose) and negative (no carbon source) controls.

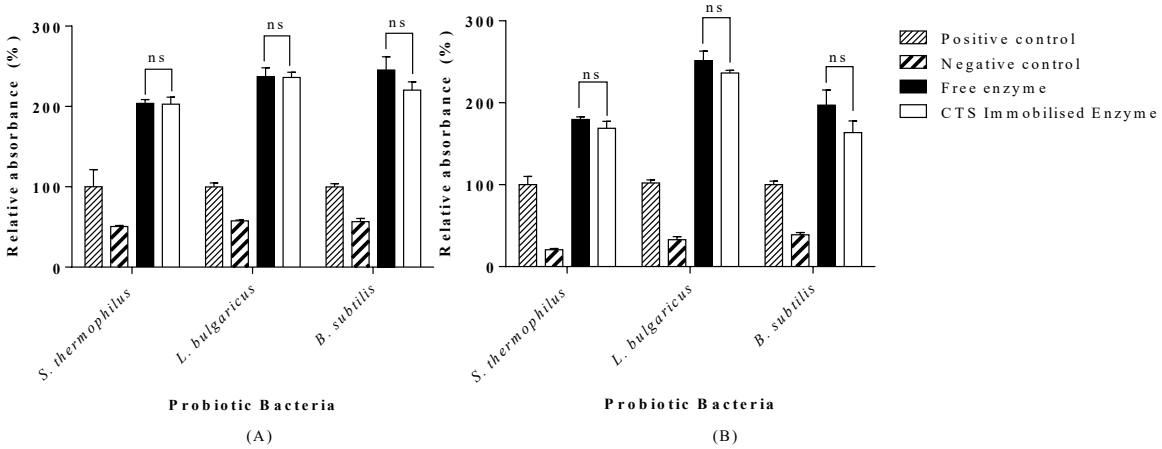


**Figure 3.8:** The evaluation of the prebiotic potential of MOS (0.155 mg/ml) generated using free and CTS immobilised endo-1,4-β-mannanase by *in vitro* fermentation by probiotic bacteria (*S. thermophilus, B. subtilis and L. bulgaricus*); (A) cell viability and (B) cell density. Statistical analysis was conducted using *t*-test for prebiotic effect of reducing sugars produced by the free and immobilised enzyme, key: ns ($p > 0.05$).

The probiotic strains, *S. thermophilus, B. subtilis,* and *L. bulgaricus* showed a significant difference in cell viability when grown on the different carbon sources, with higher survival in the presence of sugars produced from SBM by free and immobilised enzymes compared to their positive control (P = 0.0016; P <0.0001; P = 0.0001 and P = 0.0012; P < 0.0001; P = 0.0001, respectively) (Figure 3.8A). Similarly, the cell density study (Figure 3.8B) showed that

probiotics amassed more cell mass in the presence of SBM-produced sugars over the positive control of glucose. These values showed a greatly significant difference for the probiotic strains *S. thermophilus*, *B. subtilis*, and *L. bulgaricus* of the free and CTS immobilised enzymes compared to their positive controls ($P = 0.0008$; $P<0.0001$; $P = 0.0018$; and $P = 0.0002$; $P < 0.0001$; $P = 0.0009$, respectively). The results confirmed that there were no significant differences in the probiotic response, in relation to cell viability and cell density, for the SBM-produced sugars by the free and immobilised enzymes for the probiotics *S. thermophilus*, *B. subtilis* and *L. bulgaricus* ($P = 0.8754$; $P = 0.9261$; 0.0902; and $P = 0.1096$; $P = 0.1049$; 0.06085, respectively).

### 3.4.6 Antimicrobial Activity: Resazurin Assay

To establish the antimicrobial activity of MOS previously utilised by probiotic bacteria, *S. thermophilus, L. bulgaricus* and*, B. subtilis*, a resazurin assay was completed. This analysis compared the cell viability of pathogenic bacteria treated with secondary metabolites produced by probiotics which digested SBM-produced sugars, to the cell viability of a positive and negative control. In preparation for the assay, a bacterial log phase (Appendices, Figure G) was established for each of the pathogenic bacteria under investigation, *K. pneumonia* (Figure 3.9A), *S. aureus* (Figure 3.9B), and *E. coli* (Figure 3.9C).

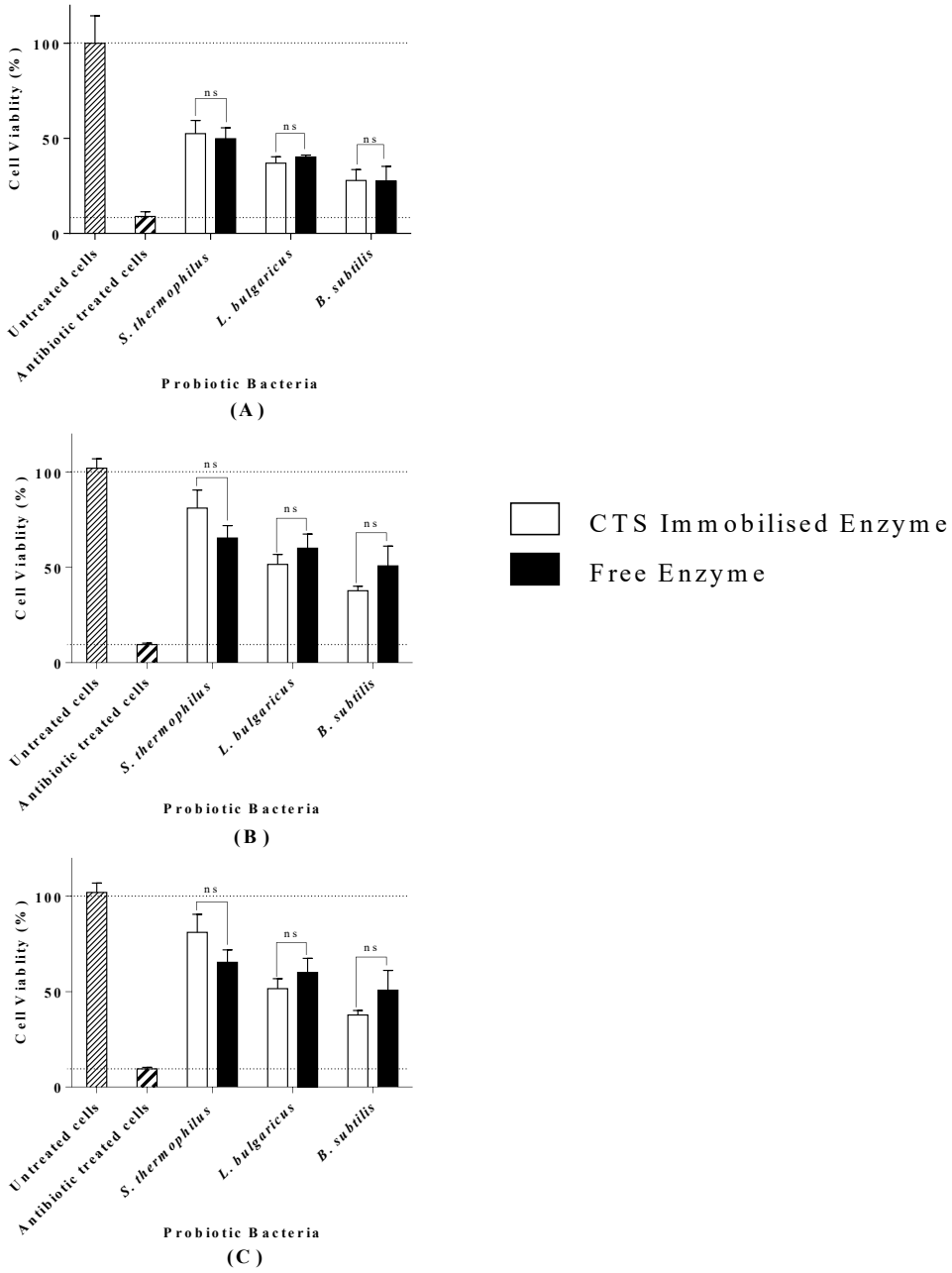


**Figure 3.9:** Evaluation of the antimicrobial activity of MOS on (A) *K. pneumoniae*, (B) *S. aureus*, and (C) *E. coli* after incubation with SBM-produced sugars digested by *S. thermophilus*, *L. bulgaricus*, and *B. subtilis*. A 50 µg/ml kanamycin was used as the positive control. Deionised water was the negative control. Statistical analysis was conducted using a *t*-test for the antimicrobial activity of reducing sugars produced by the free and immobilised enzymes, key: ns ($p > 0.05$).

The logarithmic phase was assumed to be the most linear portion of the graph, at 2.5 hours for all pathogenic bacteria under investigation. Looking at the results for the resazurin assay (Figure 3.9A – Figure 3.9C), it was noted that there was no significant difference in the utilised sugars from the probiotic bacteria between the immobilised SBM-produced sugars and the free SBM-produced sugars ($P > 0.05$). This confirmed that the hydrolysis by the immobilised and free enzymes did not affect the hydrolysis products or the way in which probiotics were able to digest the produced sugars.

Based on the cell viability (Figure 3.9), it is presumed that the solution of SBM-produced sugars contained bacterocins to some extent. *L. bulgaricus* and *B. subtilis* consumed sugars produced by SBM, resulting in the greatest loss of pathogenic cell viability, with a 50% decrease observed for all pathogenic bacteria investigated. The greatest loss in cell viability was seen against *K. pneumoniae*, with *B. subtilis* digested SBM-produced sugars reducing pathogenic cell viability by 75% for both the free and immobilised enzyme samples.

### 3.5 Discussion

The polysaccharide structures of SBM cannot be broken down by digestive enzymes; therefore, this chapter investigated the use of exogenous enzymes, produced in Chapter 2, for the effective breakdown of galactomannans in SBM (Sharma et al., 2018). Based on the success of immobilisation and how the altered enzymes competed with the free enzyme (Chapter 2), the immobilised and free enzymes were investigated for their efficiency against the insoluble, complex substrate, SBM.

The substrate composition analysis by Megazyme kits (Table 3.1) showed that the major monomeric sugar in SBM was glucose (4.116%). Islam et. al. (2018) also confirmed that this was the most prominent monomeric sugar in SBM - 5.1% of the SBM was in the form of glucose. Literature report indicate that the proportion of mannose within the structural carbohydrate should be between 0.3 and 5% of the total sugar composition (Irish and Blanave, 1993; Bach Knudsen, 1997; Karr-Lilientha et al., 2005; Choct et al., 2010; Islam et al., 2018; Chen et al., 2021) – our study showed a mannose content of 0.366%. SBM composition differs between geographical regions, creating a large variation within the literature (Choct et, al. 2010; Chen et al. 2021). Although mannose quantities were quite low, analysis has been completed at levels as low as 0.358%, where an effective production of mannose was described (Chen et al., 2021; Kiarie et al., 2021). β-mannans in SBM have a detrimental effect on poultry,

with limited information available regarding their breakdown (Sinha and Khare, 2017; White et al., 2021). For this reason, the concentrations of mannose were deemed sufficient, as the need for treatments of ANFs such as β-mannans, would provide valuable information for the poultry industry. For this reason, a further investigation into the hydrolysis of the galactomannan portion of SBM for MOS production was deemed feasible.

Before optimisation, research on SBM hydrolysis revealed that reducing the size of the substrate could promote enzymatic hydrolysis – for this reason, SBM was ground to a finer particle size before hydrolysis (Islam et al., 2018). SBM was then analysed by FTIR (section 3.3.3.3) and SEM analysis (section 3.3.3.4), in order to investigate the characteristic features of hydrolysis by the endo-1,4-β-mannanase, as well as to explain the efficiency of hydrolysis.

FTIR analysis of the various forms of SBM (Figure 3.2) showed a spectrum typical of a hemicellulose structure with well characterised bands at 3342 $cm^{-1}$, 2954 cm-1, 1760 $cm^{-1}$ and 1433 $cm^{-1}$, representing OH and N-H stretching vibrations, C-H stretching vibrations, and COOH, respectively (Fang et al., 2000; Sun and Tomkinson, 2003; Tian et al., 2017; Li et al., 2019). The strong band at 1040 $cm^{-1}$ provides evidence of a C-O stretching vibration, as previously seen by Yuan, et al. (2017), supporting the presence of a C-O-C glycosidic linkage in galactomannan (Fang et al., 2000; Nadaroglu and Sonmez, 2016; Sadaqat et al., 2022). A peak at 931 $cm^{-1}$ supported the presence of a β-1,4-glycosidic linkage, illustrating linkages between mannose and galactose within the SBM sample – further confirming the presence of galactomannan (Yuan, et al., 2017). This was previously observed by Sun and Tomkinson, (2003) at 901 $cm^{-1}$, where it was attributed to the β-glycosidic linkages within the xylose backbone of hemicellulose.

It was noted by Li et al. (2019) that the intensity of bands can be correlated to the quantity of various functional groups. There was a steady increase in functional groups with each step of the hydrolysis procedure (ground SBM < prewetted SBM < hydrolysed SBM). This was not the case for every functional group, as can be seen for the OH and N-H functional groups, the C-H stretching vibrations, as well as amide I, amide II, and amide III. Due to the mechanism of hydrolysis of the glycoside hydrolase, endo-1,4-β-mannanase, it is expected that the hydrolysis of SBM would result in the breaking of β-1,4-glycosidic linkages within the galactomannan structure (Sharma et al., 2018). This, in turn, is hypothesised to cause a decrease in the intensity of the peak at 901 $cm^{-1}$ after hydrolysis. This was, however, not the case in this study, as an increase in peak intensity was observed. This is believed to be as a result of the

processing of SBM, providing increased access to the materials' structure. An increase at 3342 $cm^{-1}$ was also hypothesised to occur after hydrolysis, due to exposure of hydroxyl groups, although due to the conclusion above it is assumed that a similar mechanism occurred, where new hydroxyl groups were not exposed but rather made more accessible for FTIR analysis.

Galactomannan is a component of hemicellulose, situated in the cell walls of plant structures (Sharma et al., 2020; Van Zyl et al., 2009). On the basis of this information, it was expected that degradation and enzyme hydrolysis would occur to a greater extent in this region. The SEM images of SBM samples, showed an increase in degradation of the cell wall throughout the hydrolysis procedure, with the least degradation observed in ground SBM (Figure 3.3A and Figure 3.3B) and the most in the hydrolysed SBM (Figure 3.3E and Figure 3.3F). Hydrolysis of enzymes in the SBM structure provided further confirmation that grinding, prewetting and hydrolysis exposed the mannan-rich portions of the SBM, leading to an increase in the production of reducing sugars such as MOS.

After a thorough evaluation of the efficiency of hydrolysis, both visually and chemically, it was important to evaluate the kinetic parameters of the enzymatic hydrolysis. This study was completed according to Section 3.3.5 and the data was shown in Figure 3.4 and Table 3.2.

The kinetic parameters, obtained by non-linear regression of the Michaelis-Menten plot, was employed to analyse the performance of the enzymes against the insoluble SBM substrate (Figure 3.4 and Table 3.2). The immobilised enzymes had a stronger affinity ($K_M$) for the insoluble substrate than the free enzyme. The $K_{M,}$ values for the free, CTS, and MAGS-CTS enzymes were 53.43 mM, 10.26 mM, and 21.80 mM, respectively. This result was unexpected: due to the substrate and the immobilised enzymes being insoluble, it was anticipated that access to active sites would prove more difficult. Though this could also be attributed to interference by the molecules produced by the enzyme, this supported by the $K_M$ for the free enzyme. However, a proportion of SBM galactomannan is soluble, potentially explaining the obtained results (Chen et al., 2021).

Further investigation into the kinetic parameters of the enzymatic hydrolysis of SBM suggested that the reaction was operating under sub-optimal conditions. The analysis of free, CTS and MAGS-CTS enzymes showed low $V_{max}$ values of 0.03099 U/mg, 0.02672 U/mg, and 0.01517 U/mg, respectively. It should be noted that the free enzyme hydrolysed SBM with the greatest success, however, only marginally – a result commonly reported after immobilisation (Al-Najada et al., 2019; Dhiman et al., 2020; Mohapatra, 2021; Behera et al., 2022). The $k_{cat}$ values

indicated that CTS outperformed the free and MAGS-CTS enzymes to convert the substrate to product.

The reusability of CTS and MAGS-CTS was assessed in section 3.3.6 and shown in Figure 3.5. The results of this study indicated that the separation of CTS from the insoluble SBM by centrifugation was not possible. This made reusability of CTS impossible. This challenge could be overcome by investigating soluble substrates, or sufficient soaking the substrate to extract the soluble galactomannan portion from SBM. In contrast, it was possible to separate the MAGS-CTS from the insoluble SBM substrate using a magnetic field; however, its reaction capabilities were rapidly depleted after the first cycle, with an 82.03% decrease in relative activity. This could be attributed to the lack of thermostability of the MAGS-CTS enzyme – deactivating the enzyme before the completion of cycle 2. Hydrolysis using an immobilised enzyme against an insoluble substrate has been used widely across literature; however, these reactions employed short reaction times of approximately 30 minutes – unlike this study which utilised a 48-hour hydrolysis period (Kumar and Gupta, 1998; Perwez et al., 2017).

TLC and HPLC analysis identified three prominent bands, before and after hydrolysis of SBM (Figure 3.6 and Figure 3.7), with one weak band present. These bands could not be identified by comparison with the MOS standards. Possible explanations for this could be the presence of glucose and galactose, previously seen between M1 and M2 standards (Chantorn et al., 2018). It is also hypothesised that MOS was produced from hydrolysis, however it was linked to branches composed of galactose. This would influence the size and therefore the migration of the residues on the TLC and HPLC – with this it is suggested that GM2 and GM3 were produced during hydrolysis. Literature has reported the presence of GM2 and GM3 between M3 and M4 and M4 and M5, respectively, correlating with the results obtained in this study (Han et al., 2010). Various sources present the breakdown of the galactomannan backbone to mannose; however, few describe specific MOS species produced after catalysis – making the comparison of results difficult (Islam et al., 2018; Chen et al., 2021). The sugar composition of SBM (Table 3.1) showed that SBM varies significantly between geographical regions, which, in turn, would likely result in a diverse range of hydrolysis products (Irish and Blanave, 1993; Bach Knudsen, 1997; Karr-Lilientha et al., 2005; Choct et al., 2010; Islam et al., 2018; Chen et al., 2021).

MOS exhibits the best prebiotic ability over the M2 – M5 range (Srivastava and Kapoor, 2017; Tiwari et al., 2020; Zhang et al., 2021). As these sugars could not be identified after hydrolysis,

it was then investigated whether the hypothesised sugars of galactose, glucose, galactomannobiose and galactomannotriose could facilitate probiotic growth.

The evaluation of the prebiotic potential of SBM produced sugars was performed using three probiotic strains: *S. thermophilus, B. subtilis* and *L. bulgaricus*, by analysing the effect of the sugar source on probiotic cell viability and cell density. These characteristics have previously been used to describe the efficient growth and metabolic activity of probiotics (Suhaibani et al., 2021).

The probiotic bacterium, *B. subtilis*, was investigated for its ability to utilise prebiotic sugars produced by SBM. With the knowledge of *B. subtilis* containing PUL, and its capacity to utilise mannose towards glycolysis, it was expected that this bacterium would show a high level of success towards utilising MOS (Suhaibani et al., 2021). Previous studies which investigated SBM fermentation by *B. subtilis* showed that bacterial growth increased by 20%, after which the growth rate was maintained – these results were substantially more successful than various other bacteria under investigation (Shi et al., 2017). Fermented SBM (FSBM) using *B. subtilis* has been studied in detail in the literature, with many positive effects on agricultural livestock, such as a decrease in blood pressure (Dai et al., 2017). The results from this study confirmed the ability of *B. subtilis* to utilise SBM-produced sugars, yielding results that far outcompeted the bacterial density (Figure 3.8B) and viability (Figure 3.8A) of the positive control of glucose.

Similarly, the results of cell density and viability with respect to *L. bulgaricus* and *S. thermophilus* suggested that these probiotics benefited enormously from the consumption of sugars produced by SBM.

After the prebiotic capabilities of the SBM-produced sugars were confirmed, Kango et al. (2022) investigated whether the compounds produced from the prebiotic evaluation, short-chain fatty acids and branched amino acids, otherwise termed bacteriocins, had the capacity to prevent pathogenic bacterial growth (Kango et al., 2022). A drop in pH often occurs after inoculation of the SBM-produced sugar with probiotics, a typical result expected with the use of lactic acid bacteria (Mora-Escobedo et al., 2018; Kango et al., 2022). However, no drop in the pH was observed in the bacterial samples. It was therefore suspected that bacteriocins were produced from the digestion of SBM-produced sugars, which facilitated the suppression of pathogenic bacterial growth.

The SBM-produced sugars digested by *L. bulgaricus*, *B. subtilis*, and *S. thermophilus* were analysed for their ability to suppress the growth of pathogenic bacteria; *K. pneumoniae*, *S.*

*aureus*, and *E. coli*. This analysis showed a similar correlation to the prebiotic study, in that there was no significant difference ($p > 0.05$) between the results obtained for the free and immobilised enzyme/SBM-produced sugars. It has been documented that SBM digested by probiotic bacteria has many beneficial qualities, with a major benefit being its capability to suppress the growth of pathogenic bacteria such as *S. aureous* and *E. coli* (Su et al., 2018). The probiotic extracts showed that pathogenic cell viability could be suppressed by up to 75%, with reference to the untreated positive control. Reports in the literature have assigned the antimicrobial properties of SBM to various peptides and bioactive compounds, often referred to as bacteriocins (Chikindas et al., 2018; Freitas et al., 2019; Chen et al., 2021).

Bacteriocins extracted from the probiotic digestion of SBM-produced sugars are typically found as peptides or produced as secondary metabolites from probiotic digestion (Mora-Escobedo et al., 2018). Bacteriocins have various mechanisms of action available to suppress the growth of pathogenic bacteria, such as the weakening of their cell walls (De Vuyst and Leroy, 2007; Mora-Escobedo et al., 2018). Lactic acid bacteria, such as *S. thermophilus* and *L. bulgaricus*, produce secondary metabolites, such as hydrogen peroxide, organic acids and various bacteriocins, with a potent inhibitory effect against various pathogenic bacterial species such as *S. aureus, E. coli,* and *K. pneumoniae* (Biswas et al., 2017; Mora-Escobedo et al., 2018). This supports our finding, which showed that pathogenic *S. aureus, E. coli,* and *K. pneumoniae* were suppressed after exposure to probiotic extracts of *S. thermophilus* and *L. bulgaricus.* The probiotic extract with the most significant effect on pathogenic inhibition was *B. subtilis*. It could be seen that a 50% decrease in pathogenic cell viability was experienced for all strains under investigation – which could potentially be attributed to the production of antibiotic compounds with a wide-spectrum effect against various pathogenic bacteria (Mora-Escobedo et al., 2018).

### 3.6 Conclusion

Immobilised and free endo-1,4-β-mannanases derived from *A. niger* were tested for their catalytic efficiency in hydrolysing the substrate SBM. It was first confirmed by acid hydrolysis that 0.366% of the total reducing sugars within SBM was composed of D-mannose. It was confirmed via SEM and FTIR that structural changes occurred in the substrate, exposing the galactomannan portion of SBM. The FTIR confirmed the presence of hemicellulose, possessing prominent characteristics of SBM and provided evidence of the β-1,4-glycosidic linkage. Recyclability analysis confirmed that the immobilised enzymes were not yet ready for

industrial use, as the recyclability of both immobilised enzymes (CTS and MAGS-CTS) with the SBM substrate showed that a second cycle was not yet achievable. The evaluation of the kinetic parameters showed that the free enzyme and CTS were the most productive for the generation of hydrolysis products. An evaluation of SBM-produced sugars showed that the galactomannans (GM2 and GM3) were not broken down further. These sugars were then evaluated for their effect on probiotic growth. SBM-produced sugars were successful in promoting probiotic growth, as well as displaying major potential as an antibiotic alternative with their capacity to reduce the growth of pathogenic bacterial strains by up to 75%. This study has therefore shown the potential for SBM-produced sugars to be used indirectly as antibiotic alternatives. Further optimisation is required to promote effective recyclability and increase catalytic efficiency. These results illustrate promising findings for an alternative AGP production, which could be validated after further optimisation of the enzyme recycling and activity experiments.

# CHAPTER 4: GENERAL DISCUSSION

The poultry industry is a major contributor to employment and protein distribution across South Africa (OECD/FAO, 2018; OECD, 2021). To ensure high yields of animal protein, good quality feeds are vital to enable the healthy production of poultry (Ravindran, 2013 van der Poel et al., 2020). SBM is a significant component of poultry feed, delivering valuable proteins and amino acids essential for growth and maintenance (Dozier and Hess, 2011; Ravindran, 2013; Zahir et al., 2019). SBM is largely beneficial - however, the presence of ANFs within its structure can be detrimental to poultry health (Sinha and Khare, 2017; Vangroenweghe et al., 2021). Galactomannans are ANFs within the SBM structure, which, unlike most ANFs, cannot be easily degraded by heat treatments (Sinha and Khare, 2017; White et al., 2021). These components have proven deleterious to poultry health, and have been shown in literature to stimulate an energy wasteful immune response as well as increase intestinal viscosity, impeding the natural absorption of nutrients from feed (Hsiao et al., 2006; Shastak et al., 2015; Scapini et al., 2018; Vangroenwghe et al., 2021). Various methods have been employed to investigate the effective breakdown of galactomannans in SBM, with the use of exogenous enzymes showing great potential (Shastak et al., 2015; Scapini et al., 2018).

Endo-1,4-β-mannanases are glycoside hydrolases, which function to hydrolyse the β-1,4-glycosidic linkages within the galactomannan backbone (Malgas et al., 2015a; Sharma et al., 2018). Although highly efficient catalysts, these enzymes are expensive and their consecutive use within the poultry industry is unpractical and unaffordable for long-term use (Dawood and Ma, 2020). This can be overcome by immobilising the enzyme onto a solid matrix, such as CTS and MAGS-CTS, to promote the reusability of the enzyme; decreasing the overall costs of the reaction (Puri and Abraham, 2016). Enzyme immobilisation is highly beneficial for the industrial applications of enzymes as it promotes increased stability, thermostability, and reusability – all of which allow for a more consistent and sustainable reaction (Puri and Abraham, 2016).

The hydrolysis of the galactomannan portion of SBM by an endo-1,4-β-mannanase produces MOS, a well-characterised prebiotic component (Shastak et al., 2015; Chacher et al., 2017; Saeed et al., 2017; Dawood and Ma, 2020; Jana et al., 2021). Prebiotics are specialised plant fibres, primarily digested by probiotic bacteria as a food source (Tiwari et al., 2020). Promoting the growth of probiotic bacteria within an organism is known to increase nutrient uptake and probiotic colonisation – benefiting the organism's overall health (Kango et al. 2022). It is

expected that probiotics fed with prebiotic MOS will suppress pathogenic bacterial growth to a greater extent than probiotics fed a sugar solution. This is a result of MOS utilisation by probiotics, producing valuable bacteriocins, branched amino acids and short-chain fatty acids (Šušković et al., 2010; Dobson et al., 2012; Kango et al., 2022). The use of prebiotics has shown great potential as an antibiotic alternative, assisting in addressing the exponential rise in antimicrobial resistance (Kango et al., 2022). Antibiotic alternatives are vital in creating a sustainable food production system (van der Poel et al., 2020).

This study was conducted to evaluate whether a recyclable reaction to hydrolyse the antinutritional galactomannan portion of SBM could efficiently produce prebiotic MOS, a component with the potential to assist in disease prevention in monogastric animals such as poultry. Before an effective analysis of enzymatic hydrolysis could be conducted, it was established by acid hydrolysis that 0.366% mannose was present. The quantities of mannose within SBM are low; however, the choice of further study was necessitated by the need for strategies to remove ANFs such as β-mannans from SBM (Sinha and Khare, 2017; Kiarie et al., 2021; White et al., 2021). As β-mannans are not deactivated by typical heat-treating methods and are not digested by endogenous enzymes, a method for their efficient removal is required (Kiarie et al., 2021). The reaction of the free enzyme was optimised with regards to SBM (Figure 3.1) to provide an effective method of hydrolysis, which was then further characterised using FTIR (Figure 3.2) and SEM (Figure 3.3) to establish that the enzyme could effectively hydrolyse the galactomannan portion of SBM situated in the cell wall of the plant structure (Sharma et al., 2020; Van Zyl et al., 2009).

The immobilisation of an endo-1,4-β-mannanase derived from *A. niger* was then investigated for immobilisation onto chitosan and magnetic particle supports. A model substrate of LBG was employed to evaluate the hydrolytic efficiency of the immobilised enzymes. This substrate was selected due to it being soluble and well characterised in literature, with a ratio of galactomannan comparable to that of SBM (Kashef et al., 2008; Malgas et al., 2015a; Surywanshi and Kango, 2021). Immobilisation strategies were validated by determining the immobilisation and activity yield (%) (Table 2.1), as well as the FTIR (Figure 2.2), and XRD (Figure 2.3) spectra for CTS and MAGS-CTS. This showed that the endo-1,4-β-mannanase was covalently immobilised onto the chitosan supports with an 81.14% immobilisation yield. FTIR results (Figure 2.2A) confirmed this claim, indicating that chitosan was effectively activated by glutaraldehyde by imine bond (C=N) formation. After this, the covalent immobilisation of the endo-1,4-β-mannanase was proved by a similar mechanism (Collins et

al., 2011; Klein et al., 2012; Mohapatra, 2021). This result was supported by the XRD analysis (Figure 2.3A), showing altered peaks and intensity which correlated with literature, suggesting the immobilisation was successful (Li et al., 2013; Galan et al., 2021; Sadaqat et al., 2022). The success of the MAGS-CTS immobilisation was less convincing, with the results from FTIR (Figure 2.2B) and XRD (Figure 2.3B) suggesting that further optimisation of the solid carrier was necessary. The FTIR analysis (Figure 2.2B) indicated that enzyme immobilisation was not sufficiently effective to a level where sufficient functional groups could be detected. This finding was supported by the XRD spectra (Figure 2.3B), where a homogenous pattern was witnessed for all forms of the MAGS-CTS, unlike what was observed for the CTS (Figure 2.3A).

Biochemical characterisation of the free, CTS, and MAGS-CTS enzymes was then conducted, in terms of physicochemical characteristics in the presence of LBG (Figure 2.7), as well as kinetic parameters in the presence of the soluble substrate LBG (Figure 2.9, Table 2.2) and insoluble substrate SBM (Figure 3.4, Table 3.2). This analysis showed an optimum temperature was maintained at 60°C, with no variation between the free and immobilised enzymes. This was, however, not the case for the pH optimum, as the CTS and MAGS-CTS immobilised enzymes were seen to favour a more acidic pH (pH 3.0), compared to the free enzyme (pH 5.0). This is likely be due to a conformational change in the enzyme after immobilisation (Blibech et al., 2011, Panwar et al., 2017; Sadaqat et al., 2022). Immobilisation has been noted in literature to increase the thermostability of various enzymes (Blibech et al., 2011; Sadaqat et al., 2022). However, this was not the case for the CTS and MAGS-CTS immobilisations. The CTS maintained a similar thermostability to the free enzyme whilst the MAGS-CTS showed a decrease in its thermostability. The kinetic parameters of the free, CTS and MAGS-CTS were similar when these enzymes acted on their LBG and SBM substrates. Regarding their $K_{m.}$ values, CTS and MAGS-CTS held higher affinities for the substrates compared to the free enzyme. Besides this aspect, the free enzyme was observed to be the most successful in terms of its catalytic capability when hydrolysing LBG, while the CTS enzyme was the most efficient when hydrolysing SBM. The MAGS-CTS immobilised enzyme was the least successful when hydrolysing both substrates. The kinetic parameters of MAGS-CTS, when hydrolysing SBM, were significantly less favourable - this was attributed to enzymes being less effective at hydrolysing insoluble substrates, due to the increased difficulty for the enzyme to access the galactomannan portion (Singh et al., 2013; Vaghari et al., 2015).

The reusability of the immobilised enzymes was then tested for effectiveness against LBG and SBM. The reusability for the CTS immobilised enzyme was achievable, showing success up to six cycles for hydrolysis with a soluble substrate such as LBG (Figure 2.6A); however this was impractical for hydrolysing an insoluble substrate such as SBM (Figure 3.5A) due to the problem of separating the enzyme and substrate. The MAGS-CTS immobilised enzyme was shown to be unproductive with regards to reusability (recyclability) in the hydrolysis of LBG (Figure 2.6B) and SBM (Figure 3.5B). However, unlike the CTS immobilised enzyme, the MAGS-CTS could be efficiently removed from the reaction medium by employing the use of a permanent magnet. Due to the lack of reusability and activity of the MAGS-CTS enzyme, further analysis into inhibitors of the endo-1,4-β-mannanase should be investigated, to investigate whether the $Fe_3O_4$ particles are contributing to unproductive hydrolysis, as has previously been reported in the literature (Zahura et al., 2010; Liao et al., 2014; Yoo et al., 2015; Ratnakomala et al., 2022).

An investigation of the LBG and SBM hydrolysis products was completed using HPLC and TLC analysis for the free, CTS and MAGS-CTS enzymes. These analysis showed that the various enzymes held a similar capacity to hydrolyse the various substrates, producing sugars of the same quantity and composition. The prominent sugars from LBG hydrolysis were M2, M3, M4, and M6. The predominant sugars of SBM were expected to be galactomanno-oligosaccharides arising from the breakdown of the galactomannan – seen by the bands between M3 and M4 (GM2), and the faint band between M4 and M5 (GM3). The expectation with the endo-1,4-β-mannanase, was that the β-1,4-glycosidic linkages within the galactomannan backbone would be hydrolysed, as has been documented in literature (Malgas et al., 2015b; Sharma et al., 2018). This was successful with regard to LBG, however with results obtained from SBM it should be noted that it is likely that no hydrolysis occurred. The similarity between the substrate control and enzyme hydrolysis samples were identical in composition and differed only partially in reducing sugar content. Therefore, it is likely that glucose, galactose, GM2 and GM3 were present before hydrolysis and not as a result of hydrolysis. Insoluble substrates, such as 10% (w/v) copra meal, hydrolysed by endo-1,4-β-mannanases, showed that M1-M6 could be produced (Ariandi et al., 2015). However, analysis of coffee mannan hydrolysed similarly only produced M1-M3 (Sachslehner et al., 2000). These results varied across a variety of substrates, both soluble and insoluble, indicating that the efficiency of hydrolysis is highly dependent on the structure of the substrate.

With the identification of sugars produced from SBM, we then investigated whether the SBM-produced MOS could be effectively utilised as a prebiotic by the probiotic bacteria (Figure 3.8), *S. thermophilus, B. subtilis* and *L. bulgaricus*. This study showed that sugars produced from SBM could increase the viability and density of probiotic bacteria to a far greater extent than the positive control of glucose (Figure 3.8). As hydrolysis was deemed to be inefficient, this result shows that the probiotic bacteria prefer a combination of sugars for sustainability, rather than a single, pure source of sugars. SBM is therefore an effective substrate for probiotic digestion, increasing the cell density (Figure 3.8B) and viability (Figure 3.8A) by up to 115% for all tested probiotics. Poultry fed SBM-produced MOS are likely to benefit from a healthy gut microbiome due to the strengthening of the probiotic bacterial population within the gut. However, this analysis (Figure 3.8) was completed *in vitro* and, therefore, *in vivo* analysis will need to be completed to confirm this finding, before a firm statement can be made regarding the prebiotic effect within poultry.

It was then investigated whether the probiotics utilising SBM-produced sugars could indeed be utilised as antibiotic alternatives – by determining whether the secondary metabolites, bacteriocins, short-chain fatty acids, and branched amino acids have an effect on preventing the growth of pathogenic bacteria (Mora-Escobedo et al., 2018). This analysis showed that the products of probiotic digestion could effectively inhibit the growth of pathogenic bacteria (Figure 3.9). Although not as effective as the antibiotic kanamycin, the results did show a significant drop in pathogenic bacterial growth. An efficient analysis was completed by comparing the results of the probiotic extract with those for untreated cells, which showed that growth was not hindered by the strategy employed for analysis. Similar to the results obtained for probiotic growth analysis (Figure 3.8), the immobilised and free enzyme samples were able to inhibit pathogenic growth to a similar extent. This showed that probiotic extracts of SBM-produced (MOS) sugars have potential for use as an antibiotic alternative. Again, *in vivo* studies are required to the confirm the impact of this study on the health of poultry. Therefore, for the present, it can be concluded that *in vitro* results suggest that the SBM-produced (MOS) sugars can be utilised as an antibiotic alternative, and as a strategy to reduce the use of AGPs within poultry.

## Conclusion

The consumption of SBM within poultry feed has been reported to be beneficial; however, the negative impacts of ANFs have proven detrimental to poultry health. Although various methods are employed to remove the ANFs in feed, galactomannans have been shown to be resistant. Many detrimental factors of SBM have been overcome by employing AGPs within the feed, leading to a rise in antibiotic resistance worldwide – this, in turn, has led to a search for antibiotic alternatives. This study was conducted in an attempt to address both of these challenges.

This study involved the successful covalent immobilisation of an endo-1,4-β-mannanase derived from *A. niger* onto CTS. Further optimisation of the immobilisation of MAGS-CTS particles is however required. The immobilised and free enzymes were biochemical characterised. The optimum temperature for the free, CTS, and MAGS-CTS immobilised enzymes was established as 60ºC. The free and CTS enzymes exhibited similar thermostabilities, with MAGS-CTS being notably different, indicating that this form of immobilisation had an adverse effect on the performance of the enzymes. The pH optimum of the CTS and MAGS-CTS was more acidic (pH 3.0) than the free enzyme (pH 5.0). Enzyme kinetic studies showed that the free enzyme displayed the highest catalytic activity on LBG, while the CTS was the most active on the insoluble substrate SBM. CTS and MAGS-CTS could not be effectively recycled in the presence of SBM; however, this was not the case for LBG. The sugars produced from the hydrolysis of both LBG confirmed that the CTS and MAGS-CTS were able to hydrolyse the substrate to the same extent as the free enzyme. The hydrolysis of SBM was deemed inefficient, though further testing of the sugars was performed in terms of their prebiotic effect. The probiotics preferred the complex substrate SBM as a source of nutrients to the positive control glucose. The compounds produced from the digestion of SBM-produced sugars by probiotic bacteria showed significant potential in suppressing the growth of pathogenic bacteria. This study revealed that an immobilised endo-1,4-β-mannanase could be efficiently utilised for producing reducing sugars from LBG. The SBM-produced sugars show great potential for utilisation as an antibiotic alternative, displaying effective prebiotic characteristics that may promote probiotic growth and inhibit pathogenic bacterial proliferation.

**Future Studies**

This project confirmed that an endo-1,4-β-mannanase could not efficiently hydrolyse the galactomannan portion of SBM. However, sugars present within SBM produced a prebiotic effect which, in turn, showed potential antimicrobial activity. In future, certain limitations to this study may be addressed; these include:

- The MAGS-CTS immobilisation recyclability could be further optimised to promote additional reaction cycles.
- Increasing the efficiency of the SBM hydrolysis by washing the substrate prior to the reaction procedure.
- CTS showed the greatest potential for reusability- however, due to the impracticality of separating the insoluble immobilized enzyme and substrate, more than one hydrolysis cycle could not be completed when hydrolysing SBM. Possible strategies which could be employed to increase the efficiency of separation could be:
  - altering the colour of the CTS particles, making them more easily identifiable from the SBM substrate;
  - employing more stringent centrifugation, to facilitate the effective separation of CTS and SBM, with regards to the difference in their densities.
- The immobilisation method was successfully optimised and validated. However, the enzymes were not tested for inhibitors and promoters of enzyme activity. This could be investigated going forward to better understand the capabilities of the immobilised endo-1,4-β-mannanase derived from *A. niger*.
- The immobilised enzymes could efficiently hydrolyze LBG in a reusable manner. However, the recyclability of the hydrolysis of SBM by MAGS-CTS proved challenging. This may be addressed by reducing the time of hydrolysis or by genetically altering the enzyme to enhance thermostability.
- Size determination of the various CTS and MAGS-CTS particles was estimated according to the Scherrer Equation (*Eq. 3*). Through an accurate size determination method, a more definitive analysis may be completed by employing the use of High-Resolution Electron Microscopy (HR-TEM), though this instrument was not available at the time of the study.
- Assessing the *in vivo* capabilities of the SBM-produced sugars for probiotic growth and inhibition of pathogenic proliferation. This will better illustrate the prebiotic capabilities of the MOS/reducing sugars as an antibiotic alternative.

**References**

Abushaheen, M. A.; Muzaheed; Fatani, A. J.; Alosaimi, M.; Mansy, W.; George, M.; Acharya, S.; Rathod, S.; Divakar, D. D.; Jhugroo, C.; Vellappally, S.; Khan, A. A.; Shaik, J.; Jhugroo, P. Antimicrobial resistance, mechanisms and its clinical significance. *Disease-a-Month*. **2020**, 66(6), 100971.

Ajdić, D.; Pham, V.T.T. Global transcription analysis of *Streptococcus mutans* sugar transporters using microarrays. *Journal of Bacteriology.* **2007**, 189(14), 5049-5059.

Alnadari, F.; Xue, Y.; Zhou, L.; a med, Y. S.; Taha, M.; Foda, M. F. Immobilization of β-Glucosidase from *Thermatoga maritima* on Chitin-functionalized Magnetic Nanoparticle via a Novel Thermostable Chitin-binding Domain. *Scientific Reports*. **2020**, 10(1), 1663.

Al-Najada, A.; Almulaiky, Y. Q.; Aldhahri, M.; El-Shishtawy, R. M.; Mohamed, S. A.; Baeshen, M.; AL-Farga, A.; Abdulaal, W. H.; Al- a rbi, S. A. Immobilisation of α-amylase on activated amidrazone acrylic fabric: a new approach for the enhancement of enzyme stability and reusability. *Scientific Reports*. **2019**, 9, 12672.

Ariandi, A.; Yopi, Y.; Meryandini, A. Enzymeatice Hydrolysis of Copra Meal by Mannanase from *Streptomyces* sp. BF3.1 for the Production of Mannooligosaccharides. *HAYATI Journal of Biosciences*. **2015**, 22(2), 79-86.

Arsenault, R. J.; Lee, J. T.; Latham, R.; Carter, B.; Kogut, M. H. Changes in immune and metabolic gut response in broilers fed β-mannanase in β-mannan-containing diets. *Poultry Science*. **2017**, 96, 4307-4316.

Arunrattanamook, N.; Wansuksri, R.; Uengwetwanit, T.; Champreda, V. Engineering of β-mannanase from *Aspergillus niger* to increase product selectivity towards medium chain length mannooligosaccharides. *Journal of Bioscience and Bioengineering*. **2020**, 130(5), 443-449.

Ayoola, A. A.; Malheiros, R. D.; Grimes, J. L.; and Ferket, P. R. Effect of dietary exogenous enzyme supplementation on enteric mucosal morphological development and adherent mucin thickness in Turkeys. *Frontiers of Veterinary Science*. **2015**, 2(45).

Bach Knudsen, K. E. Carbohydrate and lignin contents of plant materials used in animal feeding. *Animal Feed Science and Technology*. **1997**, 67(4), 319-338.

Baroudi, A.; García-Payo, C.; Khayet, M. Structural, mechanical, and transport properties of electron beam-irradiated chitosan membranes at different doses. *Polymers. J.* **2018**, 10(117), 1-23.

Bäuerle, F.; Zotter, A.; Schreiber, G. Direct determination of enzyme kinetic parameters from single reactions using a new progress curve analysis tool. *Protein Engineering, Design and selection*. **2017**, 30(3), 151-158.

Bele, A. A.; Khale, A. An overview on thin layer chromatography. *International Journal of Pharmaceutical Sciences and Research.* **2011**, 2(2), 256-267.

Belowicha, M. E.; Stoddart, J. F. Dynamic imine chemistry. *Chemistry Society Reviews*. **2012**, 41(6).

Bien-Cuong, D.; Thi-Thu, D.; Berrin, J.; Haltrich, D.; Kim-Anh, T.; Sigoillot, J.; Yamabhai, M. Cloning, expression in *Pichia pastoris*, and characterization of a thermostable GH5 mannan endo-1,4-β-mannosidase from *Aspergillus niger* BK01. *Microbial Cell Factories*. **2009**, 8(59), 1-12.

Bilal, M.; Zhao, Y.; Rasheed, T.; Iqbal, H. M. N. Magnetic nanoparticles as versatile carriers for enzymes immobilization: A review. *International Journal of Biological Macromolecules*. **2018**, 120, 2530-2544.

Biswas, K.; Upadhayay, S.; Rapsang, G. F.; Joshi, S. R. Antibacterial and synergistic activity against β-lactamase-producing nosocomial Bacteria by Bacteriocin of LAB isolated from lesser known traditionally fermented products of India. *HAYATI Journal of Biosciences*. **2017**, 24(2), 87-95.

Blair, R. Nutrition and feeding of organic poultry. *Animal Feed Science and Technology*. **2009**, 151(1-2), 172-173.

Blibech, M.; Chaari, F.; Bhiri, F.; Dammak, I.; Ghorbel, R. E.; Chaabouni, S. E. Production of manno-oligosaccharides from locust bean gum using immobilized *Penicillium occitanis* mannanase. *Journal of Molecular Catalysis B: Enzymatic.* **2011**, 73, 111-115.

Bradford, M. M. A rapid and sensitive method for the quantitation of microgram quantities of protein utilizing the primnciple of protein-dye binding. *Analytical Biochemistry,* **1976**, 72, 248-254.

Britton, H. T. S. ; Robinson, R. A. Universal buffer solutions and the dissociation constant of veronal. *Journal of the Chemical Society* **1931**, 1, 1456-1462.

Chacher, M. F. A.; Kamran, Z.; Ahsan, U.; Ahmad, S.; Koutoulis, K. C.; Qutab Ud Din; H. G.; Cengiz, Ö. Use of mannan oligosaccharide in broiler diets: an overview of underlying mechanisms. *Worlds Poultry Science Journal.* **2017**, 73, 1-14.

Chantorn, S.; Buengsrisawat, K.; Pokaseam, A.; Sombat, T. Optimization of extracellular mannanase production from *Penicillium oxalicum* KUB-SN2-1 and application for hydrolysis property. *Songklanakarin Journal of Science and Technology*. **2013**, 35(1), 17-22.

Chantorn, S.; Piyapittayanun, C.; Dangpram, P. Bioconversion of Agricultural Wastes to Mannooligosaccharides and Their Prebiotic Potential. *Chiang Mai Journal of Science*. **2018**, 45(1), 60-67.

Chen, L.; Zhao, Z.; Yu, W.; Zheng, L.; Li, L.; Gu, W.; Xu, H.; Wei, B.; Yan, X. Nutritional quality improvement of soybean meal by *Bacillus velezensis* and *Lactobacillus plantarum* during two-stage solid- state fermentation. *AMB Express*. **2021**, 11(23).

Chen, M.; Wang, J.; Wei, W.; Shen, Y.; Wei, D. High-level expression of a β-mannanase (manB) in *Pichia pastoris* GS115 for mannose production with *Penicillium brevicompactum* fermentation pretreatment of soybean meal. *Bioprocess and Biosystems Engineering*. **2021**, 44, 549-561.

Chikindas, M. L.; Weeks, R.; Drider, D.; Chistyakov, V. A.; Dicks, L. M. T. Functions and emerging applications of bacteriocins. *Current opinion in Biotechnology*. **2018**, 49, 23-28

Choct, M.; Dersjant-Li, Y.; McLeish, J.; Peisker, M. Soy Oligosaccharides and soluble non-starch polysaccharides: A review of digestion, nutritive and anti-nutritive effects in pigs and poultry. *The Asian-Australasian Association of Animal Production societies*. **2010**, 23(10), 1386-1398.

Choi, B.; Rempala, G. R.; Kim, J. K. Beyond the Michaelis-Menten equation: Accurate and efficient estimation of enzyme kinetic parameters. *Scientific Reports*. **2017**, 7, 17018.

Ciaccia, M.; Cacciapaglia, R.; Mencarelli, P.; Manolini, L. Stefano, S. D. Fast transimination in organic solvents in the absence of proton and metal catalysts. A key to iminemetathesis catalyzed by primary amines under mind conditions. *Chemical Science.* **2013**, 5, 2253-2261.

Collins, S. E.; Lassalle, V.; Ferreira, M. L. FTIR-ATR characterization of free *Rhizomucor meihei* lipase (RML), Lipozyme RM, IM and chitosan-immobilized RML. *Journal of Molecular Catalysis B: Enzymatic.* **2011***, 72*, 220-228.

Coskun, O. Separation techniques: Chromatography. *Northen Clinics of Istanbul*, **2016**, 3(2), 156-160.

Dai, C.; Ma, H.; He, R.; Huang, L.; Zhu, S.; Ding, Q.; Luo, L. Improvement of nutritional value and bioactivity of soybean meal by solid-state fermentation with *Bacillus subtilis. Lebensmittel-Wissenschaft & Technologie.* **2017**, 86, 1-7.

Dai, W.; Shao, F.; Szczerbiński, J.; McCaffrey, R.; Zenobi, R.; Jin, Y.; Schlüter, A.D.; Zhang, W. Synthesis of a two-dimensional covalent organic monolayer through dynamic imine chemistry at the air/water interface**.** *Angewandte Chemie International Edition.* **2016**, *55*, 213-217.

Daub, C. D.; Mabate, B.; Malgas, S.; Pletschke, B. I. Fucoidan from *Ecklonia maxima* is a powerful inhibitor of the diabetes-related enzyme, α-glucosidase. *International Journal of Biological Macromolecules*. **2020**, 151, 412-420.

Dawood, A.; Ma, K. Applications of microbial β-mannanases. *Frontiers in Bioengineering and Biotechnology*. **2020**, 8, 1-17.

De Vuyst, L.; Leroy, F. Bacteriocins from lactic acid bacteria: Production, purification, and food applications. *Journal of Molecular Microbiology and Biotechnology*. **2007**, 13(4), 194-199.

Dei, H. K. Soybean as a feed ingredient for livestock and poultry. *Recent Trends for Enhancing the Diversity and Quality of Soybean Products.* **2011**, (ed. D. Krezhova).

Dhiman, S.; Srivastava, B.; Singh, G.; Khatri, M.; Kumar Arya, S. Immobilization of mannanase on sodium alginate-grafted-β-cyclodextrin: An easy and cost effective approach for the improvement of enzyme properties*. International journal of biological macromolecules*. **2019**, 1(156) .

Divya, K.; Jisha, M. S. Chitosan nanoparticles preparation and applications. *Environmental Chemistry Letters.* **2018**, 16, 101-112.

Dobson, A.; Cotter, P. D.; Ross, R. P.; Hill, C. Bacteriocin production: A probiotic trait? *Applied and Environmental Microbiology*. **2012**, 78(1), 1-6.

Dozier, W. A.; Hess, J. B. Soybean meal quality and analytical techniques: chapter 6. In: Hany El-Shemy (Ed.), *Soybean and Nutrition*. **2011.**

Eddya, M.; Bouazza, T.; EL-Hami, K. A comparison of chitosan properties after extraction from shrimp shells by diluted and concentrated acids. *Heliyon*. **2020**, 6(2), e03486.

Elshikh, M.; Ahmed, S.; Funston, S.; Dunlop, P.; McGaw, M.; Marchant, R.; Banat, I. M. Resaqurin-based 96-well plate microdilution method for the determination of minimum inhibitory concentration of biosurfactants. *Biotechnology Letters*. **2016**, 38(6), 1015-1019.

Fan, Y.; Chen, J.; Wang, Z.; Tan, T.; Li, S.; Li, J.; Wang, B.; Zhang, J.; Cheng, Y.; Wu, X.; Yang, W.; Yang, F. Soybean (*Glycine max L. Merr.*) seedlings response to shading: leaf structure, photosynthesis and proteomic analysis. *BMC Plant Biology*. **2019**, 19(34), 1-12.

Fang, J. M.; Sun, R. C.; Tomkinson, J.; Fowler, P. Acetylation of wheat straw hemicellulose B in a new non-aqueous swelling system. *Carbohydrate Polymers*. **2000**, 41, 379-387.

Freitas, C. S.; Vericimo, M. A.; Leal da Silva, M.; Verissimo da Costa, G.; Pereira, P. R.; Paschoalin, V. M. F.; Mere Del Aguila, E. Encrypted antimicrobial and antitumoral peptides recovered from a protein-rich soybean (*Glycine max*) by-product. *Journal of Functional Foods.* **2019**, 54, 187-198.

Galan, J.; Trilleras, J.; Zapata, P. A.; Arana, V. A.; Grande-Tovar, C. D.; Optimization of chitosan glutaraldehyde-crosslinked beads for reactive blue 4 anionic dye removal using a surface response methodology. *Life*. **2021**, 11(2), 85.

Galanakis, C. M.; Patsioura, A.; Gekas, V. Enzyme kinetics modeling as a tool to optimize food industry: A pragmatic approach based on amylolytic enzymes. *Critical Reviews in Food Science and Nutrition*. **2015**, 55(12), 1758-1770.

Garnica-Palafox, I. M.; Sánchez-Arévalo, F. M. Influence of natural and synthetic crosslinking reagents on the structural and mechanical properties of chitosan-based hybrid hydrogels. *Carbohydrate Polymers.* **2016**, 151, 1073-1081

Gűr, S. D.; İdil, N.; Aksöz, N. ptim ization of enzyme co-immobilization with sodium alginate and glutaraldehyde-activated chitosan beads. *Applied Biotechnology & Biotechnical Equipment.* **2018**, 184(2), 538-552.

Guzik, U.; Hupert-Kocurek; K.; Wojcieszyńska, D. Immobilization as a strategy for improving enzyme properties – application to oxidoreductases. *Molecules*, **2014**, 19(7), 8995-9018.

Halas, V.; Nochta, I. Mannan oligosaccharides in nursery pig nutrition and their potential mode of action. *Animals*. **2012**, 2, 261-274.

Han, Y.; Dodd, D.; Hespen, C. W.; Ohene-Adjei, S.; Schroeder, C. M.; Mackie, R. I.; Cann, I. K. O. Comparative Analyses of two thermophilic enzymes exhibiting both β-1,4 Mannosidic and β-1,4 glucosidic cleavage activities from *Caldanaerobius polysaccharolyticus*. *Journal of Bacteriology*. **2010**, 192(16), 4111-4121.

Harnpicarnchai, P.; Pinngoen, W.; Teanngam, W.; Sornlake, W.; Sae-Tang, K.; Manitchotpisit, P.; Tanapongpipat, S. Production of high activity *Aspergillus niger* BCC 5 25 β-mannanase in *Pichia pastoris* and its application for mannooligosaccharides production from biomass hydrolysis. *Bioscience, Biotechnology, and Biochemistry*. **2016**, 80(12), 2298-2305.

Hazrati, S.; Rezaeipour, V.; Asadzadeh, S. Effects of phytogenic feed additives, probiotics and mannan-oligosaccharides on performance, blood metabolites, meat quality, intestinal morphology, and microbial population of Japanese quail. *British Poultry Science*. **2019**.

Hedman, H. D.; Vasco, K. A.; Zhang, L. A Review of antimicrobial resistance in poultry farming within low-resource settings. *Animals*. **2020**, 10(8), 1264.

Hoa, L. T. M.; Dung, T. T.; Danh, T. M.; Duc, N. H.; Chien, D. M. Preparation and characterization of magnetic nanoparticles coated with polyethylene glycol. *Journal of Physics: Conference Series.* **2009**, 187, 012048.

Holland, C.; Ryden, P.; Edwards, C. H.; Grundy, M. M. Plant cell walls: Impact on nutrient bioaccessibility and digestibility. *Advanced Research in Food Digestion*. **2020**, 9(2) 201.

Homaei, A. A.; Sriri, R.; Vianello, F.; Stevanato, R. Enzyme immobilization: an update. *Journal of Chemical Biology*. **2013**, 6(4), 185-205.

sia o, . Y.; Anderson, D. M.; Dale, N. M. Levels of β-mannan in soybean meal. *Poultry Science*. **2006**, 85(8), 1430-1432.

Irish, G. G.; Balnave D. Non-starch polysaccharides and broiler performance on diets containing soyabean meal as the sole protein concentrate. *Australian Journal of Agricultural Research*. **1993**, 44(71), 1483-1499

Islam, S. M. M.; Loman, A. A.; Ju, L. K. High monomeric sugar yields from enzymatic hydrolysis of soybean meal and effects of mild heat pretreatments with chelators. *Bioresource Technology*. **2018**, 256, 438-445.

Jamalifar, H.; Rahmini, H. R.; Samadi, N.; Shahverdi, A. R.; Sharifian, Z.; Hossesini, F.; Eslahi, H.; Fazeli, M. R. Antimicrobial activity of different *Lactobacillus* species against multi-drug resistant clinical isolates of *Pseudomonas aeruginosa. Iranian Journal of Microbiology.* **2011**, 3(1), 21-25.

Jana, U. K.; Suryawanshi, R. K.; Prajapati, B. P.; Kango, N. Prebiotic mannooligosaccharides: Synthesis, characterization and bioactive properties. *Food Chemistry*. **2021**, 342, 1-13.

Jankowska, K.; Ciesielczyk, F.; Bachosz, K.; Zdarta, J.; Kaczorek, E.; Jesionowski, T. Laccase immobilized onto zirconia–silica hybrid doped with $Cu^{2+}$ as an effective biocatalytic system for decolorization of dyes. *Materials*. **2019**, 12, 1252.

Jonović, M.; Jugović, B.; Žuža, M.; Dordević, V.; Milašinović, N.; Bugarski, B.; Knežević-Jugović, Z. Immobilisation of horseradish peroxidase on magnetite-alginate beads to enable effective strong binding and enzyme recycling during anthraquinone dyes' degradation. *Polymers*, **2022**, 14(2614), 1-26.

Joseph, B.; Dhas, B.; Hena, V.; Raj, J. Bacteriocin from *Bacillus subtilis* as a novel drug against diabetic foot ulcer bacterial pathogens. *Asian Pacific Journal of Tropical Biomedicine*. **2013**, 3(12), 942-946.

Kamada, N.; Chen, G. Y.; Inohara, N.; Núñez, G. Control of pathogens and pathobionts by the gut microbiota. *Nature Immunology*. **2013**, 14(7), 685-690.

Kango, N.; Jana, U. K.; Choukade, R.; Nath, S. Advances in prebiotic mannooligosaccharides. *Food Science.* **2022**, 47, 100883.

Karr-Lilienthal, L. K.; Kadzere, C. T.; Grieshop, C. M.; Fahey Jr., G. C. Chemical and nutritional properties of soybean carbohydrates as related to nonruminants: A review. *Livestock Production Science*. **2005**, 97, 1-12.

Kashef, R. K. H.; Hassan, H. M. M.; Afify, A. S.; Ghabbour, S. I.; Saleh, N. T. Effect of Soybean Galactomannan on the activities of α-Amylase, Trypsin, Lipase and Starch Digestion. *Journal of Applied Sciences Research*. **2008**, 4(12), 1893-1897.

Kiarie, E. G.; Steelman, S.; Martinez, M.; Livingston, K. Significance of single β-mannanase supplementation on performance and energy utilization in broiler chickens, laying hens, turkeys, sows, and nursery-finish pigs: a meta-analysis and systematic review. *Translational Animal Science*. **2021**, 5(4):

Kim, J. S.; Lee, S. Immobilization of trypsin from porcine pancreas onto chitosan Nonwoven by covalent bonding. *Polymers*. **2019**, 11(9), 1462.

Kim, S. A.; Jang, M. J.; Kim, S. Y.; Yang, Y.; Pavlidis, H. O.; Ricke, S. C. Potential for prebiotics as feed additives to limit foodborne *Campylobacter* establishment in the poultry gastrointestinal tract. *Frontiers in Microbiology*. **2019**, 10(91), 1-12.

Kim, S.; Lee, M.; Lee, E.; Nam, Y.; Seo, D. Characterization of mannanase from *Bacillus* sp., a novel *Codium Fragile* cell wall-degrading bacterium. *Food Science and Biotechnology*. **2018**, 27(1), 115-122.

Klein, M. P.; Nunes, M. R.; Rodigues, R. C.; Benvenutti, E. V.; Costa, T. M. H.; Hertz, P. F.; Ninow, J. L. Effect of the support size on the properties of β-galactosidase immobilized on chitosan: advantages and disadvantages of macro and nanoparticles. *Biomacromolecules.* **2012***, 13*, 2456-2464.

Kocher, A.; Connolly, A.; Zawadzki, J.; Gallet, D. The challenge of finding alternatives to antibiotics growth promoters. *International Society of Animal Hygiene*. **2004**, 227-227.

Kulkarni, V. H.; Kulkarni, P. V.; Keshavayya, J. Glutaraldehyde-crosslinked chitosan beads for controlled release of diclofenac sodium. *Journal of Applied Polymer Science*. **2007**, 103, 211–217

Kumar, A.; Gupta, M. N. Immobilization of trypsin on an enteric polymer Eudragit S-100 for the biocatalysis of macromolecular substrate. *Journal of Molecular Catalysis B: Enzymatic*. **1998**, 5(1-4), 289-294.

Kumar, S.; Dutta, P. K.; Koh, J. A physico-chemical and biological study of novel chitosan-chloroquinoline derivative for biomedical applications. *International Journal of Biological Macromolecules*. **2011**, 49(3), 256-261.

Kumar, S.; Koh, J. Physiochemical, optical and biological activity of chitosan-chrome derivative for biomedical applications. *International Journal of Molecular Science.* **2012**, 13, 6102-6116.

Latham, R. E.; Williams, M. P.; Walters, . G.; Carter, B.; Lee, J. T. Efficacy of β-mannanase on broiler growth performance and energy utilization in the presence of increasing dietary galactomannan. *Poultry Science*. **2018**, 97, 549-556.

Lee, C. H.; Jin, E. S.; Lee, J. H.; Hwang, E. T. Immobilization ad stabilization of enzyme in biomineralized calcium carbonate microspheres. *Frontiers in Bioengineering and Biotechnology*. **2020**, 6, 2296-4185.

Li, B.; Shan, C. L.; Zhou, Q.; Fang, Y.; Wang, Y. L.; Xu, F.; Han, L. R.; Ibrahim, M.; Guo, L. B.; Xie, G. L.; Sun, G. C. Synthesis, characterisation, and antibacterial activity of cross-linked chitosan-glutaraldehyde. *Marine Drugs*. **2013**, 11, 1534-1552.

Li, J.; Zhang, B.; Li, X.; Yi, Y.; Shi, F.; Guo, J.; Gao, Z. Effects of typical soybean meal type on the properties of soybean-based adhesive. *International Journal of Adhesion and Adhesives*. **2019**, 90, 15-21.

Liao, H; Li, S.; Zheng, H.; Wei, Z.; Liu, D.; Raza, W.; Shen, Q.; Xu, Y. A new acidophilic thermostable endo-1,4-β-mannanase from *Penicillium oxalicum* GZ-2: cloning, characterization and functional expression in *Pichia pastoris. BMC Biotechnology.* **2014**, 14, 90.

Licandro-Seraut, H.; Scornec, H.; Pédron, T.; Cavin, J.F; Sansonetti, P. Functional genomics of *Lactobacillus casei* establishment in the gut. *Proceedings of the National Academy of Sciences of the United States of America.* **2014**, 111(30), 3101-3109.

Lisboa, C. G. S.; Tonini, P. P.; T.; M. A. S.; Buckeridge, M. S. Endo-β-mannanase from the endosperm of seeds of *Sesbania virgata* (Cav.) Pers. (Leguminosae): purification, characterisation and its dual role in germination and early seedling growth. *Brazilian Journal of Plant Physiology*. **2006**, 18(2), 269-280.

Liu, J.; Basit, A.; Miao, T.; Zheng, F.; Yu, H.; Wang, Y.; Jiang, W.; Cao, Y. Secretory expression of β-mannanase in *Saccharomyces cerevisiae* and its high efficiency for hydrolysis of mannans to mannooligosaccharides. *Applied Microbiology and Biotechnology*. **2018**, 102, 10027-10041.

Mafa, M. S.; Malgas, S. Towards an understanding of the enzymatic degradation of complex plant mannan structures. *World Journal of Microbiology and Biotechnology*. **2023**, 39, 302.

Magengelele, M.; Hlalukana, N.; Malgas, S.; Rose, S. H.; van Zyl, W. H.; Pletschke, B. I. Production and *in vitro* evaluation of prebiotic manno-oligosaccharides prepared with a recombinant *Aspergillus niger* endo-mannanase, Man26A. *Enzyme and Microbial Technology*. **2021**, 150, 109893.

Mahamed, S. A.; Al-Malki, A. L.; Kumosani, T. A. Horseradish peroxidase and chitosan: Activation, immobilization and comparative results. *International Journal of Biological Macromolecules.* **2013**, 60, 295-300.

Malgas, S.; Dyk, S. J. v.; Pletschke, B. I. A review of the enzymatic hydrolysis of mannans and synergistic interactions between β-mannanase, β-mannosidase and α-galactosidase. *World Journal of Microbiology and Biotechnology* **2015a**, 31, pp. 1167-1175.

Malgas, S.; Dyk, S. J.; Pletschke, B. I. β-Mannanase (Man2 A) and α-galactosidase (Aga27A) synergism – A key factor for the hydrolysis of galactomannan substrates. *Enzyme and Microbial Technology*. **2015b**, 70, 1-8.

Manyi-Loh, C.; Mamphweli, S.; Meyer, E.; Okoh, A. Antibiotic Use in Agriculture and Its Consequential Resistance in Environmental Sources: Potential Public Health Implications. *Molecules*, **2018**, 23(4), 795.

Markowiak, P.; Śliżewska, K. The role of probiotics, prebiotics and synbiotics in animal nutrition. *Gut Pathogens*. **2018**, 10(1), 1-20.

Miller, G. L. Use of dinitrosalicylic acid reagent for determination of reducing sugar. *Analytical Chemistry* **1959**, 31(3), 426-428.

Mohapatra, B. R. Characterization of β-mannanase extracted from a novel *Streptomyces* species Alg-S25 immobilized on chitosan nanoparticles. *Biotechnology & Biotechnological Equipment.* **2021**, *35(1)*, 150-161.

Mora-Escobedo, R., Del Carmen Robles-Ramírez, M., Delia Román-Gutiérrez, A., Castro-Rosas, J., Baruchs Muñoz-Llandes, C., & Araceli Guzmán-Ortiz, F. Peptides and Microorganisms Isolated from Soybean Sources with Antimicrobial Activity. *Soybean - Biomass, Yield and Productivity*. **2019**, 1-18.

Morsy, M.; Mostafa, K. M.; Amyn, H. A. M; El-Ebissy, A. A. H.; Salah, A. M.; Youssef, M. A. Synthesis and characterization of free dryer chitosan nanoparticles as multifunctional eco-friendly finish for fabricating easy care and antibacterial cotton textiles. *Egyptian Journal of Chemistry*. **2019**, 62(7), 1277-1293.

Nadaroglu, H.; Sonmez, Z. Purification of an endo-1,4-β-mannanase from *Clitocybe geotropa* and immobilization on chitosan-coated magnetite nanoparticles: application for fruit juices. *Digest Journal of Nanomaterials and Biostructures*. **2016**, 11(2), 685-697.

Naganagouda, K.; Salimath, P. V.; Mulimani, V. H. Purification and characterization of endo-beta-1,4 mannanase from Aspergillus niger gr for application in food processing industry. *Journal of Microbiology and Biotechnology*. **2009**, 19(10), 1184-1190.

Najavand, S.; Habibnejad, M.; Amani-Ghadim, A. R.; Rahimizadeh, P.; Pazhang, M. Optimized immobilization of endoglucanase Cel9A onto glutaraldehyde activated chitosan nanoparticles by response surface methodology: The study of kinetic behaviors. *Biotechnology Progress*. **2020**, 36(3), 2960.

Nakano, Y.; Yamaguchi, M.; Endo, H.; Rejab, N. A.; Ohtani, M. NAC-MYB-based transcriptional regulation of secondary cell wall biosynthesis in land plants. *Frontiers in Plant Science*. **2015**, 6, 1-18.

Neira, H. D.; Herr, A. E. Kinetic analysis of enzymes immobilized in porous film arrays. *Journal of Analytical Chemistry*. **2018**, 89(19), 110311-10320.

Nguyen, V. D.; Styevkó, G.; Madaras, E.; Haktanirlar, G.; Tran A. T. M.; Bujna, E.; Dam, M. S.; Nguyen, Q. D. Immobilization of β-galactosidase on chitosan-coated magnetic nanoparticles and its application for synthesis of lactulose-based galactooligosaccharides. *Process Biochemistry*. **2019**, 84, 30-38.

Nigam, P. S. Microbial enzymes with special characteristics for biotechnological applications. *Biomolecules*. **2013**, 3(3), 597-611.

Nkukwana, T. T. Global poultry production: Current impact and future outlook on the South African poultry industry. *South African Journal of Animal Science*. **2018**, 48, 869-884

OECD. Meat consumption worldwide from 1990 to 2021, by meat type* (in million tons). [Online] **2021**. Available at: https://www.statista.com/statistics/274522/global-per-capita-consumption-of-meat/ [Accessed 17 September 2021].

OECD/FAO. OECD-FAO Agriculutral outlook 2018-2027, **2018**. Paris: OECD Publishing and Agriculture organisation of the United Nations.

Onem, H.; Cicek, S.; Nadaroglu, H. Immobilization of a thermostable phytase from Pinar melkior (*Lactarius piperatus*) onto magnetite chitosan nanoparticles. *CyTA – Journal of Food*. **2016**, 14(1), 74-83.

Osuna, Y.; Gregorio-Jauregui, K. M.; Gaona-Lozano, J.; Garza-Rodriguez, I. M.; Ilyna, A.; Barriga-Castro, E. D.; Saade, .; López, R. G. Chitosan-coated magnetic nanoparticles with low chitosan content prepared in one-step. *Journal of Nanomaterials*. **2012**, 1-7.

Pan, D.; Yu, Z. Intestinal microbiome of poultry and its interaction with host and diet. *Gut Microbes*. **2014**, 5(1), 108-119.

Patrikiadou, E.; Patrikidou, A.; Hatzidaki, E.; Papandreou, C. N.; Zaspalis, V.; Nalbandian, L. Magnetic nanoparticles in medical diagnostic applications. Synthesis, characterization, functionalization, and proteins conjugation. *Current Nanoscience*. **2015**, 12, 1-1.

Perwez, M.; Ahmad, R.; Sardar, M. A reusable multipurpose magnetic nanobiocatalyst for industrial applications. *International Journal of Biological Macromolecules*. **2017**, 103, 16-24.

Peternele, W. S.; Fuentes, V. M.; Fascineli, M. L.; Da Silva, J. R.; Silva, R. C.; Lucci, C. M.; Betentes de Azevedo, R. Experimental investigation of the coprecipitation method: An approach to obtain magnetite and maghemite nanoparticles with improved properties. *Journal of Nanomaterials*. **2014**, 1-10.

Phiwphech, S.; Luang-In, V.; Deseenthum, S.; Rattanasuk, S. Locust bean gum hydrolysis for mannooligosacharide (MOS) production using *Bacillus methylotrophicus* KS1. *ICoFAB2019 Proceedings*, **2019**, 14, 69-73.

Podrepšek, G. .; Željko, K.; Maja, L. Development of chitosan functionalized magnetic nanoparticles with bioactive compounds. *Nanomaterials*. **2020**, 10(10), 1913.

Puri, M.; Abraham, R. E. Strategies to Enhance Enzyme Activity for Industrial Processes in Managing Agro-Industrial Waste. In Agro-Industrial Wastes as Feedstock for Enzyme Production (pp. 299–312). **2016**, Elsevier.

Raafat, D.; Sahl, H. G. Chitosan and its antimicrobial potential – a critical literature survey. *Microbial Biotechnology*. **2009**, 2(2), 186-201.

Ramírez-Ramírez, L. G.; Zazueta-Álvarez, D, E.; Fileto-Pérez, H. A.; Reyes-Jáquez, D.; Núñez-Núñez, C. M.; de Dios Galindo-De la Rosa, J.; López-Miranda, J.; Vázquez-Ortega 1, P. G. Improvement in the thermostability of a recombinant β-glucosidase immobilized in zeolite under different conditions. *Molecules*. **2022**, 27, 4105.

Ratnakomala, S.; Kahar P.; Kashiwagi, N.; Lee, J.; Kudou, M.; Matsumoto, H.; Apriliana, P.; Yopi, Y; Prasetya, B.; Ogino, C.; Kondo, A. Manno-oligosaccharide production from biomass

hydrolysis by using endo-1,4-β-mannanase (ManNj6-379) from *Nonomuraea jabiensis* ID06-379. *Processes*. **2022**, 10(20), 269.

Ravindran, V. Poultry feed availability and nutrition in developing countries. *Poultry Development Review*. **2013**, 60-63.

Rebroš, M.; Rosenberg, M.; Mlichova, Z.; Kristofikova, L. ydr olysis of sucrose by invertase entrapped in polyvinyl alcohol hydrogel capsule. *Food Chemistry.* **2007***, 102(3)*, 784-787.

Rehm, F. B. H.; Chen,, S.; Rehm, B. H. A. Enzyme engineering for *in situ* immobilization. *Molecules.* **2016**, 21, 1-19

Reshmy, R.; Narisetty, V.; Ayon, Tarafdar, A.; Bachan, N.; Madhavan, A.; Tiwari, A.; Chaturvedi, P.; Varjani, S.; Sirohi, R.; Kumar, V.; Awasthi, M. K. Cellulase immobilisation by nanoparticles for biofuel applications: Strategies and perspectives. *BioEnergy Research*. **2022**.

Sachslehner, A.; Foidl, G.; Foidl, N.; Gubitz, G.; Haltrich, D. Hydrolysis of isolated coffee mannan and coffee extract by mannanases of *Sclerotium rolfsii. Journal of Biotechnology*. **2000**, 80, 127-134.

Sadaqat, B.; Sha, C.; Dar, M.A.; Dhanavade, M.J.; Sonawane, K.D.; Mohamed, H.; Shao, W.; Song, Y. Modifying thermostability and reusability by immobilization on glutaraldehyde cross-linked chitosan beads. *Biomolecules*. **2022**, 12(7), 999.

Saeed, M.; Ahmad, F.; Arain, M. A.; Abd El-Hack, M.; Emam, M.; Bhutto, Z. A.; Moshaveri, A. Use of mannan-oligosaccharides (MOS) as a feed additive in poultry nutrition. *Journal of Poultry Research*. **2017**, 7(3), 94-103.

Samrot, A. V.; Shobana, N.; Sruthi, P. D.; Sahithya, C. S. Utilization of chitosan-coated superparamagnetic iron oxide nanoparticles for chromium removal. *Applied Water Science*. **2018**, 8(192), 1-9.

Saravanakumar, T.; Palvannan, T.; Kim, D. H.; Park, S. M. Optimized immobilization of peracetic acid producing recombinant acetyl xylan esterase on chitosan coated-$Fe_3O_4$ magnetic nanoparticles. *Process Biochemistry*. **2014**, 49(11), 1920-1928.

Scapini, L. B.; Rorig, A.; Ferrarini, A.; Füber, L. M.; Canavese, M.; Silva, A. M. Nutritional evaluation of soybean hulls with or without β-mannanase supplement on performance, intestinal morphometric and carcass yield of broilers chickens. *Brazilian Journal of Poultry*. **2018**, 20(4), 633-642.

Shalaby, A. S. G.; Esawy, M. A.; Huessein, M. D. M. Comparative study between free and immobilized *Penicillium chrysogenum* mannanase: a local fungal isolate. *Journal of Applied Pharmaceutical Science.* **2017**, 7(6), 97-104.

Sharma, K.; Dhillon, A.; Goyal, A. Insights into structure and reaction mechanisms of β-mannanases. *Current Protein and Peptide Science*. **2018**, 19, 34-47.

Sharma, P.; Sharma, S.; Ramakrishna, G.; Srivastava, H.; Gaikwad, K. A comprehensive review on leguminous galactomannans: structural analysis, functional properties, biosynthesis process and industrial applications. *Critical Reviews in Food Science and Nutrition*. **2020**, 62(2), 443-465.

Shastak, Y.; Ader, P.; Feuerstein, D.; Ruehle, R.; Matuschek, M. β-Mannan and mannanase in poultry nutrition. *World's Poultry Science Journal*. **2015**, 71, 161-174.

Shi, C.; Zhang, Y.; Lu, Z.; Wang, Y. Solid-state fermentation of corn-soybean meal mixed feed with *Bacillus subtilis* and *Enterococcus faecium* for degrading antinutritional factors and enhancing nutritional value. *Journal of Animal Science and Biotechnology*. **2017**, 50(8), 1-9.

Shoaib, M.; Zhouping, W. Application of chitosan as an antimicrobial agent. J*ournal of Food and Nutritional Health.* **2020**, 1(1), 1-11.

Silva, D. F.; Rosa, H.; Carvalho, A. F. A.; Oliva-Neto, P. Immobilization of papain on chitin and chitosan and recycling of soluble enzyme for deflocculation of *Saccharomyces cerevisiae* from Bioethanol Distilleries. *Hindawi Publishing Corporation*. **2015**, 2015(1), 1-10.

Singh, R. K.; Tiwari, M. K.; Singh, R.; Lee, J. K. From protein engineering to immobilization: Promising strategies for the upgrade of industrial enzymes. *International Journal of Molecular Sciences*. **2013**, 14(1), 1232-1277.

Sinha, K.; Khare, V. Review on: Antinutritional factors in vegetable crops. *The Pharma Innovation Journal.* **2017**, 6(12), 353-358.

Solis-Cruz, B., Hernandez-Patlan, D., Hargis, B.M., Tellez, G. Use of prebiotics as an alternative to antibiotic growth promoters in the poultry industry, in: Franco-Robles, E., Ramírez-Emiliano, J. (Eds.), Prebiotics and probiotics. **2019,** IntechOpen, Rijeka.

Soni, H.; Rawat, H. K.; Pletschke, B. I.; Kango, N. Purification and characterization of β-mannanase from *Aspergillus terreus* and its applicability in depolymerization of mannans and saccharification of lignocellulosic biomass. *Biotechnology Journal*. **2016**, 6(136), 1-11.

Srivastava, P. K.; Kapoor, M. Production, properties, and applications of endo-β-mannanases. *Biotechnology Advances*. **2017**. 35, 1-19.

Su, L.; Cheng, Y.; Hsiao, F. S.; Han, J.; Yu. Optimization of mixed solid-state fermentation of soybean meal by *Lactobacillus* species and *Clostridium butyricum. Polish Journal of Microbiology.* **2018**. 67(3), 297-305.

Suhaibani, A. A.; Bacha, A. B.; Alonazi, M.; Bhat, R. S.; El-Ansary, A. Testing the combined effects of probiotics and prebiotics against neurotoxic effects of propionic acid orally administered to rat pups. *Food Science & Nutrition.* **2021***, 9(8)*, 4440-4451.

Sun, D.; Zhang J.; Li C.; Wang, T. F.; Qin, H. M. Biochemical and structural characterization of a novel thermophilic and acidophilic β-mannanase from *Aspergillus calidoustus*. *Enzyme and Microbial Technology*. **2021**, 150, 1-7.

Sun, R. C.; Tomkinson, J.; Characterization of hemicelluloses isolated with tetraacetylethylenediamine activated peroxide from ultrasound irradiated and alkali pre-treated wheat straw. *European Polymer Journal*. **2003**, 39, 751-759.

Suryawanshi, R. K.; Kango, N. Production of mannooligosaccharides from various mannans and evaluation of their prebiotic potential. *Food Chemistry*. **2021**, 331, 127428.

Šušković, J.; Kos, B.; Beganović, J.; Pavunc, A. L.; a bjanič, K.; Matošić, S. Antimicrobial activity – The most important property of probiotic and starter lactic acid bacteria. *Food technology and Biotechnology.* **2010**, 48(3), 296-307.

Suthama, N.; Wibawa, P. J. Amino acids digestibility of pelleted microparticle protein of fish meal and soybean meal in broiler chickens. *Journal of the Indonesian Tropical Animal Agriculture*. **2018**, 43(2), 169-176.

Swartz, M. HPLC detectors: A brief review. *Journal of Liquid Chromatography & Related Technologies.* **2010**, 33(9-12), 1130-1150.

Thamilarasan, V.; Sethuraman, V.; Gopinath, K.; Balalakshmi, C.; Govindarajan, M.; Mothana, R. A.; Siddiqui, N. A.; Khaled, N. A.; Benelli, G. Single step fabrication of chitosan nanocrystals using *Penaeus semisulcatus*: Potential as new insecticides, antimicrobials and plant growth promoters. *Journal of Cluster Science*. **2018**, 29, 375-384.

Tian, Z.; Chen, J.; Ji, X.; Wang, Q.; Yang, G.; Fatehi, P. Dilute sulfuric acid hydrolysis of *Pennisetum* (sp.) Hemicellulose. *Bioresources*. **2017**, 12(2), 2609-2617.

Tiwari, U. P.; Fleming, S. A.; Abdul Rasheed, M. S.; Jha, R.; Gilger, R. N. The role of oligosaccharides and polysaccharides of xylan and mannan in gut health of monogastric animals. *Journal of Nutritional Science.* **2020**, 9, 1-9.

USDA WASDE. 2022. United States Department of Agriculture World Agricultural Supply and Demand Estimates. Accessed June 2022. https://www.usda.gov/oce/commodity/wasde/wasde0622.pdf

Vaghari, H.; Jafarizadeh-Malmiri, H.; Mohammadlou, M.; Berenjian, A.; Anarjan, N.; Jafari, N.; Nasiri, S. Application of magnetic nanoparticles in smart enzyme immobilization. *Biotechnology Letters*. **2015**, 38, 223-233.

Van der Poel, A. F. B.; Abdollahi, M. R.; Cheng, H.; Colovic, R.; Hartog, L. A; Miladinovic, D.; Page, G.; Sijssens, K.; Smillie, J. F.; Thomas, M.; Wang, W.; Yu, P.; Hendriks, W. H. Future directions of animal feed technology research to meet the challenges of a changing world. *Animal Feed Science and Technology*, **2020**, 270, pp. 1-32.

Van Zyl, P. J.; Moodley, C.; Rose, S. H.; Roth, R. L.; van Zyl, W. H. Production of the *Aspergillus aculeatus* endo-1,4-b-mannanase in *A. niger. Journal of Industrial Microbiology and Biotechnology.* **2009**, 36(4), 611-617.

Vangroenweghe, F.; Poulsen, K.; Thas, . Supplementation of a β-mannanase enzyme reduces post-weaning diarrhea and antibiotic use in piglets on an alternative diet with additional soybean meal. *Porcine Health Management.* **2021**, 7(8), 1-12.

Vaz, R. P.; Filho, E. X. F. Exchange Chromatography for enzyme immobilization. *Applications of Ion Exchange Materials in Biomedical Industries*. **2019**, 13-27

Verma, M. L.; Kumar, S.; Das, A.; Randhawa, J. S.; Chamundeeswari, M. Chitin and chitosan-based support materials for enzyme immobilization and biotechnological applications. *Environmental Chemistry Letters.* **2020**, 18, 315-323.

Waifalkar, P. P.; Parit, S. B.; Chougale, A. D.; Sahoo, S. C.; Patil, P. S.; Patil, P. B. Immobilization of invertase on chitosan coated γ-$Fe_2O_3$ magnetic nanoparticles to facilitate magnetic separation. *Journal of Colloid and Interface Science*. **2016**, 482, 159-164.

Wang, D.; Zhang, H.; Wu, F.; Li, T.; Liang, Y.; Duan, X. Modification of pectin and hemicellulose polysaccharides in relation to aril breakdown of harvested longan fruit. *International Journal of Molecular Sciences*. **2013**, 14, 23356-23368.

Wang, L. Y.; Gu, Y. H.; Zhou, Q. Z.; Ma, G.H.; Wan, Y. H.; Su, Z. G. Preparation and characterization of uniform-sized chitosan microspheres containing insulin by membrane emulsification and a two-step solidification process. *Colloids Surfaces B*. **2006**, 50, 126–135.

White, D. Adhikari, R.; Wang, J.; Chen, C.; Lee, J. H.; Kim, W. K. Effects of dietary protein, energy and β-mannanase on laying performance, egg quality, and ileal amino acid digestibility in laying hens. *Poultry Science*. **2021**, 100(9), 101312.

Xie, J.; Pan, L.; e, Z.; Liu, W.; Zheng, D.; Zhang, Z.; Wang, B. A novel thermophilic β-mannanase with broad-range pH stability from *Lichtheimia ramosa* and its synergistic effect with α-galactosidase on hydrolyzing palm kernel meal. *Process Biochemistry*. **2020**, 88, 51-59.

Yuan, Z.; Chang, X. F.; Kapu, N. S.; Beatson, R.; Martinez, D. M. An eco-friendly scheme to eliminate silica problems during bamboo biomass fractionation. *Biorefinery*. **2017**, 32(1), 4-13.

Yoo, H. Y.; Pradeep, G. C.; Lee, S. K.; Park, D. H.; Cho, S. S.; Choi, Y. H.; Yoo, J. C.; Kim, S. W. Understanding β-mannanase from *Streptomyces* sp. CS147 and its potential application in lignocellulose based biorefining. *Biotechnology Journal*. **2015**, 10(12), 1894-1902.

Younes, I.; Marguerite, R. Chitin and chitosan preparation from marine sources: Structure, properties and applications. *Marine Drugs*. **2015**, 13(3), 1133-1174.

Zahir, M.; Fogliano, V.; Capuano, E. Effect of soybean processing on cell wall porosity and protein digestibility. *Food and Function.* **2019**, 11, 285-296.

Zahura, U. A.; Rahman, M. M.; Inoue, A.; Tanaka, H. An endo-β-1,4-mannanase, AkMan, from the common sea hare *Aplysia kurodai*. *Comparative Biochemistry and Physiology, Part B*. **2010**, 157, 137-143.

Zhang, R.; Li, X. Y.; Cen, X. L.; Gao, Q.H.; Zhang, M.; Li, K. Y.; Wu, Q.; Mu, Y. L.; Tang, Z. H.; Zhou, J. P. Huang, Z. X. Enzymatic preparation of manno-oligosaccharides from locust bean gum and palm kernel cake, and investigations into its prebiotic activity. *Electronic Journal of Biotechnology*. **2021**, 49, 64-71.

Zhou, C.; Xue, Y.; Ma, Y. Characterization and high-efficiency secreted expression in *Bacillus subtilis* of a thermo-alkaline β-mannanase from an alkaliphilic *Bacillus clausii* strain S10. *Microbial Cell Factories.* **2018**, 17(124), 1-19.

Zuluaga, L. V.; Giraldo, O. H.; Orrego, C. E. Immobilization of mannanase on magnetic chitosan microspheres. *Revista Mexicana de Fisica.* **2012**, 58(2), 39-43.

Zyl, W. .; Rose, S. .; Trollope, K.; Görgens, J. F. Fungal β-mannanases: Mannan hydrolysis, heterologous production and biotechnological applications. *Process Biochemistry*. **2010**, 45, 1203-1213.

## Appendices

**Table A:** XRD size determination analysis of CTS

| Particle Type | Parameters | | Calculations | | Particle Size | |
|---|---|---|---|---|---|---|
| | ***K*** | **λ** | **Peak position (2θ)** | **FWHM β** | ***D* (nm)** | **Average *D* (nm)** |
| **Chitosan** | 0.94 | 0.15 | 10.65 | 1.58 | 5.27 | 8.02 |
| | | | 19.72 | 1.68 | 5.02 | |
| | | | 42.55 | 1.02 | 8.76 | |
| | | | 49.50 | 0.70 | 13.05 | |
| **A-CTS** | | | 18.16 | 0.79 | 10.63 | 12.28 |
| | | | 42.61 | 0.62 | 14.33 | |
| | | | 49.33 | 1.07 | 8.53 | |
| | | | 52.10 | 0.59 | 15.63 | |
| **CTS** | | | 31.15 | 1.04 | 8.25 | 10.07 |
| | | | 33.24 | 1.41 | 6.13 | |
| | | | 42.67 | 0.85 | 10.51 | |
| | | | 49.50 | 0.65 | 14.07 | |
| | | | 45.60 | 0.79 | 11.39 | |

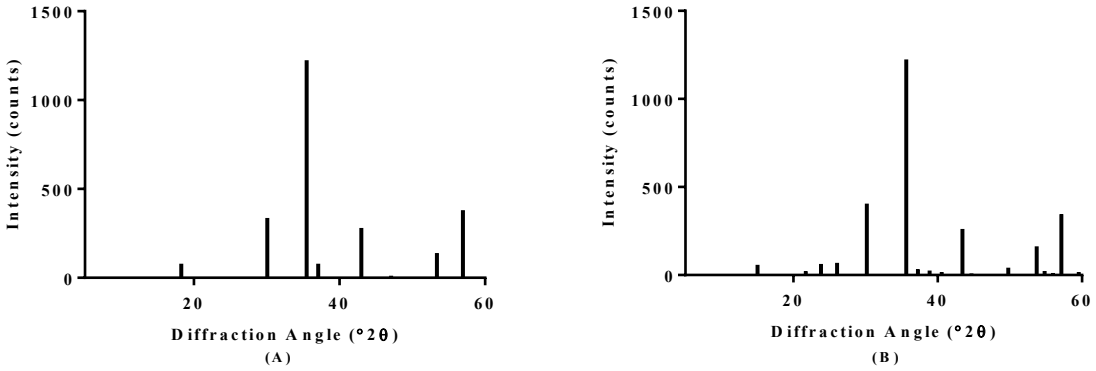


**Figure A:** X-ray Diffraction (XRD) patterns of **(A)** magnetite and **(B)** maghemite.

**Table B:** XRD size determination analysis of MAGS-CTS

| **Particle Type** | **Parameters** | | **Calculations** | | **Particle Size** | |
|---|---|---|---|---|---|---|
| | ***K*** | **λ** | **Peak position (2θ)** | **FWHM β** | ***D* (nm)** | **Average *D* (nm)** |
| **MAGS** | 0.94 | 0.15 | 29.62 | 1.36 | 6.33 | 8.38 |
| | | | 34.99 | 0.73 | 11.85 | |
| | | | 42.66 | 1.47 | 6.07 | |
| | | | 56.67 | 1.02 | 9.27 | |
| **MAGS-chitosan** | | | 29.56 | 0.65 | 13.22 | 11.06 |
| | | | 34.82 | 1.07 | 8.11 | |
| | | | 42.50 | 0.90 | 9.84 | |
| | | | 49.46 | 0.54 | 16.88 | |
| | | | 56.33 | 1.30 | 7.25 | |
| **MAGS-A-CTS** | | | 29.68 | 1.55 | 5.52 | 8.15 |
| | | | 35.10 | 0.96 | 9.07 | |
| | | | 42.90 | 1.24 | 7.17 | |
| | | | 53.13 | 0.85 | 10.85 | |
| | | | 56.68 | 1.16 | 8.12 | |
| **MAGS-CTS** | | | 29.79 | 0.87 | 9.81 | 8.06 |
| | | | 35.38 | 0.99 | 8.81 | |
| | | | 42.89 | 1.50 | 5.96 | |
| | | | 53.39 | 1.21 | 7.65 | |

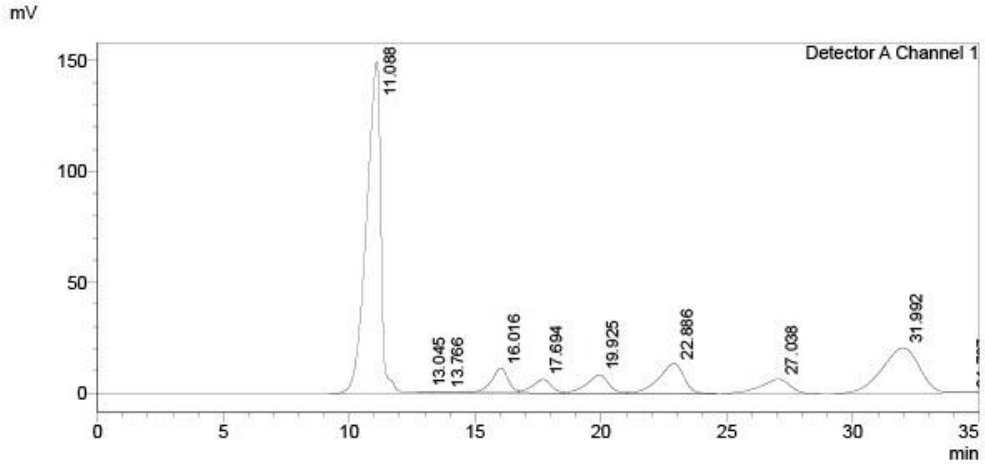


**Figure B:** MOS standards. Analysis was conducted using a Carbosep CHO 411 column, with a flow rate of 0.26 ml/min and a refractive index detector (RID).

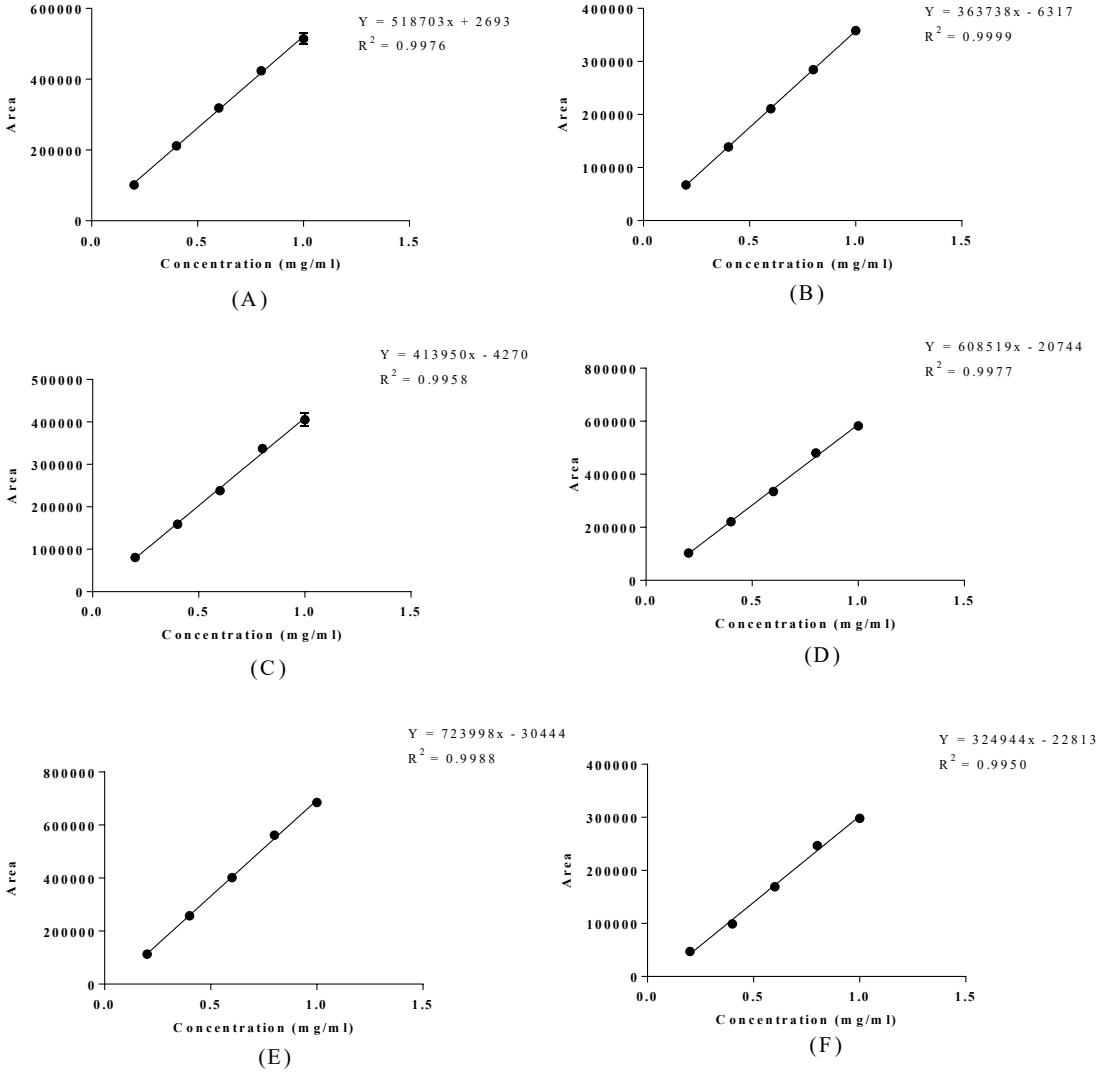


**Figure C:** Standard curves representing the MOS standards used in HPLC analysis: (A) M1, (B) M2, (C) M3, (D) M4, (E) M5, and (F) M6.

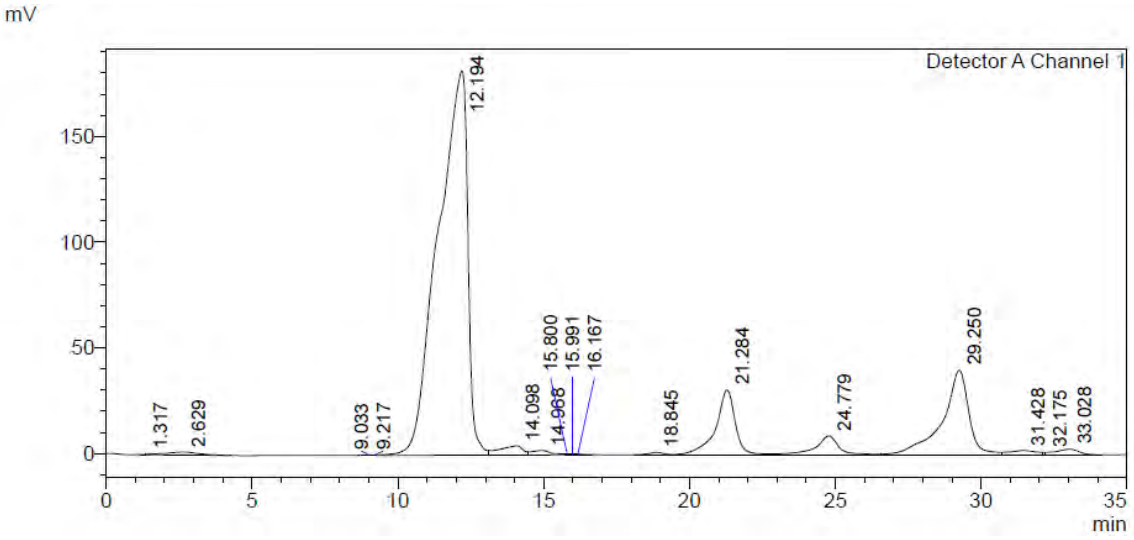


**Figure D:** HPLC Full Analysis Report of 6% (w/v) SBM hydrolysed with free endo-1,4-β-mannanase. Analysis was conducted using a Carbosep CHO 411 column, with a flow rate of 0.26 ml/min and a refractive index detector (RID).

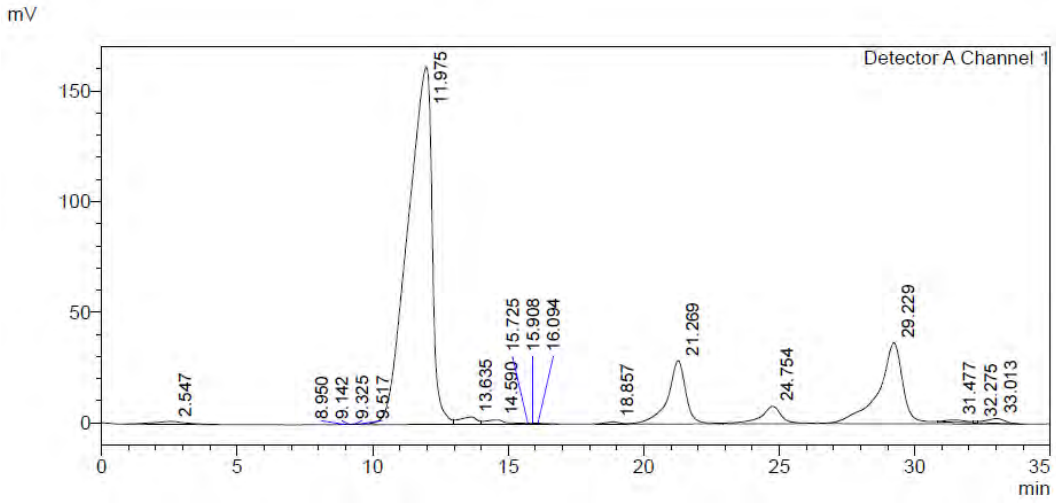


**Figure E:** HPLC Full Analysis Report of 6% (w/v) SBM hydrolysed with CTS endo-1,4-β-mannanase. Analysis was conducted using a Carbosep CHO 411 column, with a flow rate of 0.26 ml/min and a refractive index detector (RID).

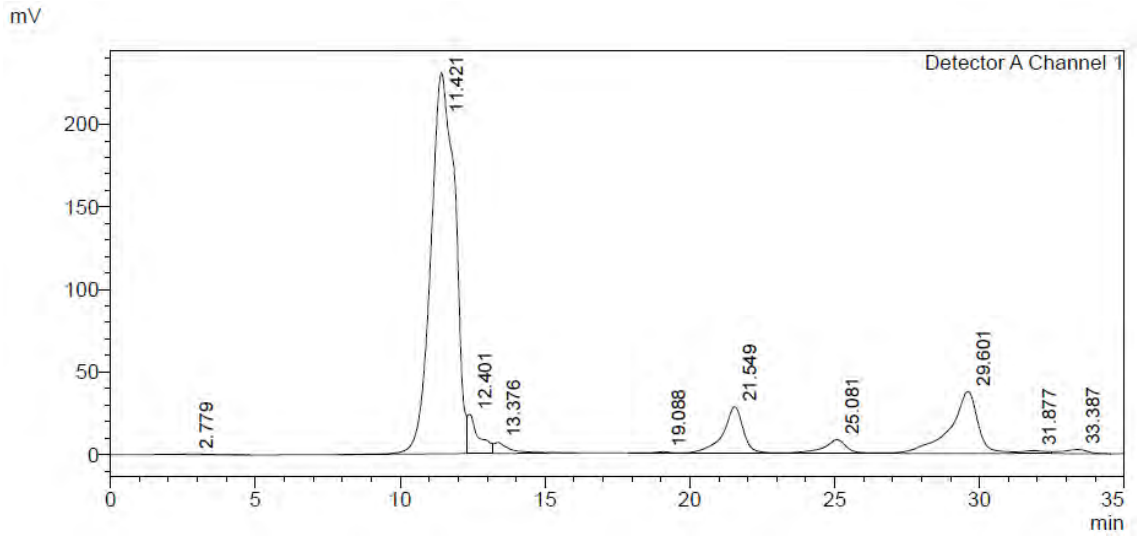


**Figure F:** HPLC Full Analysis Report of 6% (w/v) SBM hydrolysed with MAGS-CTS endo-1,4-β-mannanase

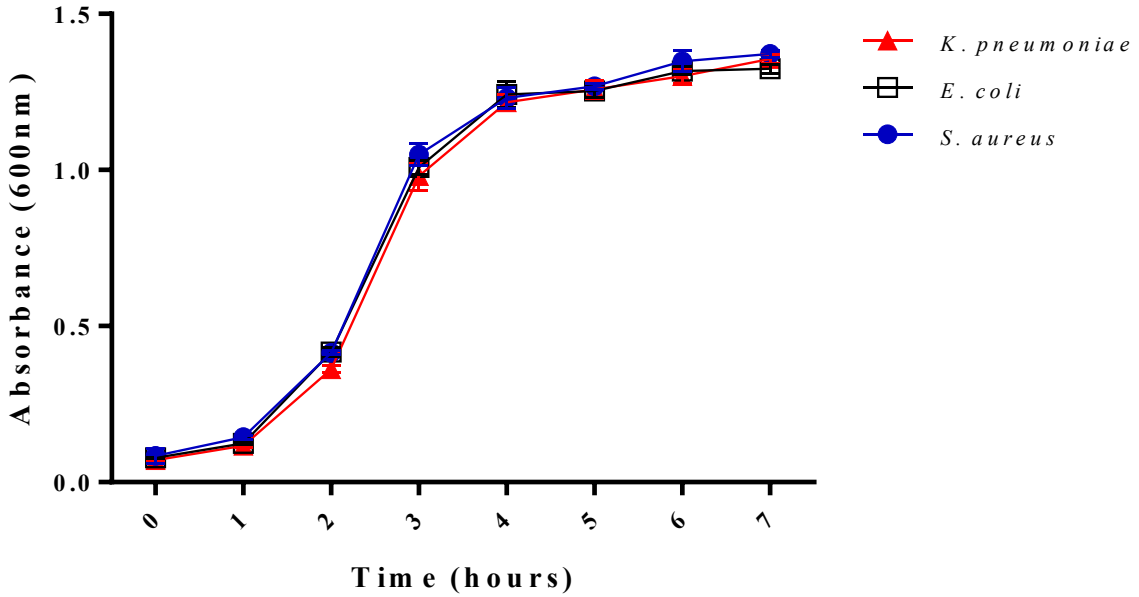


**Figure G:** Bacterial log phases of the various pathogenic bacteria.

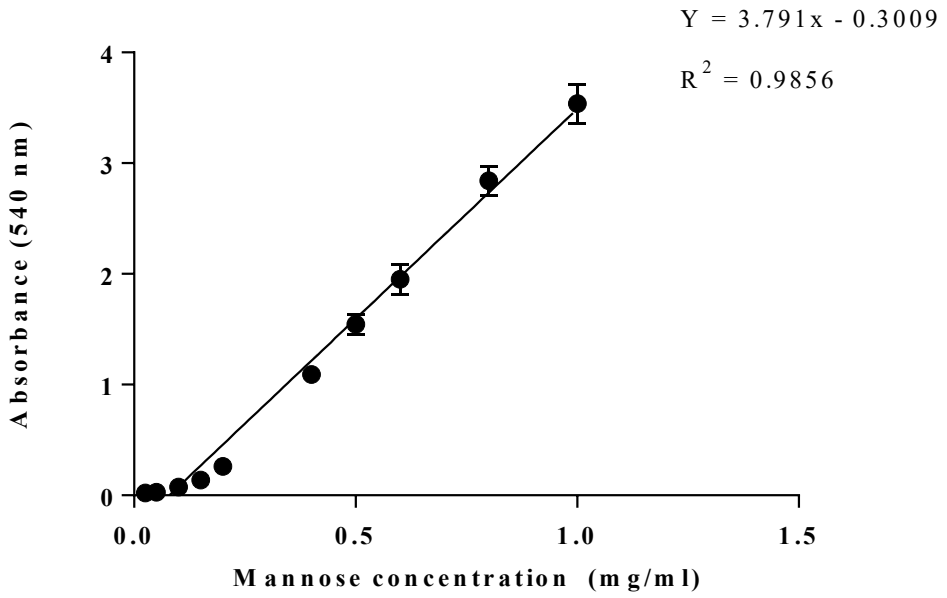


**Figure H:** Mannose standard curve. Reducing sugars were analysed via a DNS assay. Each value in the graphs represents the means ± SD (n = 3).

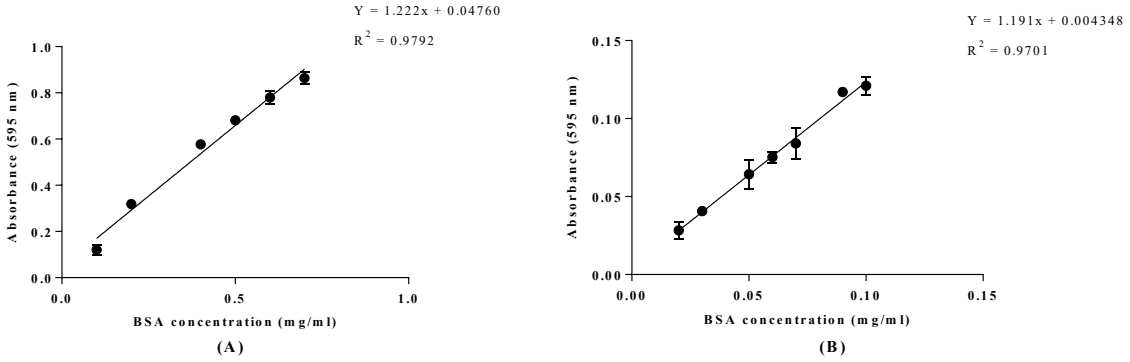


**Figure I:** BSA protein standard curves in the (A) 0.1 – 0.7 mg/ml and (B) 0.01 – 0.1 mg/ml concentration ranges.